

Developing Next Generation Technologies  
for Spatially Targeted Proteomics

By

Daniel Joseph Ryan

Dissertation

Submitted to the Faculty of the  
Graduate School of Vanderbilt University  
in partial fulfillment of the requirements

for the degree of

DOCTOR OF PHILOSOPHY

in

Chemistry

June 30th, 2019

Nashville, Tennessee

Approved:

Richard M. Caprioli, Ph.D.

Jeffrey M. Spraggins, Ph.D.

John A. McLean, Ph.D.

Lars Plate, Ph.D.

Kevin L. Schey, Ph.D.

Copyright © 2019 by Daniel Joseph Ryan  
All Rights Reserved

## ACKNOWLEDGEMENTS

It is with the help of many people that I am afforded the unique privilege of being able to sit here and write out an acknowledgements section for my dissertation. First and foremost, I would like to thank both of advisors, Dr. Richard Caprioli and Dr. Jeff Spraggins. Richard, you have pushed me both scientifically and personally. You have led by example and I am very grateful to have had the opportunity to spend my graduate career in your laboratory, it is not something I take for granted. Jeff, you helped me gain traction upon entering the lab, gave me direction, and have been an integral part of my journey while at Vanderbilt. You went above and beyond what is expected of any advisor to help mold me into the scientist I am today, and I am grateful to call you a mentor and more importantly, a friend. To my entire committee, Kevin Schey, John McLean, and Lars Plate; I am forever thankful for the time you have taken to help push me towards excellence throughout this journey.

I want to thank my lab mates, who are also my closest friends, for their support and friendship throughout this period of my life. Thank you for dealing with my craziness and also for being as excited for Happy Hour as I am, I couldn't imagine going through this process with another group of people. I will always hold the many memories involving late night Patriots at Dukes, SatCo porch beers, and appropriately priced snacks at Answer close to my heart, and consider them a contributing factor in finishing my research at Vanderbilt. To the staff of the MSRC, you all have been instrumental in ensuring I stay happy and on track, and I am so thankful. Maureen Casey, you were truly one of the best parts of coming to lab every day, and I wish you the best in retirement.

Finally, and most importantly, I would like to thank my family and my daughter for their continued support. There is an old quote that states, “To us, family means putting your arms around each other and being there”, and I have been truly blessed with a family, with parents, who have never swayed from that motto. Only they know how truly difficult this path has been at times, and they have come to my aid whenever I needed it, and I am truly thankful for all that you guys have done. To my beautiful, smart, and funny daughter Norah, you have no idea how important your presence, whether near or far, served as the perfect distraction to all of the fuss of chemistry and graduate school. Walking to daycare after lab each day, picking up an always surprised 2 year old, or watching you shovel loads of hummus in your mouth on my couch, to nightly runs in a jogging stroller. These are some of my fondest memories in Nashville. The research detailed below is a culmination of not only my work, but our combined work as a family, and any success I have in the future, and have had in the past, is a direct result of all of you.

## TABLE OF CONTENTS

	Page
ACKNOWLEDGEMENTS .....	iii
LIST OF FIGURES .....	viii
LIST OF TABLES .....	xi
LIST OF ABBREVIATIONS .....	xii
Chapter	
I. MATRIX-ASSISTED LASER DESORPTION/IONIZATION IMAGING MASS SPECTROMETRY AND PROTEIN IDENTIFICATION	
Overview.....	1
Introduction.....	2
Matrix-Assisted Laser Desorption/Ionization and Mass Spectrometry .....	2
MALDI Imaging Mass Spectrometry and MALDI Profiling of Proteins from Tissue.....	4
Time-of-Flight Mass Spectrometry.....	8
Fourier Transform Ion Cyclotron Resonance Mass Spectrometry .....	10
Protein Identification in MALDI IMS .....	13
Protein Identification Strategies.....	16
<i>Tissue Homogenization</i> .....	17
<i>In Situ Enzymatic Digestion</i> .....	18
<i>Chemical Derivatization</i> .....	19
<i>Laser Capture Microdissection</i> .....	20
<i>Hydrogel Extraction</i> .....	20
<i>Liquid Extraction Surface Analysis</i> .....	21
Research Summary and Objectives.....	23
II. IMPROVING PROTEIN ION TRANSMISSION ON A 15T FT-ICR MS FOR MALDI IMS	
Overview.....	25
Introduction.....	25
Results.....	28
<i>Systematic Study of Source Pressure</i> .....	28
<i>Tissue Imaging and Image Fusion</i> .....	37
Discussion .....	45
Methods.....	46
<i>Mass Spectrometry</i> .....	46

<i>Imaging Mass Spectrometry</i> .....	48
<i>Data Driven Multi-Modal Image Fusion</i> .....	49

### III. SPATIALLY TARGETED PROTEOMIC ANALYSIS FROM TISSUE USING LIQUID EXTRACTION SURFACE ANALYSIS

Overview.....	51
Introduction.....	51
Results.....	55
<i>Surface Extraction Performance</i> .....	55
<i>Correlating IMS with LESApplusLC Protein Experiments</i> .....	62
Discussion .....	72
Methods.....	73
<i>Tissue Preparation</i> .....	73
<i>MALDI IMS</i> .....	74
<i>In Situ Tryptic Digestion</i> .....	75
<i>Tissue Extractions</i> .....	75
<i>Online LC-MS</i> .....	77
<i>Bottom-Up Tandem Mass Spectrometry</i> .....	77
<i>Top-Down Tandem Mass Spectrometry</i> .....	79

### IV. MICROLESA: INTEGRATING AUTOFLUORESCENCE MICROSCOPY, IN SITU MICRO-DIGESTIONS, AND LIQUID EXTRACTION SURFACE ANALYSIS FOR HIGH SPATIAL RESOLUTION TARGETED PROTEOMIC STUDIES

Overview.....	81
Introduction.....	82
Results.....	86
<i>microLESA: Achievable Spatial Resolution</i> .....	87
<i>Micro-Digestion Trypsin Concentration and Digest Sensitivity</i> .....	88
<i>Micro-Digestion Incubation Time and Tissue Thickness</i> .....	90
<i>Elucidating the Proteomic Drivers of Host-Pathogen Interactions</i> .....	92
Discussion .....	96
Methods.....	97
<i>Micro-Digestions and Autofluorescence Microscopy</i> .....	97
<i>Micro-Digestions: Spotting Specific ROI's with Trypsin</i> .....	98
<i>Liquid Extraction Surface Analysis (LESA)</i> .....	99
<i>Animals and Bacterial Strains</i> .....	99
<i>MALDI IMS of Proteins</i> .....	100
<i>Bottom-Up LC-MS/MS and Data Analysis</i> .....	102
Acknowledgements.....	103

## V. CONSPECTUS

Overview.....	105
Protein Transmission in MALDI MS/IMS .....	106
Protein Identification using LESA.....	107
microLESA and the Host/Pathogen Interface.....	109
Outlook and Continued Development of Targeted Proteomic Technologies .....	110
Conclusions.....	112

REFERENCES .....	113
------------------	-----

CURRICULUM VITAE.....	127
-----------------------	-----

## LIST OF FIGURES

Figure	Page
1.1 Schematic of matrix-assisted laser desorption/ionization.....	4
1.2 Protein MALDI IMS workflow .....	7
1.3 MALDI profiling of tissue .....	8
1.4 Schematic of MALDI TOF mass spectrometry .....	10
1.5 Excitation and measurement of ions in FT-ICR MS .....	12
1.6 Schematic of mass analysis using an FT-ICR MS.....	13
1.7 Cartoon of CID and ETD.....	15
1.8 Visual depiction of the common approaches to protein identification from tissue .....	17
1.9 LESA Overview.....	22
2.1 Overview of source modifications on a 9.4T FT-ICR MS .....	30
2.2 Vertical position of ESI capillary in relation to ion funnel.....	31
2.3 Protein abundance as a function of source pressure with minimized ESI overlap .....	33
2.4 Protein mass spectra at normal and reduced pressures with minimized ESI overlap.....	34
2.5 Protein mass spectra at normal and reduced pressures with maximized ESI overlap .....	35



2.6 Protein abundance as a function of source pressure with minimized ESI overlap, ESI flow closed off, and varying pressure by adjusting rough pump conductance .....	37
2.7 Protein abundance as a function of source pressure with maximized ESI overlap, ESI flow closed off, and varying pressure by adjusting rough pump conductance .....	38
2.8 Average mass spectra from rat brain at normal and reduced pressures .....	40
2.9 Selected mass ranges from protein MALDI IMS of rat brain at reduced and normal source pressures.....	41
2.10 Selected ion images of intact proteins from protein IMS of rat brain at reduced and normal source pressures .....	43
2.11 Selected ion images of intact proteins from protein IMS of rat kidney at reduced source pressures.....	44
2.12 Data-driven, multi-modal fusion of FT-ICR MS data and H&E microscopy of rat brain data to predict protein distributions at 10 $\mu\text{m}$ .....	46
3.1 Droplet resolution of a liquid extraction surface analysis at increasing droplet volumes .....	57
3.2 Unique protein identifications using LESA as a function of extraction droplet volume.....	60
3.3 Sequential LESA extractions and unique peptide and protein identifications.....	62
3.4 Protein MALDI IMS of a full-body section of mouse pup.....	63
3.5 Venn diagram of protein identifications from the 3 regions of mouse pup interrogated using LESA.....	64

3.6 Protein identifications from a MALDI IMS identified through accurate mass matching of a top-down MS/MS data set .....	72
3.7 TIC of proteins detected from online LESA LC-MS from mouse pup .....	73
4.1 Overview of microLESA workflow.....	88
4.2 Achievable resolution of micro-digestion.....	90
4.3 Optimization of trypsin concentration for microLESA .....	91
4.4 Protein identifications and increasing micro-digest spots per LESA extract .....	92
4.5 Protein identifications using microLESA as a function of tissue thickness .....	94
4.6 microLESA enables the identification of proteins for a MALDI IMS acquisition .....	98

LIST OF TABLES

Table	Page
3.1 Droplet resolution of LESA measured from water-sensitive paper .....	58
3.2 Protein identifications using LESApplusLC from mouse pup .....	65
4.1 Protein identifications using microLESA targeting the abscess in a <i>S. aureus</i> infected mouse kidney.....	97

## LIST OF ABBREVIATIONS

2D: 2 dimensional

3-SBASE: 3-sulfobenzoic acid succinimidyl ester

ACN: Acetonitrile

AGC: Automatic gain control

CID: Collision induced dissociation

CP: Calprotectin

d: Distance

DAN: 1,5-diaminonaphthalene

DESI: Desorption electrospray ionization

DHA: 2,5-dihydroxyacetophenone

DPI: days post infection

EIC: Extracted ion chromatogram

ESI: Electrospray ionization

ETD: Electron transfer dissociation

FA: Formic acid

FDR: False discovery rate

Fe: Iron

FT-ICR: Fourier transform ion cyclotron resonance

H&E: Hematoxylin and eosin

HPLC: High performance liquid chromatography

Hz: Hertz

IMS: Imaging mass spectrometry

IR: Infrared

ITO: Indium-tin-oxide

KE: kinetic Energy

LC: Liquid chromatography

LCM: Laser capture microdissection

LESA: Liquid extraction surface analysis

LIFT: Laser induced forward transfer

LMCO: Low mass cutoff

*m/z*: mass-to-charge

MALDI: Matrix-assisted laser desorption ionization

MS/MS: Tandem mass spectrometry

MS: Mass spectrometry

Nd:YAG: Neodymium-doped yttrium

Nd:YLF: Neodymium-doped yttrium lithium fluoride

Nm: Nanometer

PAM: Parafilm-assisted microdissection

PG: Pirani Gauge

PTM: Post-translational modification

q: Charge

Q-TOF: Quadrupole time-of-flight

RF: Radio frequency

RNA: Ribonucleic acid

RP: Rough pump

RSD: Relative standard deviation

S/N: Signal-to-noise

SA: Sinapinic acid

SIMS: Secondary ion mass spectrometry

T: Tesla

t: Time

TFA: Trifluoroacetic acid

TIC: Total ion chromatogram

TOF: Time-of-flight

UV: Ultraviolet

V: Voltage

$V_{pp}$ : Peak to peak voltage

z: charge

$\lambda$ : Wavelength

$\mu\text{m}$ : micrometer

## CHAPTER I

### MATRIX-ASSISTED LASER DESORPTION/IONIZATION IMAGING MASS SPECTROMETRY AND PROTEIN IDENTIFICATION

This chapter was adapted from the previous published Ryan et al., *Current Opinion in Chemical Biology*, Copyright 2018 by Elsevier

#### Overview

With the completion of the Human Genome Project, and the identification of some 30,000 genes, understanding normal biological processes and disease pathogenesis has transitioned from studying changes in the genome to focus more on understanding the downstream effects by studying their protein products.<sup>1</sup> Proteomic studies often aim to identify proteins and their various proteoforms that are directly involved or implicated in a disease, and identifying possible candidates for therapeutics.<sup>2</sup> As the human proteome is quite complex, with upwards of an estimated 1,000,000 possible proteoforms in a given cell, this feat is not easily achieved.<sup>3</sup> The field of proteomics has given rise to a number of new analytical technologies and advances that focus on collecting and deciphering as much proteomic information as possible from a single experiment. For example, bottom-up and top-down proteomics have revolutionized the way in which a protein is identified using mass spectrometry. Further, the coupling of mass spectrometry to multidimensional chromatography has enabled excellent proteomic coverage of a sample. Alongside MS approaches, nuclear magnetic resonance (NMR) has been applied extensively in structural proteomic studies. These developing techniques and technologies provide many means



to gather more reliable information than previously possible. However, the majority of these approaches sacrifice the spatial integrity of the sample and often focus on the analysis of proteins from cultured cells or tissue homogenates.

The ability to identify proteins and map their spatial distributions in a tissue sample is a powerful way to track possible changes associated with a specific disease, and is a major goal of those using matrix-assisted laser desorption/ionization (MALDI) imaging mass spectrometry (IMS). The analysis of proteins from a tissue sample using MALDI mass spectrometry give rise to a number of challenges ranging from analyte ionization and transmission, to identification. The work presented below looks to address and solve challenges associated with protein identification from tissue by implementing new instrumental modifications and developing new protein ID workflows.

## **Introduction**

### **Matrix-Assisted Laser Desorption/Ionization Mass Spectrometry**

Mass spectrometry (MS) is an analytical technology that allows for the direct measurement of the mass-to-charge ( $m/z$ ) of an ion of a chemical species. To transmit and detect molecules in a mass spectrometer they must first undergo an ionization event that imparts a positive or negative charge on the molecules of interest. A number of ionization techniques have been developed over the past decades that have enabled the study of molecular classes ranging from small molecules/metabolites to larger, intact proteins.<sup>4</sup> Originally developed in the late 1980s separately by Tanaka and Hillenkamp,<sup>5, 6</sup> matrix-assisted laser desorption/ionization (MALDI) is a soft ionization technique that allows for the direct measurement of analytes from surfaces, and has been

applied to study most biomolecular classes.<sup>4, 7-9</sup> In MALDI MS the analyte is first co-crystallized with a small molecule matrix, depicted in Figure 1.1. Once crystallized, a UV laser irradiates the matrix/analyte mixture. The matrix functions to absorb the UV radiation and desorb/ionize the analyte molecules. A number of particles are generated during the MALDI event, including neutrals, matrix ions, free electrons, free analyte ions, and matrix-bound analyte clusters. During the ionization event, the matrix molecule will donate, or abstract, a proton to the analyte molecule, creating an ion and thus measurable by a mass spectrometer. Historically, MALDI was accomplished using nitrogen lasers ( $\lambda$ : 337 nm). With the advancement of laser technology, the field has transitioned to primarily using solid state lasers. The most commonly employed lasers are frequency triple neodymium-doped yttrium (Nd:YAG,  $\lambda$ : 335 nm) and frequency tripled neodymium-doped yttrium lithium fluoride (Nd:YLF,  $\lambda$ : 349 nm). These lasers have much higher repetition rates and much longer lifespans than the previously used nitrogen lasers, and many matrices used for MALDI absorb efficiently at these wavelengths. For example, sinapinic acid (SA, 3,5-dimethoxy-4-hydroxycinnamic acid) is a suitable MALDI MS matrix that is used widely to analyze proteins and has an  $\lambda_{\text{max}}$  at approximately 337 nm.<sup>10</sup> Ions generated during the MALDI event are typically in low charge states ( $< 3$ ) and undergo little fragmentation and thus the resulting mass spectra are simple to interpret.

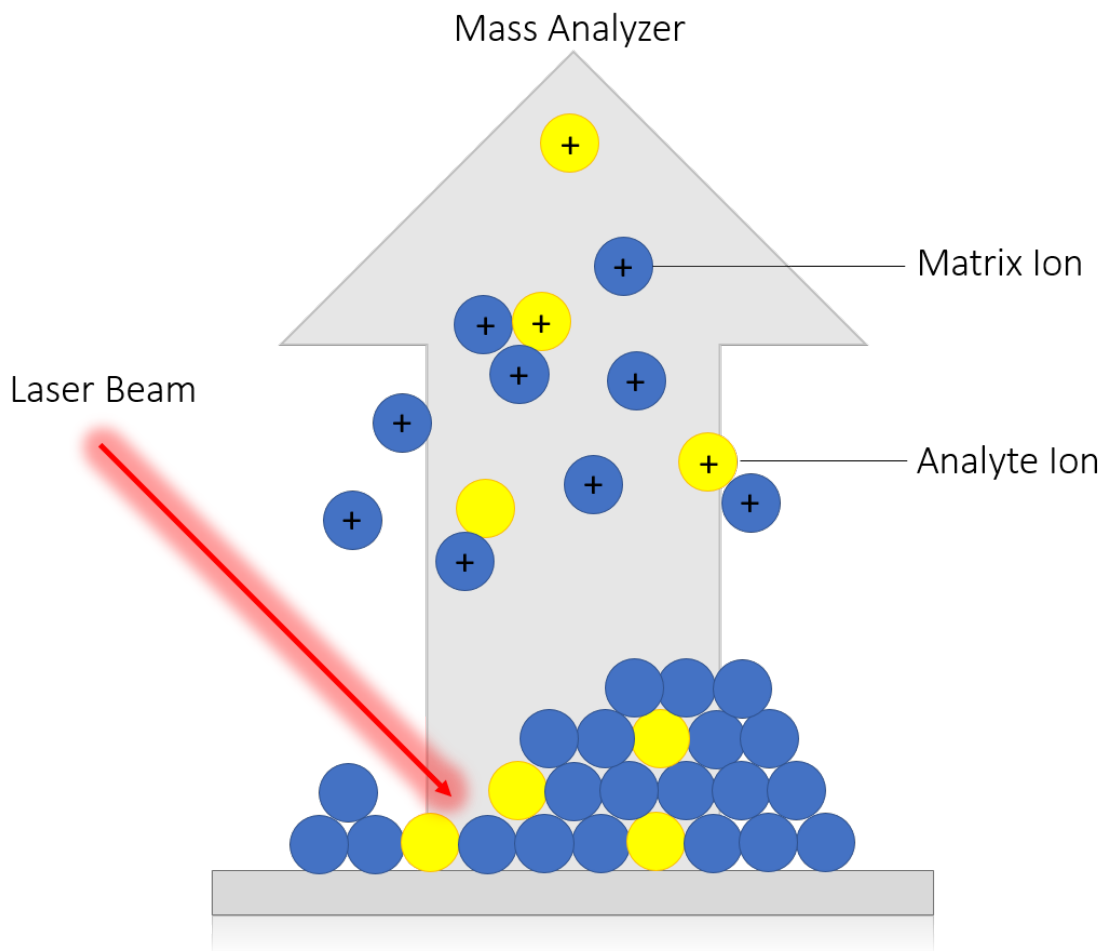


**Figure 1.1:** Schematic depicting matrix-assisted laser desorption/ionization. A UV laser, depicted as a red arrow, is used to irradiate a co-crystallized mixture of analyte and matrix molecules which are represented as yellow and blue circles, respectively. The matrix molecules absorb the irradiated light and ions and neutrals are vaporized from the surface. Analytes are ionized via gas-phase protonation from the matrix molecules and are then transmitted and measured using mass spectrometry.

### MALDI Imaging Mass Spectrometry and MALDI Profiling of Proteins from Tissue

MALDI imaging mass spectrometry (MALDI IMS) was introduced by Caprioli *et al.* in the late 1990s and has seen tremendous growth in utility and application, being employed to analyze biological substrates ranging from non-mammalian plants and insects to mammalian tissue specimens where it has had the broadest application.<sup>11-14</sup> MALDI IMS is a unique molecular

imaging modality in that it allows for the label-free, multiplex analysis of thousands of analytes across a samples surface, yielding 2-dimensional molecular maps of the localization of both an analyte and its relative abundance at a given position. The technology has been used to study a wide range of analyte classes from tissue, including metabolites, lipids, peptides, glycans, and proteins.<sup>15-18</sup> Protein analysis has garnered a lot of attention in the imaging community due to the fundamental biological role the proteome plays in the understanding of biology and disease progression.<sup>2</sup> The typical MALDI IMS workflow for protein analysis from tissue is illustrated in Figure 1.2. First, the tissue is sectioned thinly, most commonly 10-20  $\mu\text{m}$ , and thaw-mounted onto a conductive slide. Once mounted, a series of organic solvent washes is completed to remove excess salts and lipids. The slide and section are then homogenously coated with a MALDI matrix. As discussed earlier, MALDI matrices are generally small aromatic compounds that have an absorbance at the emitting MALDI laser wavelength, and often contain either a basic or acidic site.<sup>19</sup> Matrix is most commonly applied via a robotic pneumatic sprayer system, or by sublimation onto the tissue surface. Once coated, the sprayed slide can be recrystallized to better extract proteins into the matrix layer.<sup>20</sup> The sample is then loaded into the instrument and a raster of the laser is performed across the tissue surface, moving a defined lateral distance, and generating a mass spectrum at each location. Ion intensities for a selected mass range are then plotted in a coordinate system that matches the image acquisition, creating an ion image. A number of reviews highlight the merits, outlooks, and applications of MALDI imaging mass spectrometry.<sup>21, 22</sup>

Aside from MALDI IMS acquisitions from entire sections of tissue, MALDI profiling experiments can also be completed in order to generate proteomic profiles from discrete regions of tissue. This type of workflow is often utilized when looking to compare various regions of tissue, or to categorize certain disease types according to their unique MALDI profiles.<sup>23</sup> Here, the

tissue preparation is completed as discussed earlier, but instead of a laser raster across the entire section, individual mass spectra are collected at distinct locations (Figure 1.3).<sup>24</sup> This type of approach allows for a histology-directed profiling of tissue features and has been applied to study molecular classes ranging from small molecules metabolites and lipids, but is most commonly applied to study proteins as it allows for the direct  $m/z$  measurement of a protein and its various proteoforms from tissue.<sup>23, 25, 26</sup>

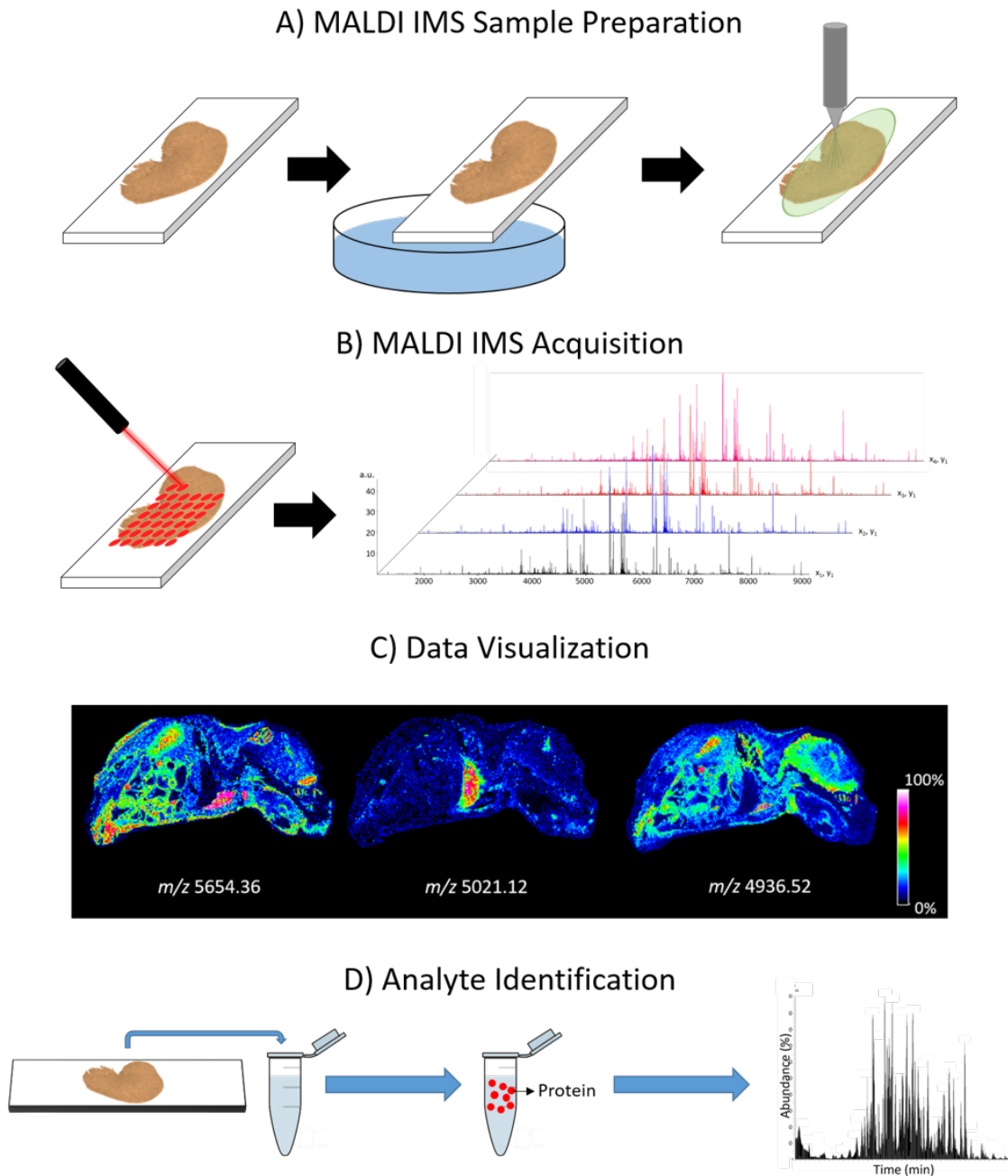


**Figure 1.2:** Overview of a protein MALDI IMS acquisition from a section of mouse pup. A) Tissue is sectioned and mounted onto a conductive slide. Lipids and interfering salts are washed away and matrix is applied homogenously to the surface. B) Mass spectra are acquired at each x and y-coordinate. C) Ion images are generated by plotting the intensity of individual protein ions across the tissue section. D) Following, or in parallel to IMS experiments, orthogonal experiments are completed in order to generate protein identifications that can be correlated to the imaging data. Figure is adapted from citation.<sup>27</sup>

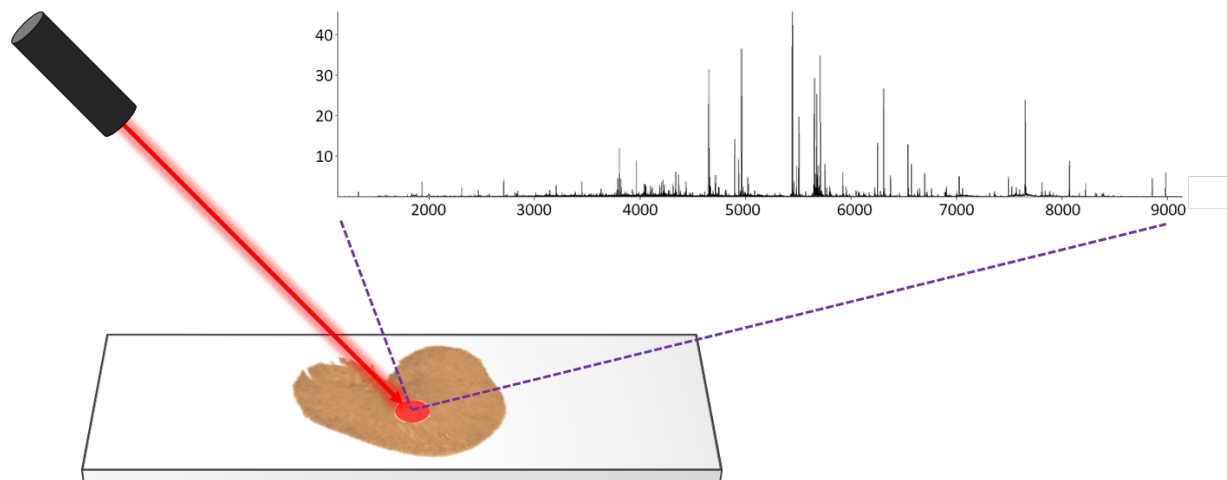


**Figure 1.3:** Visual depiction of a MALDI profiling experiment where a mass spectrum is generated from a specific region of interest (ROI) on the tissue.

### Time of Flight Mass Spectrometry

Historically, protein IMS has been carried out on time-of-flight (TOF) instruments due to their sensitivity, increased mass range (routinely up to 30,000  $m/z$  for MALDI IMS), relatively low cost, and high acquisition speed.<sup>28</sup> TOF mass spectrometers have been coupled to a number of ionization sources, such as DESI and SIMS, but MALDI is still the most commonly used ion source for tissue analysis.<sup>29, 30</sup> Mass analysis on a TOF is completed by first accelerating ions to equal kinetic energies, and focusing their trajectories through a field-free flight tube. This initial kinetic energy is defined in Equation 1.1 and is the product of the charge of the ion ( $z$ ) and the accelerating voltage ( $V$ )

$$\text{Eq. 1.1} \quad \mathbf{KE = zV}$$

Substitution of KE with the traditional equation for kinetic energy is presented in Equation 1.2, where ( $m$ ) is the mass of the ion and ( $v$ ) is the velocity

$$\text{Eq. 1.2} \quad \text{KE} = zV = \frac{mv^2}{2}$$

While traversing a known distance (i.e. the distance of the flight tube), ions will separate based on  $m/z$ , with the heavier ions requiring more time to travel the distance of the flight tube (Figure 1.4). The time necessary to traverse this distance is measured and the  $m/z$  of the ion is calculated through instrument calibration. Substituting velocity for distance ( $d$ ) and time ( $t$ ) allows the rearrangement of the equation to measure the time-of-flight and discern the  $m/z$  of the ions (detailed below in Equation 1.3).

$$\text{Eq. 1.3} \quad t = d \sqrt{\frac{m}{2zV}}$$

Advancements in TOF technology, such as delayed extraction<sup>31</sup> and reflectron time-of-flight MS<sup>32</sup>, has led to the increased use of TOF MS in a number of areas of mass spectrometry, and has allowed for its use in MALDI IMS to effectively analyze most biomolecular classes.<sup>33-35</sup> The advent of hybrid instruments, such as the quadrupole time-of-flight (Q-TOF) mass spectrometer has allowed for an increase in resolving power, and the ability to filter ions based on  $m/z$ , without sacrificing speed and sensitivity, and has been utilized for MALDI imaging of proteins.<sup>36, 37</sup> Ion mobility coupled with TOF mass spectrometry is also being leveraged in protein imaging studies, as a new means of completing gas-phase separations prior to mass analysis.<sup>38</sup> Although TOF mass spectrometers are robust, relatively affordable, and are a common choice for IMS acquisitions, they suffer from limited mass accuracy and mass resolving power, particularly when operated in linear mode for the analysis of higher  $m/z$  species (i.e. > 3000 Da). These two drawbacks are problematic for identifying proteins: there is diminished accurate mass and poor



mass resolution to determine other qualities like protein charge state or modification. As a result of this, other higher resolving power platforms have started to be used in use in MALDI IMS.

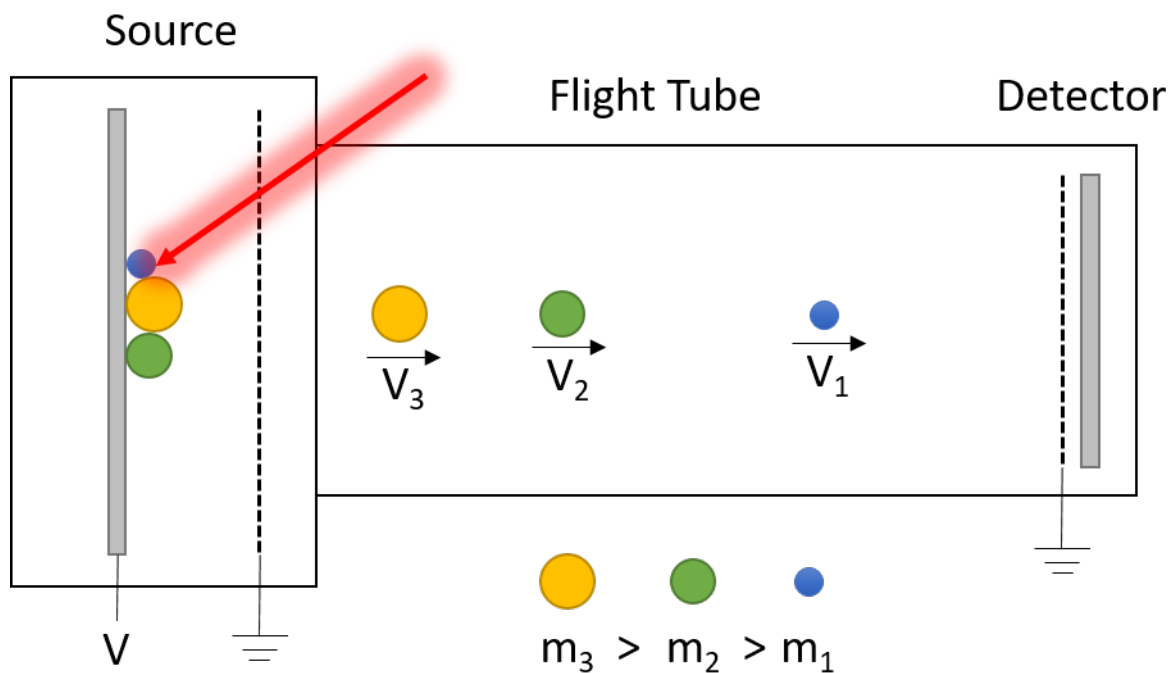


**Figure 1.4:** A schematic depicting a MALDI linear time-of-flight mass spectrometer. Three ions of varying mass, represented by the colored circles, are accelerated to same initial kinetic energy after being ionized by a laser. Ions are then accelerated down a field-free drift tube where they separate by  $m/z$ .

### Fourier Transform Ion Cyclotron Resonance Mass Spectrometry

Fourier transform ion cyclotron resonance (FT-ICR) mass spectrometers have played a critical role in the analysis of complex mixtures, such as the environment encountered in tissue. FT-ICRs have unsurpassed resolving power and mass accuracy, allowing for the separation of isotopes present in high  $m/z$  species like intact proteins. An in-depth review of FT-ICR theory is outside the goals of this dissertation and can be found elsewhere,<sup>39</sup> however, a concise explanation

on how they function in MALDI analysis is worthwhile. Briefly, ions are generated using the MALDI process and transmitted via ion optics to an ICR cell located within a super conducting magnet (normally 7-15T in strength). In the presence of a homogenous magnetic field, the ion population will begin to undergo a rotational motion due to a Lorentz force (Equation 1.4) acting upon them, and the ions will begin to bend in a circular path. In Eq. 1, (m) is the mass of the ion, (q) is the charge, and (v) is the velocity of the ion, (B) is the magnetic field strength, and (t) is time

$$\text{Eq. 1.4} \quad \text{Force} = m \cdot \text{acceleration} = m \frac{dv}{dt} = qv \times B$$

Should the ions remain at a constant speed and undergo no collisions, their path will bend into a circle with a radius (r) determined by the strength of the magnetic field. The frequency of this rotation (i.e. their cyclotron frequency) is m/z dependent, with heavier ions of the same charge rotating at lower frequencies. Equation 1.5 denotes the “unperturbed” cyclotron frequency, where ( $\nu_c$ ) represents the cyclotron frequency, ( $\omega_c$ ) is angular velocity, (m/z) is the mass-to-charge ratio of the ion, and (B) is the field strength

$$\text{Eq. 1.5} \quad \nu_c = \frac{\omega_c}{2\pi} = \frac{1.535611 \times 10^7 \text{ B}}{m/z}$$

The ions are confined radially to the ICR cell by the magnetic field, and axially by trapping electrodes. As the ions are confined to the center of the cell, and spinning in a rotational motion, resonant excitation is used to excite all ions to a larger diameter, inducing coherency among the ion populations and pushing them close to electrodes where an image current is induced (Figure 1.5). The frequency of all ions is measured simultaneously for a defined period of time (usually < 2 seconds) captured in a time-domain signal, and a Fourier transform is used to generate a

frequency spectrum. The measured frequencies are then converted to a mass spectrum (Figure 1.6) through calibration. Recently, FT-ICRs have begun to play a significant role in protein imaging and have been applied to study various biological applications.<sup>40</sup> However, the increased power of these platforms does come with drawbacks for MALDI IMS; namely, FT-ICRs require longer scan times for analysis. For comparison, high-speed TOF platforms can image upwards of 50 pixels a second, while an FT-ICR may only be capable of 0.1-3 pixels per second, creating long acquisition times, especially for higher spatial resolution or high mass resolving power imaging acquisitions. Due to these time constraints, some research labs have begun to leverage the high power afforded by an FT-ICR to help aid in protein identifications in tandem with the faster performing TOF platforms.<sup>41</sup>

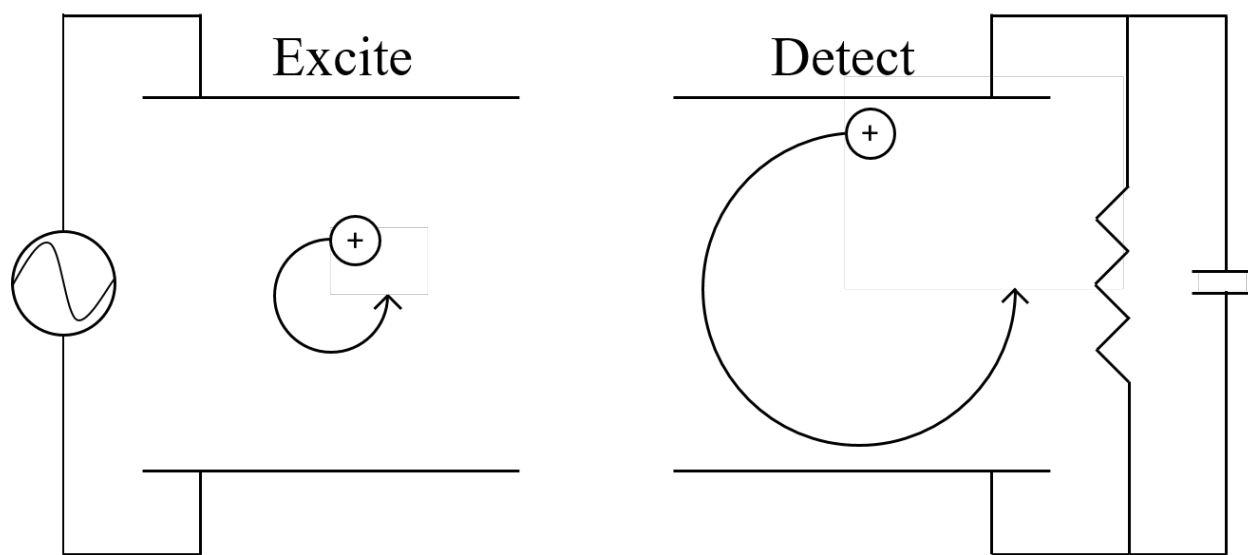


**Figure 1.5:** Spatial coherency is generated by applying an excitation waveform onto the electrodes of the ICR cell. Ions initially spinning in incoherent ICR motion become coherent, and expand to move closer to a pair of detection electrodes. An image current is induced upon these electrodes and ICR frequencies are measured. Adapted from citation.<sup>39</sup>

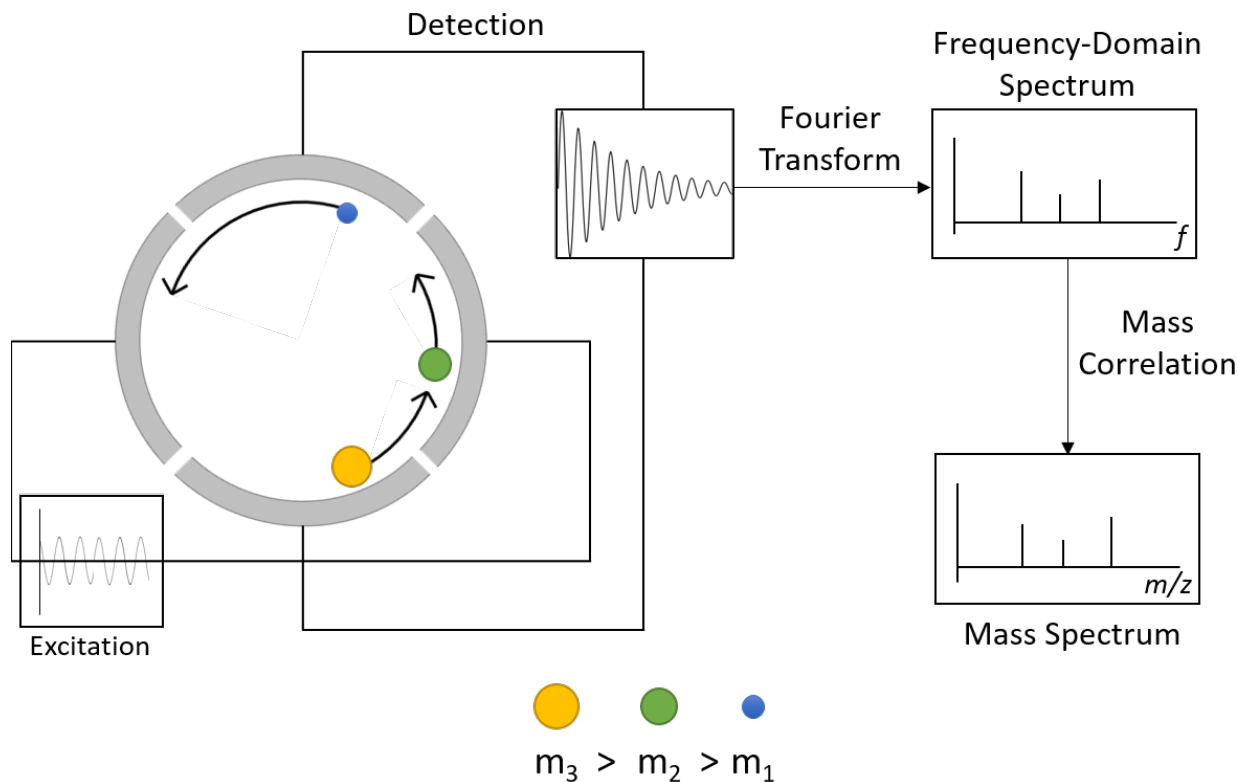


**Figure 1.6:** A schematic representing mass analysis using a Fourier transform ion cyclotron resonance mass spectrometer. Ions are generated, represented with colored circles, and transmitted to an ICR cell and begin to undergo a cyclotron motion in the presence of a large, homogenous magnetic field. Ions are excited to a larger radius by applying an excitation waveform. As the excited packets of ions move closer to detection electrodes, and image current is induced upon the electrodes and the frequencies of the ions are measured and captured in a time-domain signal. This signal undergoes a Fourier transform to a frequency-domain spectrum which is then translated into a mass spectrum.

### Protein Identification in MALDI IMS

Protein identification in MALDI MS is crucial in helping to understand the physiological role of biomolecular and cellular systems. However, identifying proteins observed in many MALDI imaging and profiling experiments can be challenging because MALDI generated ions typically have low charge states ( $< 3$ ), greatly reducing the gas-phase fragmentation efficiency and

ultimately resulting in limited sequence coverage.<sup>42, 43</sup> In general, protein identification in mass spectrometry is performed using either bottom-up or top-down sequencing.<sup>44</sup> Bottom-up protein identification methods rely on enzymatic digestion to hydrolyze larger proteins into smaller peptides that are easier to fragment, resulting in higher sequence coverage.<sup>45</sup> In top-down methods, intact proteins are injected into the mass spectrometer and subjected to fragmentation without prior digestion.<sup>46</sup> Aside from better tracking of protein modifications, an advantage of top-down protein sequencing is that it complements imaging experiments by enabling mass measurement of the intact protein that relates more directly to the MALDI IMS generated signals of intact proteins.

For both bottom-up and top-down proteomics experiments, proteins and peptides are commonly fragmented using collision induced dissociation (CID) or electron transfer dissociation (ETD). In CID, ions are accelerated and collide with a neutral gas leading to increased internal energy of the ion. Should the deposited energy exceed the critical energy of a bond, fragmentation will occur.<sup>47</sup> The ‘mobile proton model’ is used to describe the dissociation of proteins and peptides in CID studies.<sup>48</sup> This model postulates that sequence fragments of highly charged proteins result from charge directed fragmentation after the mobilization of a proton to a carbonyl on the peptide backbone. However, MALDI primarily produces low charge state ions with few protons which tend to be sequestered on highly basic amino acid side chains (e.g. lysine and arginine). Thus, MALDI generated protein ions produce fragments with poor sequence coverage. In ETD, ions are bombarded with radical anions in an ion trap resulting in electron transfer and formation of radical cations. Once the radical cation is formed, rapid dissociation along the peptide backbone occurs resulting in informative sequence fragments.<sup>49</sup> ETD requires that multiple protons are present, and the fragmentation efficiency for a given protein or peptide is highly

correlated to an increased charge state. For these reasons, the applicability of ETD to MALDI generated proteins is also limited. Figure 1.7 depicts these two fragmentation techniques.

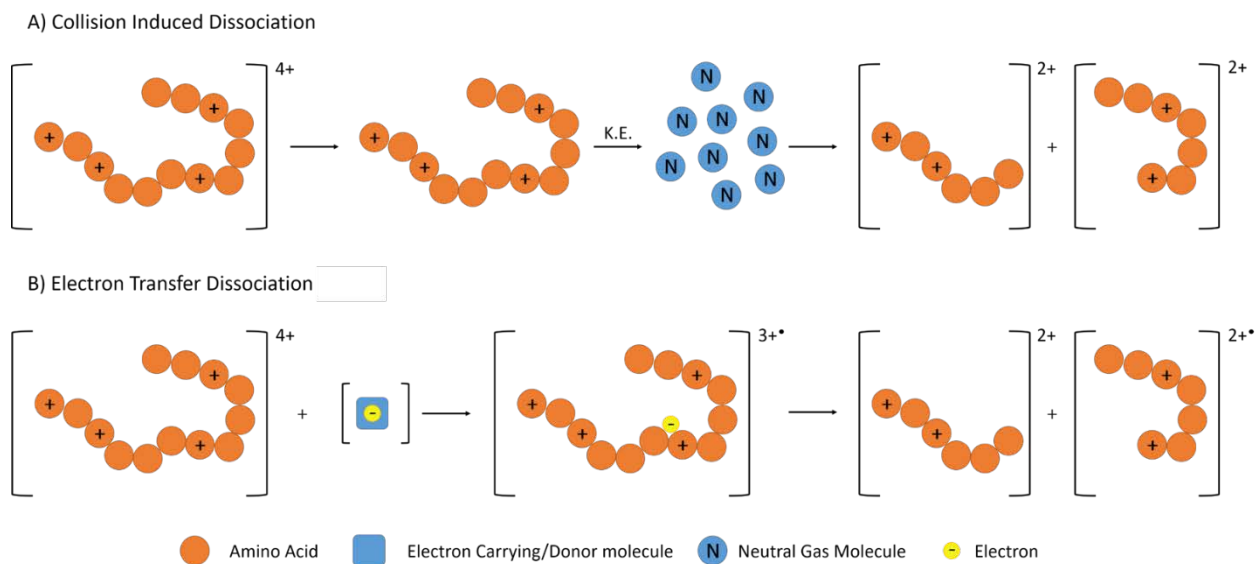


**Figure 1.7:** A cartoon schematic depicting the two common fragmentation techniques used in tandem mass spectrometry. A) CID relies on increasing the kinetic energy of the ion of interest and colliding into a neutral background gas molecule. Upon collision, kinetic energy is converted to internal energy and should the deposition be large enough, the ion will fragment. B) Electron transfer dissociation occurs via radical-induced dissociation after the capture of an electron. In ETD this exchange occurs via a charge-transfer reaction involving a molecule with a low electron affinity.

To overcome the challenges associated with identification of MALDI generated proteins, technologies and methods have been developed to enable separate, complimentary proteomics experiments to be performed as part of IMS workflows. These orthogonal experiments are typically performed on the sample following MALDI image analysis or using a serial tissue section. In general, these experiments involve the extraction of proteins from the tissue with subsequent analysis of the sample by electrospray ionization (ESI). ESI generally produces highly charged ions that are more amenable to CID and ETD fragmentation.<sup>50</sup> By completing these experiments offline, protein identifications can be made using more traditional proteomics

workflows and the resulting identifications can be correlated to the imaging data through accurate mass matching.<sup>16, 51, 52</sup>

### Protein Identification Strategies

Analytical methods for generating protein identifications in MALDI IMS and MALDI profiling workflows must balance trade-offs between the effective spatial resolution and sensitivity with respect to the number of proteins identified. The goal is to provide complimentary data by mapping protein identifications to distinct tissue substructures or cell types in the sample. Each approach has its own unique performance characteristics including spatial resolution, throughput, intact protein/peptide compatibility, and fragmentation method compatibility and is presented in Figure 1.8.

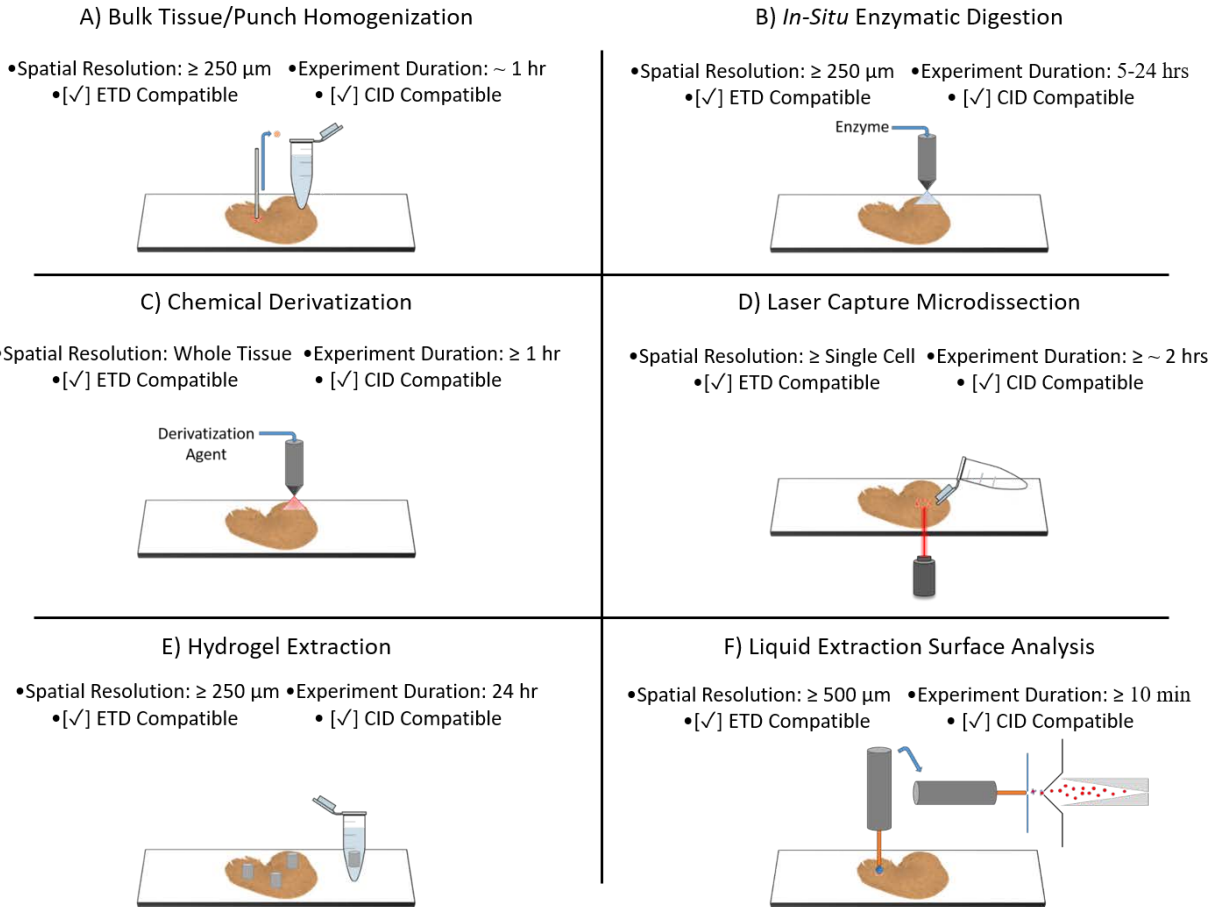


**Figure 1.8:** A schematic representing the 6 common approaches to gathering proteomic data from a tissue sample.

### *Tissue Homogenization*

Many common approaches for extracting and identifying proteins from tissue utilize bulk tissue homogenization.<sup>50, 51</sup> A number of protocols have been developed to enhance the detection of specific types of proteins (e.g. membrane and phosphorylated proteins),<sup>53, 54</sup> as well as quantitative workflows.<sup>55</sup> In general, the sample to be homogenized can be the remainder of tissue, a serial tissue section, or a punch biopsy if attempting to isolate analytes from discrete areas of tissue ( $> 250 \mu\text{m}$ ). The sample is pulverized and undergoes a cell lysis step. Cell lysis is typically performed mechanically,<sup>56</sup> and is followed by various solvent washes to solubilize and extract the



endogenous proteins. Proteins are either analyzed directly (top-down analysis) or undergo enzymatic digestion prior to MS analysis (bottom-up). Purification procedures are typically employed to increase sensitivity (i.e. removing salts, detergents, etc.). In both bottom-up and top-down workflows the complex protein mixture is fractionated by gel electrophoresis or liquid chromatography. There are many examples of researchers employing this strategy in protein IMS workflows. For example, investigators have extracted and combined proteins from serial sections of rat brain tissue that were subsequently analyzed using top-down MS in order to link identifications to a MALDI FT-ICR IMS data set using mass accuracy.<sup>40</sup> Although tissue homogenization is the most utilized strategy for tissue proteomics workflows, spatial fidelity is lost in most cases, limiting its application for the analysis of discrete foci in tissue.

#### *In Situ Enzymatic Digestion*

Ideally, proteins should be identified in an MALDI experiment workflow from their native environment; that is, directly from tissue. This allows both mass accuracy and spatial information to be used to relate imaging data to protein identification experiments. As described above, MALDI generated proteins suffer from inefficient fragmentation in the gas phase. To overcome this challenge, on-tissue enzymatic digestions can be performed to generate peptides from larger proteins that are more amenable to MS/MS experiments directly from tissue. Approaches utilizing in-situ enzymatic digestions are often performed using robotic sprayers to apply a homogenous coating of enzyme across the tissue section or by robotically depositing small (> ~200  $\mu\text{m}$ ), discrete droplets of enzyme on the surface.<sup>57, 58</sup> An incubation step is performed prior to MALDI MS analysis. Trypsin is the most commonly employed enzyme, however, other endoproteinases such as Glu-C and Asp-N have been utilized for IMS studies.<sup>59, 60</sup> Once digested, proteins can be identified by spatially targeting and sequencing peptides using traditional MS/MS approaches

directly from tissue. In an early example where trypsin was applied to lung tumor tissue micro-arrays using an automated spotter, researchers were able to differentiate specific cancer types (e.g. adenocarcinoma from squamous cell carcinoma biopsies) by peptide imaging.<sup>61</sup> In another approach, investigators combined MALDI IMS with ion mobility mass spectrometry and *in-situ* digestions from both fresh frozen and formalin fixed paraffin embedded tissue samples.<sup>62</sup> The use of ion mobility provided separation of isobaric species that would not normally be observed using conventional MALDI IMS, enabling higher peak capacity in the tissue-based bottom-up proteomics analysis. Although effective for identifying proteins, there is currently no software available to allow for automated peptide fragmentation from tissue, limiting throughput and data interpretation.

### *Chemical Derivatization*

Chemical derivatization entails modification of analytes present on the surface of the tissue to enhance analytical characteristics such as sensitivity and fragmentation efficiency.<sup>63</sup> The majority of this work has been applied to the study of small molecule analytes to enhance sensitivity of species with low ionization efficiency. However, there are a number of studies that have used chemical derivatization of proteins to simplify the resulting fragmentation data generated from bottom-up MALDI data sets.<sup>64, 65</sup> Protein IMS workflows have been developed that include N-terminal derivatization strategies that yields only y-type sequence ions during MALDI TOF/TOF experiments.<sup>66</sup> In this work a negative charge was added to the N-terminus of tryptic peptides using 3-sulfobenzoic acid succinimidyl ester (3-SBASE). This sulfonation agent was used to generate complete peptide y-fragment series from MALDI generated ions. Also, a sialic acid derivatization approach was developed for N-Glycan MALDI IMS from formalin fixed, paraffin-embedded tissues. In order to preserve the sialic acid group, which is often lost by in-

source decay during ionization and ion transfer, they utilized a linkage-specific demethylation and amidation for stabilization.<sup>67</sup> Similar to in-situ enzymatic digestion, these methods allow for the identification of proteins directly from tissue, but are throughput-limited and are better suited for targeted studies.

### *Laser Capture Microdissection*

Laser capture microdissection (LCM) facilitates the interrogation of tissue foci and is well suited for cellular analysis, having the capability to sample single cells from heterogeneous environments using microscopy combined with a laser targeting system. In LCM, a laser is used to perforate the tissue and effectively cut out the target region, separating it from adjacent tissue. The separated tissue is then collected using a non-contact approach such as laser induced forward transfer (LIFT). LCM instrumentation commonly rely on ultraviolet (UV) and/or infrared (IR) lasers for tissue perforation and collection. Once collected, the tissue sample can be subjected to homogenization protocols and bottom-up or top-down workflows. In recent studies, high resolving power FT-ICR MS with spatially targeted LCM was used to aid in identifying proteins from an IMS data set.<sup>16</sup> These two platforms were employed to study and identify proteins in a mouse model of glioblastoma and enabled proteins to be identified specifically from tumor and non-tumor regions of tissue. New workflows integrating LCM and MALDI IMS have been reported using a parafilm-assisted microdissection (PAM).<sup>68</sup> This approach enabled rapid and inexpensive LCM-based proteomic analyses in IMS workflows. LCM allows for spatially targeted proteomic information to be gathered for specific cell types in tissue, but can suffer from poor sensitivity due to tissue loss, and requires long collection times.

### *Hydrogel Extraction*

Hydrogels are a superabsorbent polymer that are characterized by the ability to retain a large amount of liquid relative to volume and are inexpensive to fabricate. Hydrogels have found use in a diverse range of applications including microfluidics,<sup>69</sup> wound care and drug delivery,<sup>70, 71</sup> and protein extractions.<sup>72, 73</sup> Briefly, a hydrogel is cast into sheets through polymerization of water soluble monomeric units such as acrylamide. After casting, a punch biopsy is used to retrieve a gel of a specific diameter. The hydrogel can then be dehydrated and subsequently rehydrated with an enzyme solution, most commonly trypsin. The gel is then placed onto the surface of the tissue, leading to spatially targeted protein digestion and peptide extraction into the gel. Peptides are then washed from the gel and analyzed by LC-MS. Hydrogels were initially investigated with applications to IMS as a cost-effective approach to generate spatially targeted protein identifications from tissue.<sup>72</sup> This approach utilized laser printed molds creating an ionotropic hydrogel that were employed to extract and digest proteins from the cerebellum of a rat brain. Hydrogel fabrication was further optimized for tissue analysis using a polyacrylamide hydrogel and were able to fabricate the gels down to a diameter of 260  $\mu\text{m}$  while still identifying hundreds of proteins species from tissue.<sup>74</sup> Although efficient at generating spatially targeted protein identifications, hydrogels are limited in throughput due to the lengthy preparation and incubation time required for peptide extraction, as well as difficulties when attempting to manipulate a small gel on a tissue surface.

#### *Liquid Extraction Surface Analysis*

Liquid micro-extractions, commonly referred to as a liquid extraction surface analysis (LESA), utilize a small volume ( $\sim 0.5\text{-}3\ \mu\text{L}$ ) of extraction solvent that can be placed on the samples surface. Analytes present in the tissue diffuse into the solvent that is subsequently aspirated off the tissue and analyzed by traditional proteomic workflows. A cartoon schematic depicting a protein

LESA from tissue is presented in Figure 1.9. Analyte classes ranging from small molecule metabolites to intact proteins have been studied using LESA technology. One of the more desirable characteristics of the experiment is the low cost associated with an experiment. Schey et al. generated liquid micro-extracts using a hand pipette and a gel loading pipette tip. Using this approach, they detected upwards of 100 intact protein species from thin tissue sections by simply dispensing 1-2  $\mu\text{L}$  of extraction solvent onto a tissue using a gel loading pipette tip, aspirating the solvent, and taking it offline for top-down LC-MS/MS.<sup>75</sup> New research has focused on making the

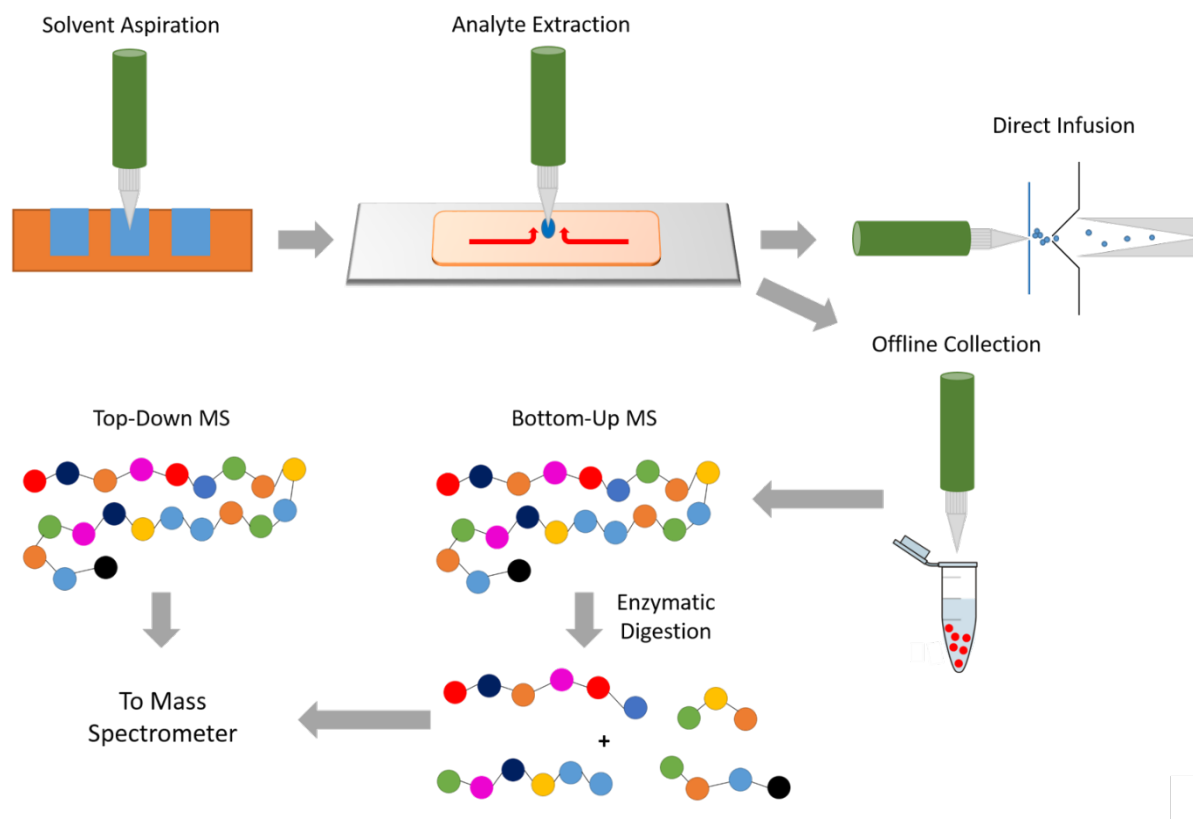


**Figure 1.9:** A schematic representing the LESA experiment extracting proteins from tissue. Extractions solvent is aspirated and dispensed onto a tissue’s surface where proteins diffuse into the solvent. The solvent is aspirated back from the tissue and can be injected directly into the mass spectrometer or taken offline and subjected to traditional bottom-up and top-down mass spectrometry approaches.

experiment more automated incorporating a robotically controlled extraction. Much of this work stems from initial research by Jack Henion and Gary Van Burkel.<sup>76, 77</sup> A challenge to the LESA experiment is the size of the droplet diameter on tissue. Typically, LESA is limited to a spatial resolution of ~500  $\mu\text{m}$  for routine use. Although limited in resolution, LESA provides a high-throughput approach to gather spatially targeted protein identifications from tissue.

### **Research Summary and Objectives**

In order to improve our current approaches to spatially targeted proteomic studies from tissue, both instrumental modifications and new methodologies were implemented. First, modifications were made to a commercial 15T FT-ICR MS to improve protein ion transmission for higher  $m/z$  species. The source region of the instrument was modified to include a second rough pump as well as new isolation valves that allowed the source pressure to be adjusted. Optimizing the pressure allowed for ions up to  $m/z$  24,000 to be transmitted, effectively doubling our analyzable mass range. Protein identification from tissue was improved by the optimization and implementation of a new robotic, liquid extraction surface analysis workflow. Online HPLC and offline proteomic strategies were developed to identify proteins that can be mapped back to the IMS data through accurate mass matching. The LESA resolution was improved by the addition of a spatially targeted, micro-enzymatic digestion, yielding a new workflow termed microLESA. This new approach incorporates both liquid micro-spotting and fluorescent microscopy to identify tissue foci and increase the resolution of analysis for a bottom-up LESA experiment. Following optimization and characterization, the new microLESA workflow was applied to study the host-pathogen interface in a *Staphylococcus aureus* infection in murine kidney. The development of these new technologies are of great importance to the imaging community, allowing for a greater visualization of the proteome, and thus a better understanding of pathology and biology. The

utilization of these new technologies enable a superior approach to proteomic studies than were previously possible.

## CHAPTER II

### IMPROVING PROTEIN ION TRANSMISSION ON A 15T FT-ICR MS FOR MALDI IMS

This chapter was adapted from the previous published Prentice, Ryan et al., *Analytical Chemistry*, Copyright 2018 by ACS<sup>78</sup>

#### Overview

The molecular identification of proteins of interest is an important part of an imaging mass spectrometry (IMS) experiment. The high resolution accurate mass capabilities of FT-ICR MS have been shown to facilitate the identification of proteins in MALDI IMS. However, these experiments are typically limited to proteins giving rise to ions of relatively low  $m/z$  due to difficulties transmitting and measuring large molecular weight ions of low charge states. Modifications to the source region of a commercial MALDI FT-ICR MS to regulate gas flow and pressure enables the transmission and detection of protein species up to  $m/z$  24,000 and the detection of proteins from tissue up to  $m/z$  22,000.

#### Introduction

The ability to efficiently sample ions generated from relatively high pressure ion sources into the instrument vacuum chamber for analysis is a key factor in determining the overall sensitivity of a mass spectrometry experiment. The advent of ambient ionization methods such as



electrospray ionization (ESI) has necessitated the development of improved methods of ion transmission across differentially pumped regions of the mass spectrometer.<sup>76, 79-85</sup> The introduction of the ion funnel, which consists of a stack of closely spaced ring electrodes with successively decreasing inner diameters, has enabled ion transmission efficiencies that approach 100%.<sup>86-88</sup> Ion funnel interfaces are now present on many commercial mass spectrometers and can transmit ions with little  $m/z$  bias.<sup>89-91</sup> While extensive studies have been performed to characterize the fundamental mechanisms of ion transmission and focusing in ion funnels for ESI-generated ions,<sup>92-96</sup> relatively little work has been done to characterize the transmission efficiency of species generated by matrix-assisted laser desorption/ionization (MALDI), which can introduce unique considerations for ions of high  $m/z$  ratios.

The efficiency of ion transport through the funnel is governed by several processes, including the collection of ions emanating from the source and the collisional focusing of these species in the ion funnel. Important to both of these processes are the gas flow dynamics and the operating pressure of the system.<sup>87, 93</sup> Off-axis gas flow can detrimentally effect the collection of ions into the mass spectrometer, and the operating pressure of the ion funnel (along with its physical dimensions and operating RF voltages) determines the effective electric field for ion confinement.<sup>92, 93</sup> At increased operating pressures, the effective potential well for ions is suppressed and a decrease in ion radial confinement is observed.<sup>97</sup> This situation is especially pronounced for ions of high  $m/z$  values (greater than 10,000) that have shallower pseudopotential well depths.<sup>96, 98, 99</sup> Most ESI-based experiments analyze ions in a more modest mass range from  $m/z$  200 to 3,000, such as analyses of singly charged metabolites and lipids and multiply charged peptides and proteins. Especially for high  $m/z$  species generated by ESI (*e.g.*, intact protein complexes), additional processes such as ion desolvation become important to consider when

determining the operating parameters of the source.<sup>92, 100-102</sup> Even these high molecular weight complexes are typically multiply charged and thus of relatively modest  $m/z$  value, perhaps explaining the scarcity of reports detailing the use of ion funnels to study ions in excess of  $m/z \sim 10,000$ .<sup>103-105</sup> In contrast to ESI, MALDI-generated protein ions are typically observed at low charge states (*i.e.*, higher  $m/z$ ) and do not undergo desolvation, although declustering during MALDI plume evolution could be an analogous process in this context.<sup>106-108</sup>

Recently, we have reported the detection of protein ions in an imaging mass spectrometry (IMS) experiment up to  $m/z \sim 12,000$  with good signal-to-noise ratios (S/N), and up to  $m/z$  17,000 with low S/N, using a commercial ion funnel-based MALDI source on a Fourier transform ion cyclotron resonance (FT-ICR) mass spectrometer.<sup>109</sup> While FT-ICR instruments have been widely used to study a variety of low molecular weight MALDI-generated ions,<sup>110-114</sup> intact protein analysis by MALDI has historically been performed on time-of-flight (TOF) mass spectrometers due to the superior sensitivity of these platforms at high  $m/z$  ratios.<sup>115, 116</sup> Most MALDI TOF instruments generally operate at high vacuum, making them incompatible with current ion funnel designs that typically operate at pressures of 0.1-30 Torr ( $\sim 0.1$ -40 mbar). Despite the superior sensitivity of TOF-based platforms, the high mass resolving power and mass accuracy afforded by FT-ICR instruments have recently been demonstrated to facilitate the identification of isotopically-resolved, MALDI-generated intact proteins in a complex mixture of species detected during a tissue imaging experiment.<sup>16, 109, 117</sup> Early work by several groups noted the benefits of FT-ICR to studying high  $m/z$  ions generated using internal MALDI sources (*i.e.*, located in the ultra-high vacuum region of the ICR cell).<sup>118-120</sup> Although relatively little research has focused on high  $m/z$  species generated by external MALDI sources due to inefficient ion transmission, advances in ion optics and the use of stronger magnetic fields are now enabling these types of experiments.

Herein, we have modified the source region of a 15T FT-ICR mass spectrometer in order to maximize the ion funnel transmission efficiency of high  $m/z$  MALDI-generated protein ions. The dual ESI/MALDI ion source on this instrument was modified to allow for control of the existing gas flow and pressure, both of which were identified to be important to ion transmission. Significant improvements in ion transmission efficiency were observed for protein standards up to  $m/z$  ~24,000 and for proteins detected from tissue up to  $m/z$  22,000, roughly doubling the normal mass range and dramatically enhancing the quality of the protein imaging data.

## Results

### *Systematic Study of Source Pressure*

In order to maximize the transmission efficiency of MALDI-generated protein ions, we sought to optimize both the operating pressure of the ion funnel as well as effects of off-axis gas flow from the ESI capillary. In an effort to minimize the effects of the off-axis gas flow, the ESI source was raised to its maximum adjustable position, reducing the overlap with the MALDI ion generation region (Figure 2.2). MALDI mass spectra of a mixture of protein standards were then acquired as a function of source pressure, which was controlled by adjusting the valve attached to the ESI capillary (V3). In this configuration, both the V1 and V2 isolation valves are fully open. In general, the abundance of most protein ions increased as the source pressure was decreased from the normal operating pressure of ~2.9 Torr (~3.9 mbar) to ~800 mTorr (~1.1 mbar) (Figure 2.3).

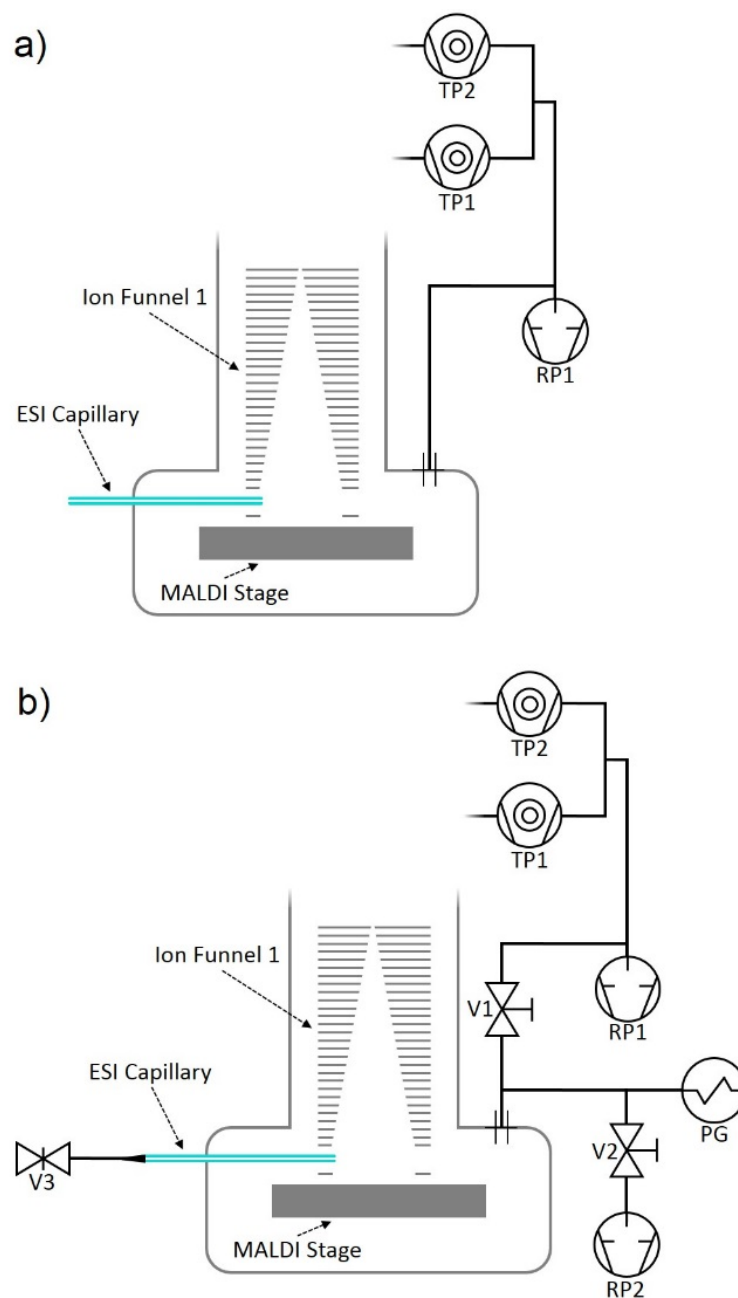


**Figure 2.1:** Schematic of selected components in the instrument source region (not to scale) showing a) the normal gas manifold and b) the gas manifold that has been modified to incorporate isolation valves (V1 and V2), an additional source rough pump (RP2), a Pirani gauge (PG), and a valve to regulate gas flow through the ESI capillary (V3).

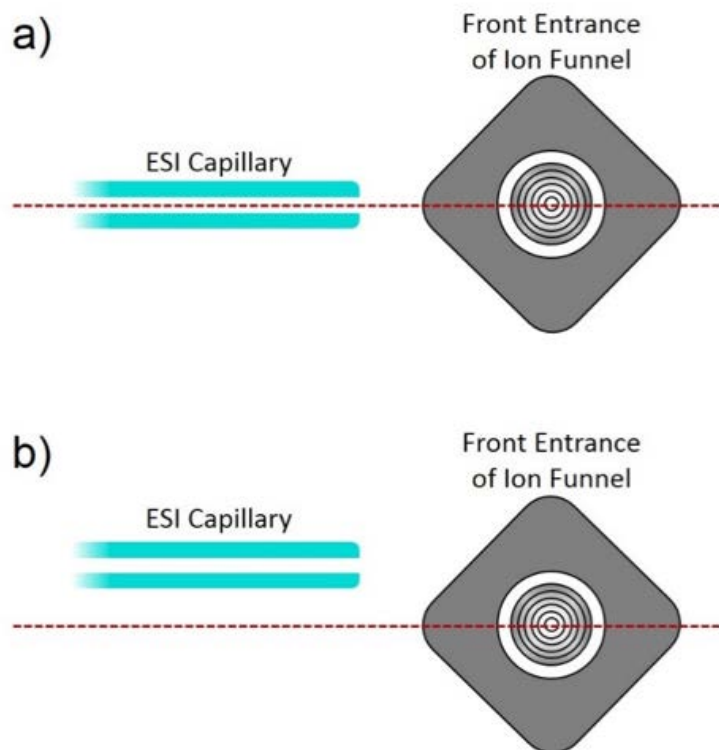


**Figure 2.2:** Vertical position of the ESI source in relation to the ion funnel to a) maximize or b) minimize overlap with the MALDI ion generation region, which occurs roughly in the center of the ion funnel.

This effect is especially pronounced for the high  $m/z$  protein species, namely singly charged ubiquitin (Figure 2.3b), apomyoglobin (Figure 2.3c), and trypsinogen cations (Figure 2.3d). This increase in ion transmission efficiency at lower pressures is consistent with a greater effective potential wall confining the radial motions of the ions within the funnel.<sup>92, 93</sup> Changes in axial gas flow dynamics and the axial DC gradient as they relate to the observed increases in ion transmission efficiency are thought to be minor under these operating conditions.<sup>92, 93, 96, 121</sup> The most efficient ion transmission for the largest  $m/z$  species (singly charged apomyoglobin and singly charged trypsinogen) occurs between 700 and 800 mTorr. The abundance of these ions, as well as  $[\text{trypsinogen} + 2\text{H}]^{2+}$ , is improved by at least an order of magnitude compared to that at the normal

source operating pressure (Figure 2.4). The signal-to-noise (S/N) improvement is especially dramatic for singly charged apomyoglobin and singly charged trypsinogen ions not observed at normal source pressure, but now readily detected.

The signal intensity of the lower  $m/z$  species, namely [ubiquitin + 2H]<sup>2+</sup>, [apomyoglobin + 2H]<sup>2+</sup>, and [trypsinogen + 3H]<sup>3+</sup>, is relatively unchanged as the pressure is decreased from 2.9 to 1.0 Torr. However, the transmission efficiency of the multiply charged ions noticeably decreases as the pressure is reduced further below 1.0 Torr. This difference in transmission between singly and multiply charged species is consistent with the effective potential being higher for multiply charged ions.<sup>92, 97</sup> The effective potential in vacuum at point (r, x) in cylindrical coordinates has been defined as:

$$\text{Eq. 2.1} \quad V^*(r, x) = \frac{q^2 E_{\text{RF}}^2(r, x)}{4m\omega^2} \sim \frac{z^2 V_{\text{RF}}^2}{f^2}$$

where  $q = ze$  is the charge of the ion,  $E_{\text{RF}}(r, x)$  is the local RF amplitude and is proportional to the RF voltage applied to the funnel ( $V_{\text{RF}}$ ),  $m$  is the mass of the ion,  $\omega = 2\pi f$  is the angular frequency, and  $z$  is the charge of the ion.<sup>93, 97</sup> According to Equation 2.1, the effective potential is proportional to the square of the ion charge state, which supports the charge-state dependent curves in Figure 2.3. As the effective potential increases, a low-mass cutoff effect (LMCO), analogous to that observed in RF multipole devices, appears to affect the stability of the lower  $m/z$  protein species. While the formation of multiply charged protein ions by MALDI has been shown by several groups to be more favorable at higher pressures,<sup>107, 122-126</sup> a pressure-dependent shift in the charge state distribution of ions produced during the MALDI process seems unlikely here given that there is no concomitant decrease in abundance of the multiply charged species while the higher  $m/z$  singly charged species increase in abundance as the pressure is decreased from 2.9 to 1.0 Torr.

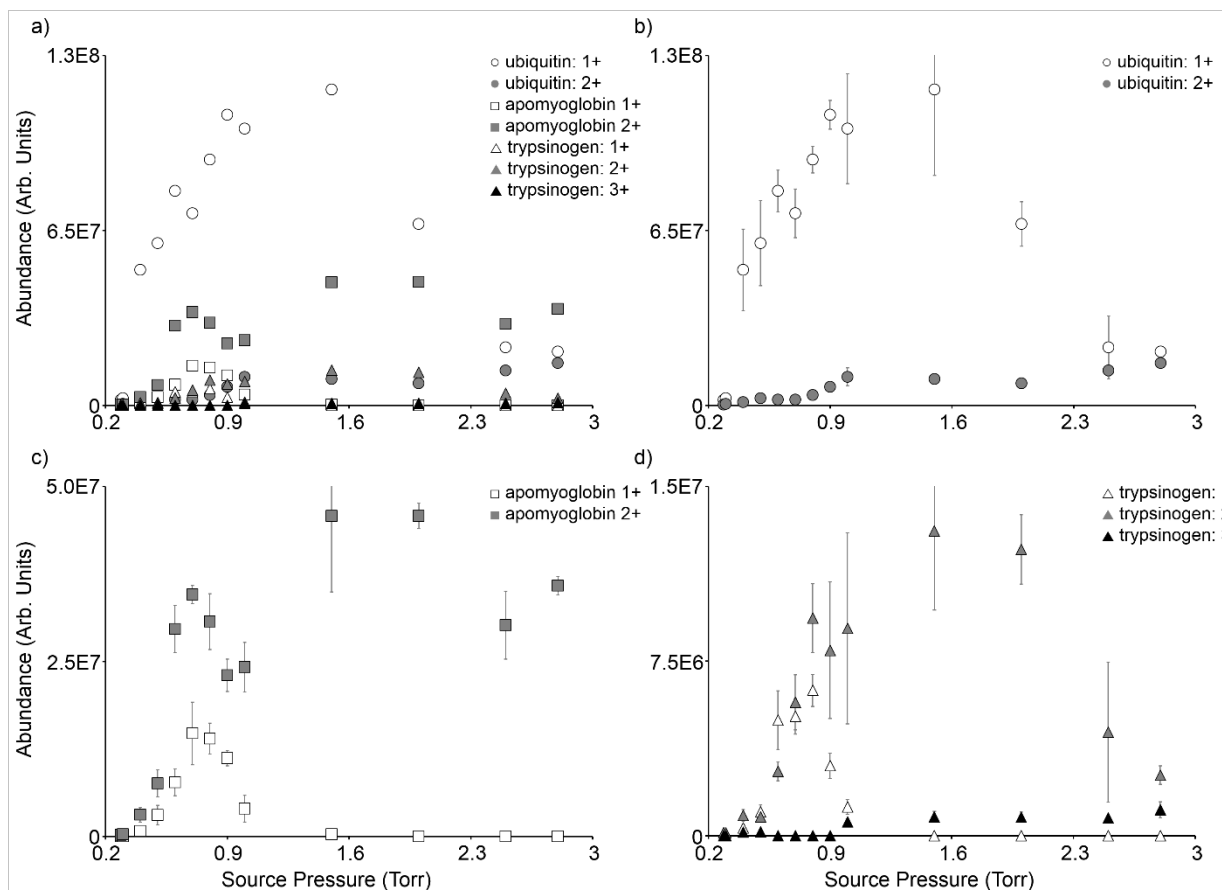


**Figure 2.3:** (a) Protein abundance as a function of source pressure for (b) ubiquitin, (c) apomyoglobin, and (d) trypsinogen. In c-d, the error bars represent the standard deviation of 3 replicates. The source pressure was varied by adjusting gas flow through the ESI capillary (V3) and the ESI source is positioned to minimize the overlap with the MALDI ion generation region.

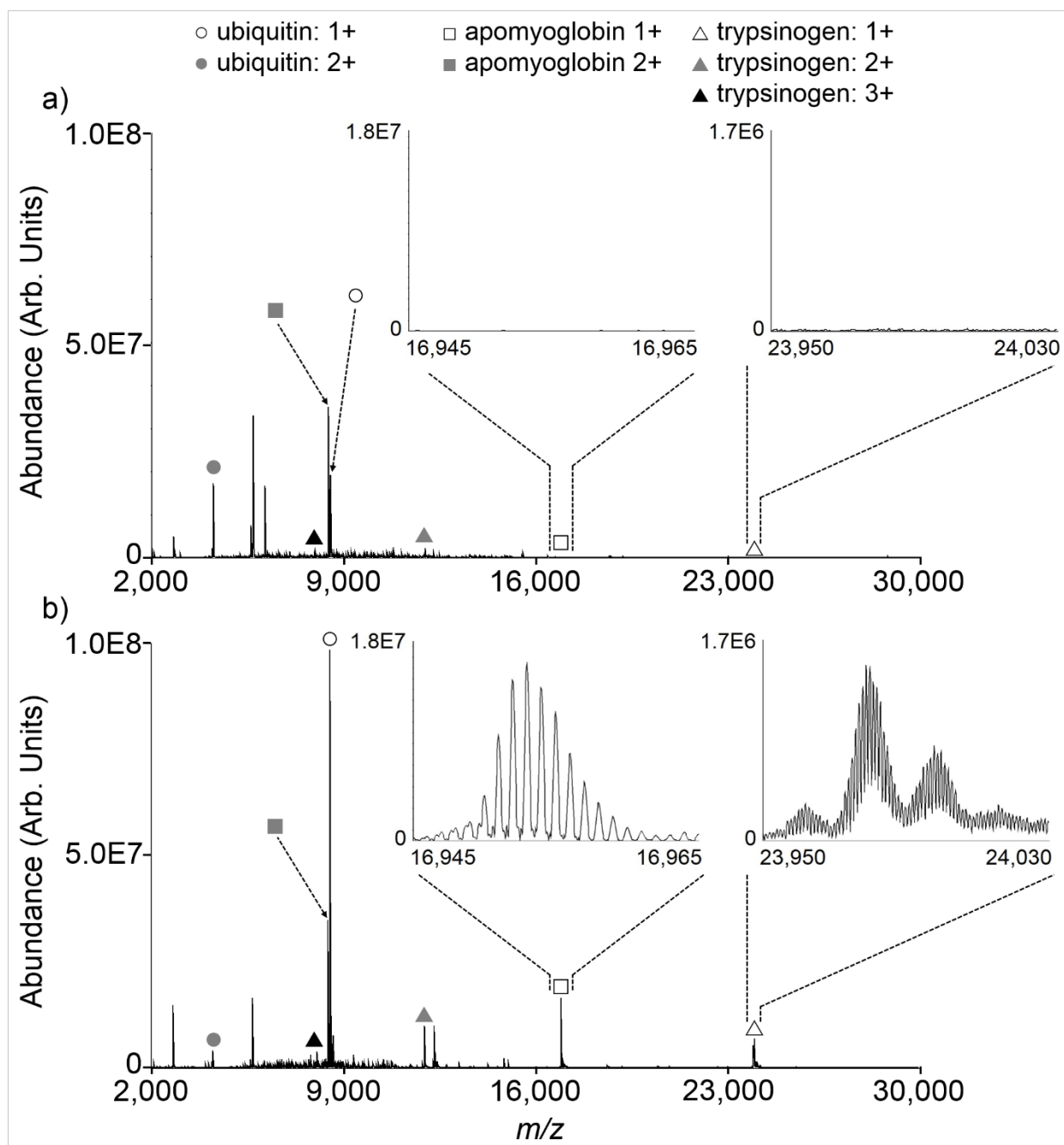


**Figure 2.4:** Representative protein standard mass spectra acquired at source pressures of a) 2.9 Torr and b) 800 mTorr. The source pressure was varied by adjusting gas flow through the ESI capillary (V3) and the ESI source is positioned to minimize the overlap with the MALDI ion generation region.



When the ESI source is lowered to maximize the overlap with the MALDI ion generation region, the abundance of most protein species again increases as the source pressure is decreased from the normal operating pressure (~2.9 Torr) to ~800 mTorr (Figure 2.5). However, the increased overlap of the gas flow through the ESI capillary with the MALDI ion generation region appears to disrupt the efficiency of ion collection by the ion funnel. In general, the abundances of the protein species are ~20-40% lower at each pressure in this experiment compared to the those in Figure 2.3 and a dramatic loss in sensitivity is observed as V3 is opened to pressures above 1.0 Torr.

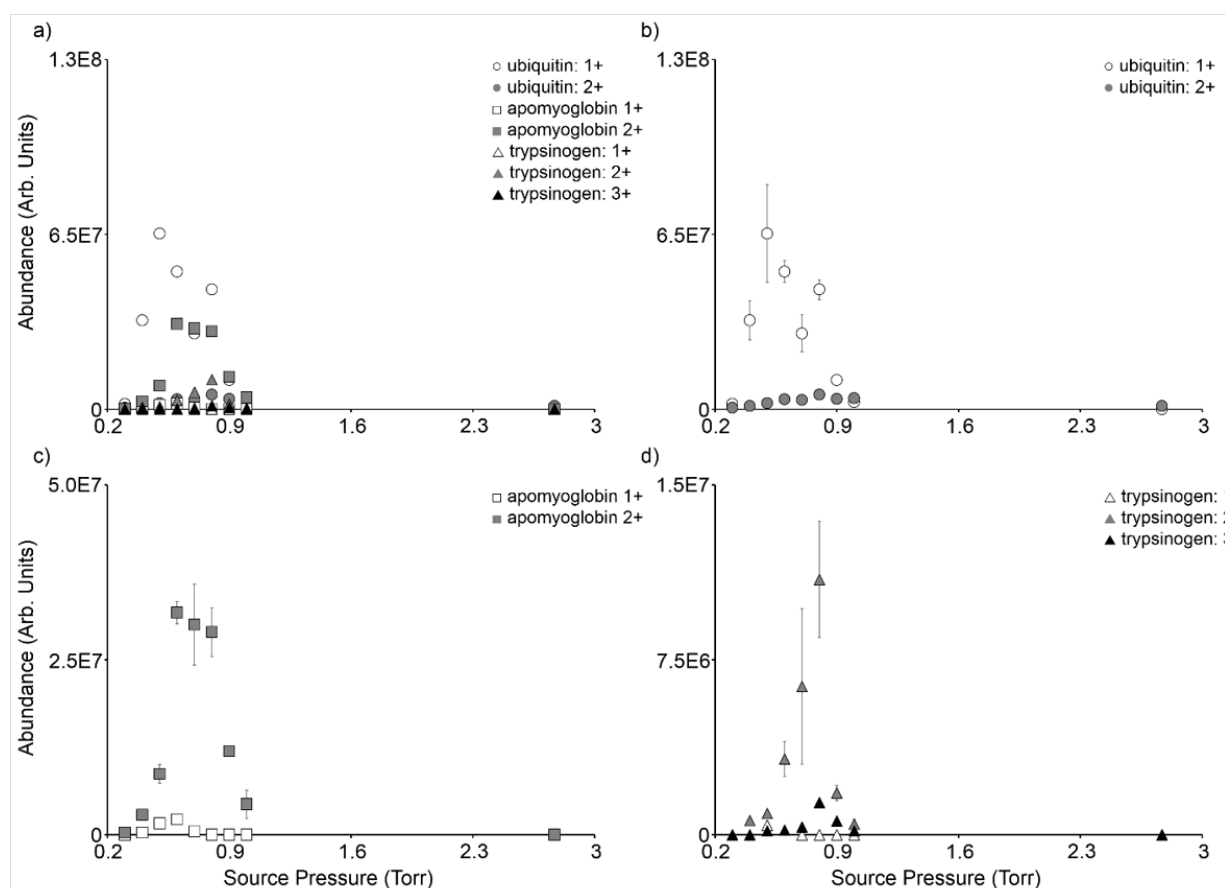


**Figure 2.5:** (a) Protein abundance as a function of source pressure for (b) ubiquitin, (c) apomyoglobin, and (d) trypsinogen. In c-d, the error bars represent the standard deviation of 3 replicates. The source pressure was varied by adjusting gas flow through the ESI capillary (V3) and the ESI source is positioned to maximize the overlap with the MALDI ion generation region (Supplemental Figure 1a).

In order to examine the effect of pressure on transmission efficiency in the absence of off-axis gas flow, V3 was closed and the pressure was systematically increased by varying V1 (V2 is closed). This minimizes the disruption of ion sampling into the funnel by largely eliminating the gas flow through the ESI capillary. Without further modifications to the vacuum system, the highest achievable pressure using this setup is 800 mTorr. For this experiment, the source was again raised to minimize overlap between the ESI capillary and the MALDI ion generation region. As the source pressure is increased from 300 to 800 mTorr, protein signal is improved (Figure 2.6), similar to the experiments in which the pressure was manipulated by adjusting V3. The signal abundances between the two sets of experiments are comparable, confirming that there is not a significant disruption of ion focusing induced by the off-axis gas flow in Figure 2.3. Also evident in Figure 2.6, while adjusting the pressure from the rough pump while the ESI port is closed off, is a difference in transmission between singly and multiply charged species. Although there are no data for source pressures above 800 mTorr, this observation is again consistent with the effective potential being higher for multiply charged ions (Equation 2.1). Finally, there is no significant difference in protein signal abundances due to the ESI source position (*i.e.*, ESI capillary not in line with the MALDI generation region [Figure 2.6] versus ESI capillary in line with the MALDI generation region [Figure 2.7]). This is expected as there is minimal off-axis gas flow emanating from the ESI source when V3 is closed and the source pressure adjusted using V1. Only when the ESI source is positioned in line with the MALDI ion generation region and V3 opened above roughly 1.0 Torr is the off-axis gas flow sufficient to disrupt ion focusing into the funnel.

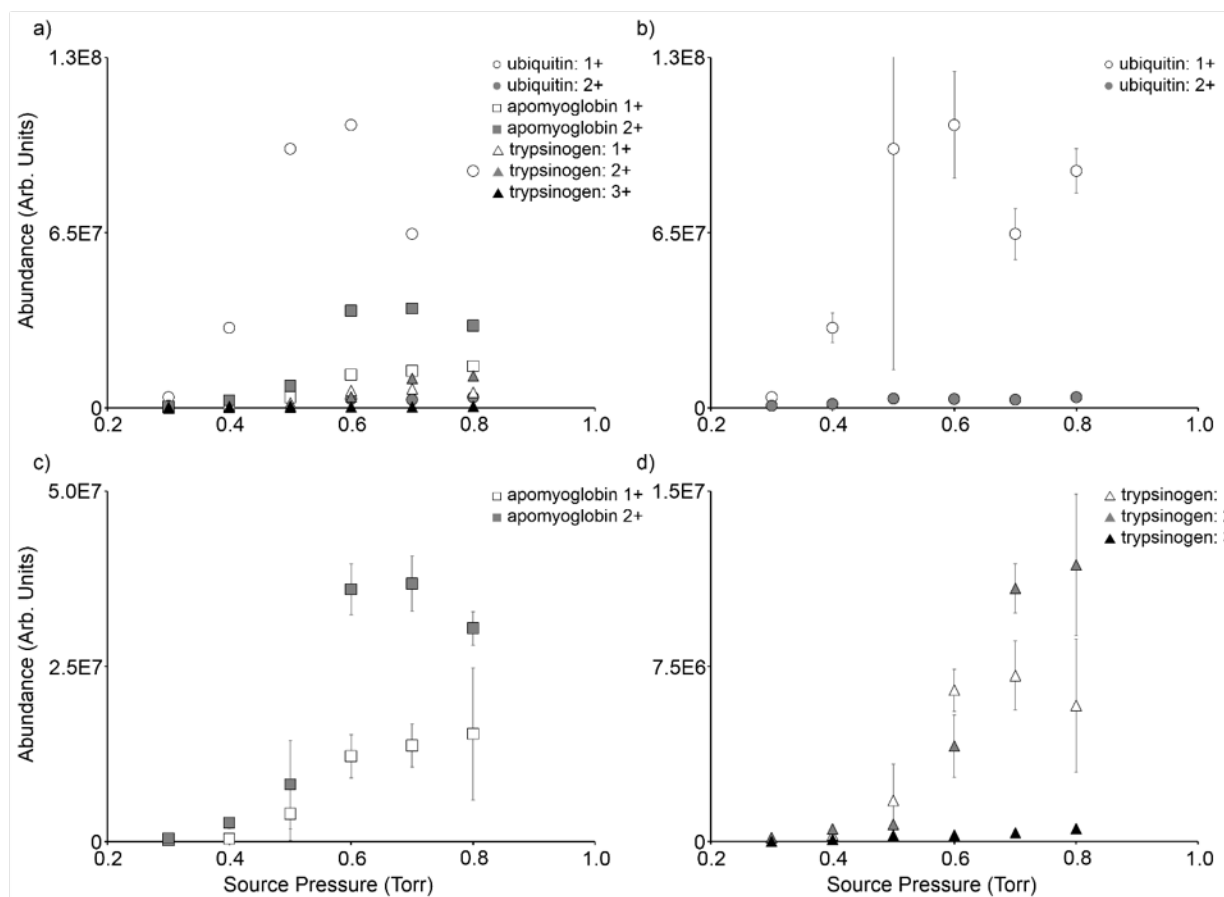


**Figure 2.6:** (a) Protein abundance as a function of source pressure for (b) ubiquitin, (c) apomyoglobin, and (d) trypsinogen. In c-d, the error bars represent the standard deviation of 3 replicates. The flow through the ESI capillary was minimized (V3 closed) and the source pressure was instead varied by adjusting rough pump conductance (V1). The ESI source is positioned to minimize the overlap with the MALDI ion generation region.

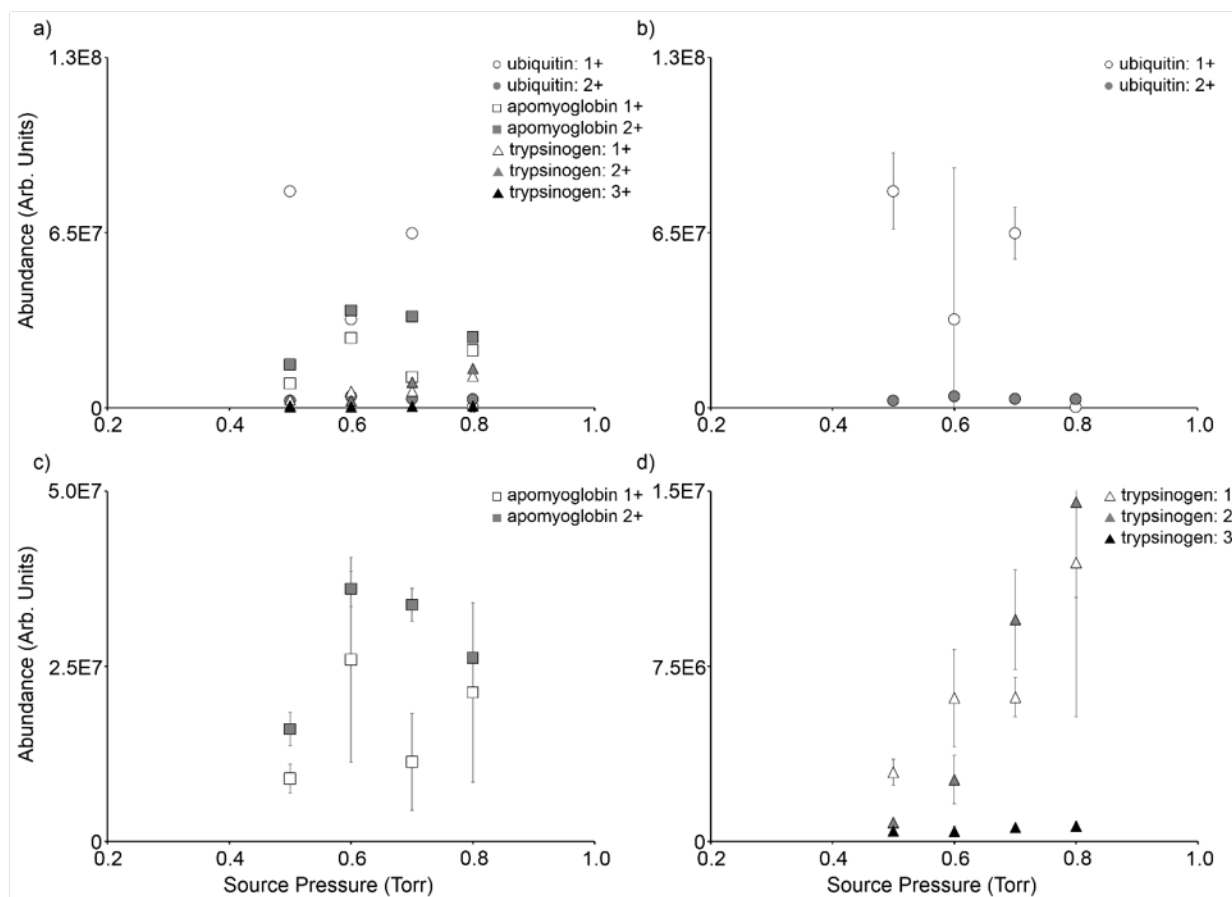


**Figure 2.7:** (a) Protein abundance as a function of source pressure for (b) ubiquitin, (c) apomyoglobin, and (d) trypsinogen. In c-d, the error bars represent the standard deviation of 3 replicates. The flow through the ESI capillary was minimized (V3 closed) and the source pressure was instead varied by adjusting rough pump conductance (V1). The ESI source is positioned to maximize the overlap with the MALDI ion generation region.

### *Tissue Imaging and Image Fusion*

The high mass resolution and accurate mass capabilities of FT-ICR MS have recently been used to facilitate protein identification in imaging mass spectrometry experiments.<sup>16, 109, 117</sup> While this technology is promising for the identification of post-translational modifications (PTMs) and the separation of overlapping proteoforms, proteins detected with good signal-to-noise ratios in these studies have been limited to  $m/z$  values of less than 15,000. Here, we have applied the source

conditions optimized as described above for high  $m/z$  ion transmission to a protein imaging experiment. One half of a transverse rat brain section was imaged using normal source conditions (2.9 mTorr) while the second half of the brain was imaged under reduced source pressure conditions (750 mTorr). Under normal source conditions, most of the protein species detected are in the mass range of  $m/z$  4,000 to 8,500, with a few species detected up to  $m/z$  ~14,000 with low S/N (Figure 2.7a). However, upon adjusting the source pressure to 750 mTorr using V3, protein signals with good S/N are observed from  $m/z$  4,000 to 22,000 (Figure 2.8b). Dramatic improvements in S/N are observed at high  $m/z$ . For example, the abundance of the singly charged species at  $m/z$  14,121.73 is improved by roughly 100-fold using the reduced source pressure (Figure 2.9a and 2.9e). Additionally, many other high  $m/z$  species that were not detected at normal source pressure are observed with good S/N using a source pressure of 750 mTorr (Figure 2.9b-d and 2.9f-h). The isotopic envelopes centered at  $m/z$  18,444.60 and 20,712.00 appear to represent doubly charged species, indicating that the reduced source pressure condition has enabled the detection of proteins with molecular weights over 40 kDa, though the incomplete resolution of these isotopic distributions cannot preclude the presence of two overlapping singly charged proteins (Figure 2.9f). Given the results from the protein standard experiments in Figure 2.3, it is likely that the abundances of protein species below  $m/z$  ~11,000 are being slightly attenuated at a source pressure of 750 mTorr (attributed to a LMCO effect). Similar to the protein standard experiments, the transmission efficiency for multiply charged species is diminished more so than that for singly charged species at lower  $m/z$ , which is consistent with the effective potential in the ion funnel being higher for multiply charged species (Figure 2.9). A more optimal source pressure for ions in this mass range is ~1.0 Torr. However, in this imaging experiment we sought to

maximize the transmission of the highest  $m/z$  species, which occurs at a source pressure of ~750 mTorr.

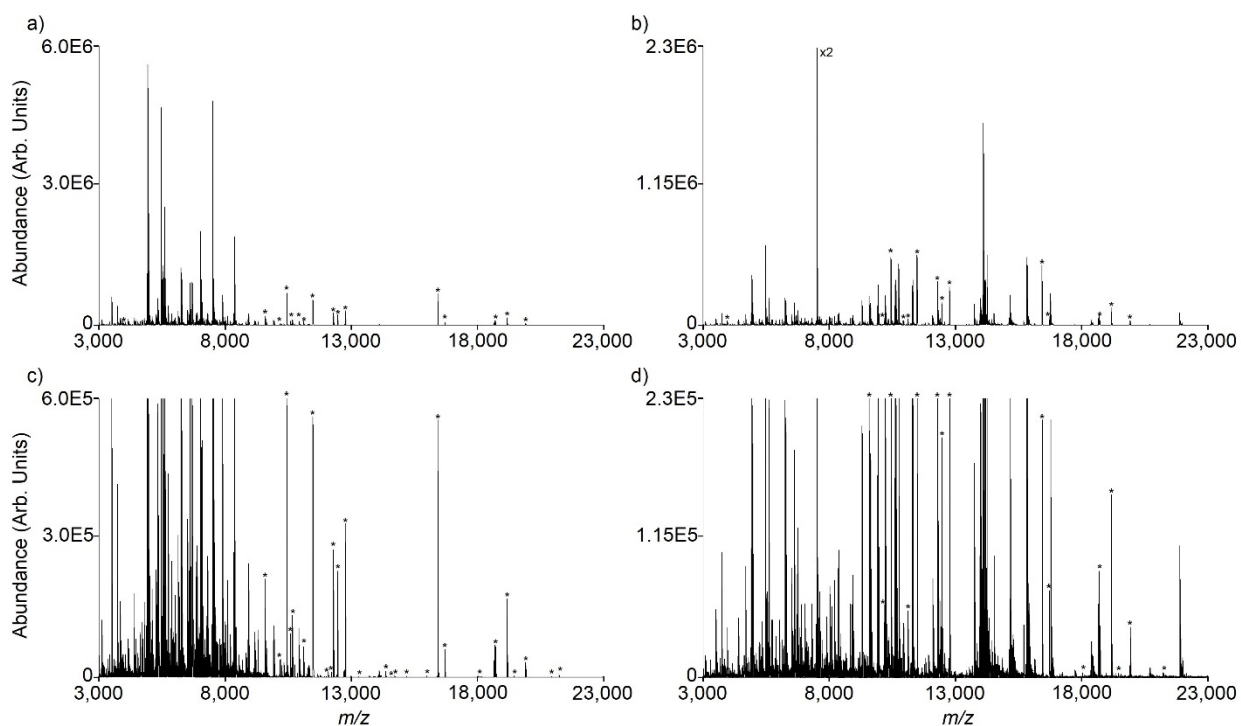


**Figure 2.8:** Average mass spectra from rat brain tissue imaging mass spectrometry experiments acquired at source pressures of a) 2.9 Torr and b) 750 mTorr. The source pressure was varied by adjusting gas flow through the ESI capillary (V3) and the ESI source is positioned to minimize the overlap with the MALDI ion generation region (Figure S1b). Spectra were background subtracted and asterisks (\*) are used to denote peaks due to electronic noise. c) and d) are 10-fold expansions of the intensity scales of (a) and (b), respectively

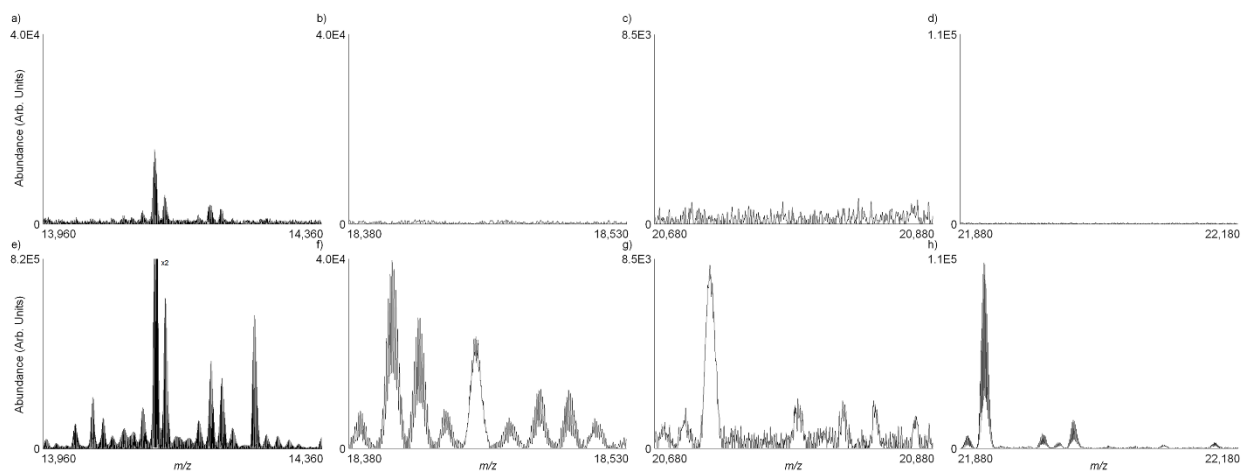


**Figure 2.9:** Selected mass ranges from Figure 4 showing average mass spectra from rat brain tissue imaging mass spectrometry acquired at source pressures of a-d) 2.9 Torr and e-h) 750 mTorr. The source pressure was varied by adjusting gas flow through the ESI capillary (V3) and the ESI source is positioned to minimize the overlap with the MALDI ion generation region (Figure S1b).

Despite the signal attenuation observed for ions at lower  $m/z$ , ion images can be produced across a broad mass range from  $m/z$  4,000 to 22,000 using the reduced source pressure, roughly doubling the mass range for which quality protein ion images can be produced (Figure 2.9). While the image quality for proteins in the lower  $m/z$  range is comparable between the two source conditions (Figure 2.10b-e), the image quality for proteins above  $m/z$  ~9,000 is dramatically improved at reduced source pressure (Figure 2.10f-o). The spatial distributions of proteins up to  $m/z$  ~22,000 are clearly visible in many brain substructures including the corpus callosum, white matter, granular layer, and molecular layer. The high mass resolving power of the FT-ICR platform allows for clear isotopic resolution of most of these high  $m/z$  protein species, and ion images are plotted using a  $\pm 0.25$  Da window of the most intense isotope in order to minimize interferences from potentially overlapping isotopic patterns. Using accurate mass measurements, tentative identifications for selected ions can be made based on previous reports of rat brain protein imaging. For example, the protein ion detected at  $m/z$  5,636.114 can be tentatively identified as

ATP synthase subunit epsilon (Figure 2.10c, 4.8 ppm).<sup>109</sup> Similarly, the protein at  $m/z$  11,348.33 can be tentatively identified as doubly acetylated and dimethylated histone H4 (Figure 2.10h, -7.3 ppm). These post-translational modifications have previously been identified by top-down proteomics (N-terminal acetylation, acetylation of lysine 17, and di-methylation of lysine 21).<sup>109</sup> Finally, the ions at  $m/z$  5,653.722 and  $m/z$  11,306.37 are tentatively identified as doubly (2.7 ppm) and singly charged (-3.5 ppm) versions of histone H4 that has an N-terminal acetylation and di-methylation of lysine 21 (Figure 2.10d and 2.10g).<sup>109</sup> Imaging mass spectrometry analysis of rat kidney tissue was also performed at a reduced source pressure, enabling the detection of protein ions up to  $m/z$  ~17,000. Similar to IMS analysis of rat brain tissue, high quality ion images are obtained here for species above  $m/z$  ~9,000 (Figure 2.10). Doubly charged ions are observed up to  $m/z$  11,654.37, allowing for the mapping of protein species of molecular weights in excess of 23 kDa (Figure 2.11d).



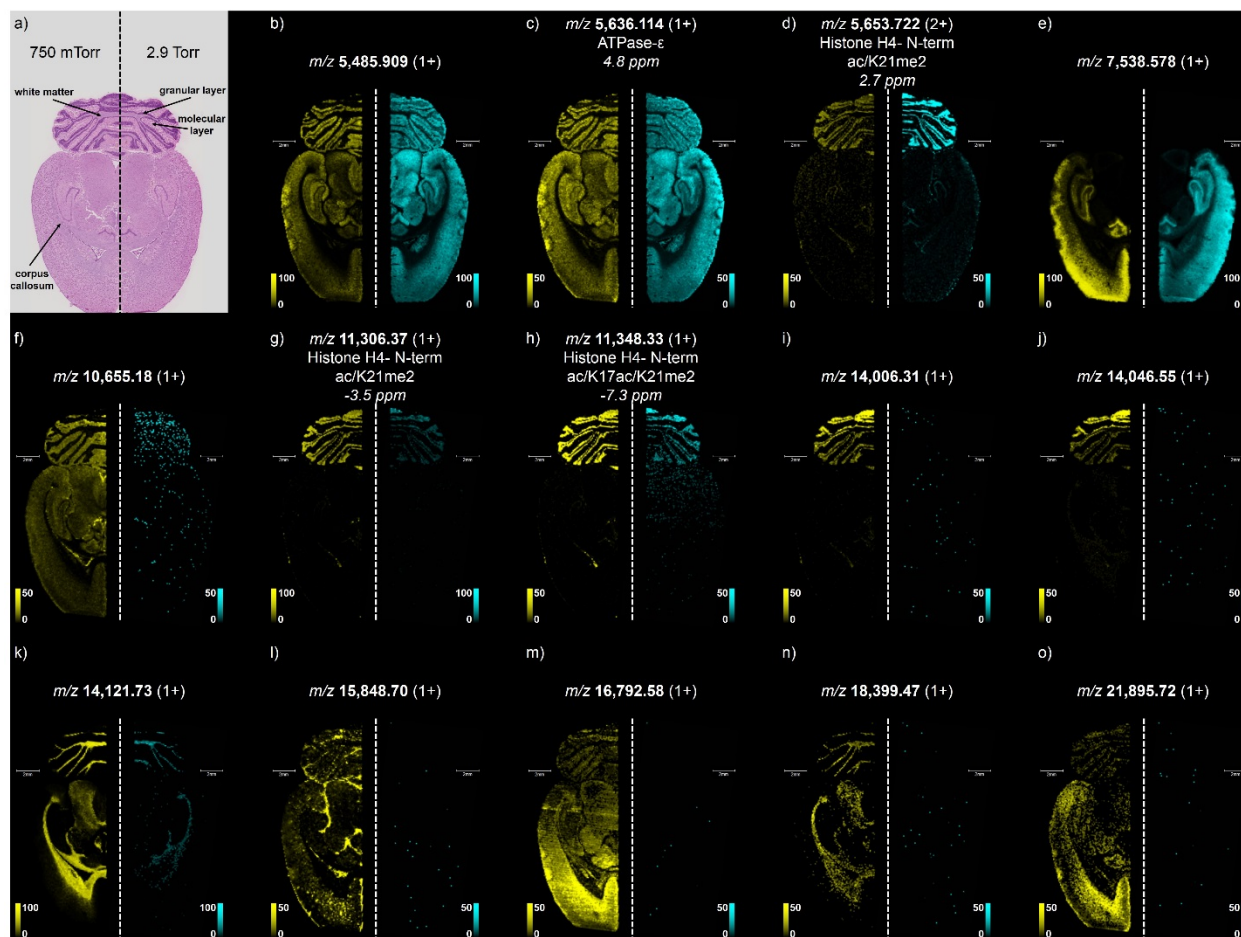


**Figure 2.10:** Selected ion images of intact proteins from the mass spectra displayed in Figure 2.9. a) An H&E stain of a serial tissue section allows for visualization of brain substructures and indicates the hemispheres of the brain that were analyzed using normal source pressure (right hemisphere) or reduced pressure source conditions (left hemisphere). b-o) The accurate mass of the most abundant isotope and the protein charge state are reported for each of the ion images. Internal mass calibration was performed using singly and doubly charged species of cytochrome c and hemoglobin  $\alpha$  using a quadratic fit. Images are displayed using root-mean-square (RMS) normalization. Ion images are plotted as  $\pm 0.25$  Da for the most intense isotope. Scale bars = 2 mm.

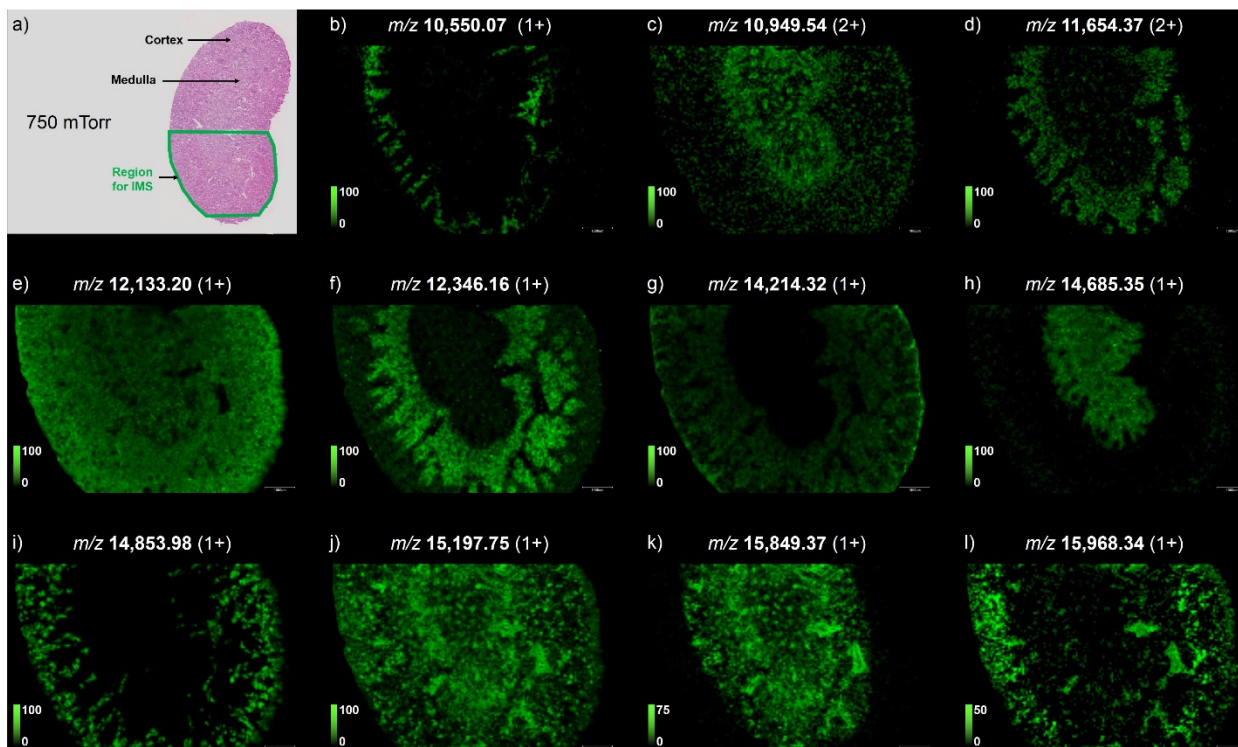


**Figure 2.11:** Selected ion images of intact proteins acquired from protein IMS of rat kidney, which was acquired at a reduced source pressure. a) An H&E stain of the tissue section following image acquisition allows for visualization of kidney substructures. b-l) The accurate mass of the most abundant isotope and the protein charge state are reported for each of the ion images. Internal mass calibration was performed using singly and doubly charged species of cytochrome c and hemoglobin  $\alpha$  using a quadratic fit. Images are displayed using root-mean-square (RMS) normalization. Ion images are plotted as  $\pm 0.25$  Da for the most intense isotope. Scale bars = 1 mm.

While the FT-ICR platform facilitates the identification of proteins in an imaging experiment, the length of the time-domain signal required to adequately resolve these high  $m/z$  ions is significant. The 4.47 s transient length used in the imaging experiment shown in Figure 2.10 provided for a resolving power of  $\sim 41,000$  at  $m/z \sim 17,000$ , but necessitated over 28 hours of instrument time to complete the two 100  $\mu\text{m}$  protein imaging experiments. As the number of pixels, and thus image acquisition time, required to sample a given area of tissue is inversely proportional to the square of the pixel size,<sup>127-131</sup> protein imaging mass spectrometry at higher spatial resolutions

using FT-ICR MS quickly becomes time-prohibitive. There is thus specific interest in using data-driven FT-ICR IMS-microscopy image fusion<sup>132</sup> to predict protein ion distributions to a higher spatial resolution than that of the original IMS experiment. In order to assess the feasibility of this approach, we performed a “spatial sharpening” application of data-driven image fusion, which predicts protein ion distributions to a spatial resolution that exceeds that of the measured ion images by ten-fold. In this workflow, the IMS protein measurements acquired at 100- $\mu\text{m}$  spatial resolution are fused with the H&E microscopy measurements acquired at 10- $\mu\text{m}$  spatial resolution in order to predict protein ion distributions at 10- $\mu\text{m}$  spatial resolution (Figure 2.12). This results in a single predictive image modality with FT-ICR-grade molecular specificity and microscopy-grade spatial resolution. These predicted images are accompanied by “reconstruction scores,” which are numerical measures of confidence that help assess the reliability of each of the ion distribution estimations.<sup>132</sup> For example, the successful predictions of protein ions at  $m/z$  7,650.009, 13,776.35, and 14,313.60 to 10  $\mu\text{m}$  is confirmed with relatively high reconstruction scores of 84.47%, 86.11%, and 79.35%, respectively ( $m/z$  7,650.009 shown in Figure 2.12c). This proof-of-concept application demonstrates the compatibility of high  $m/z$  protein FT-ICR IMS with *in silico* up-sampling techniques such data-driven image fusion, which outperforms common bilinear interpolation (data not shown). This example illustrates that predictive computational methods hold potential to offset some of the practical constraints incurred by the longer time-domain transient lengths and limited spatial resolutions used in this work.

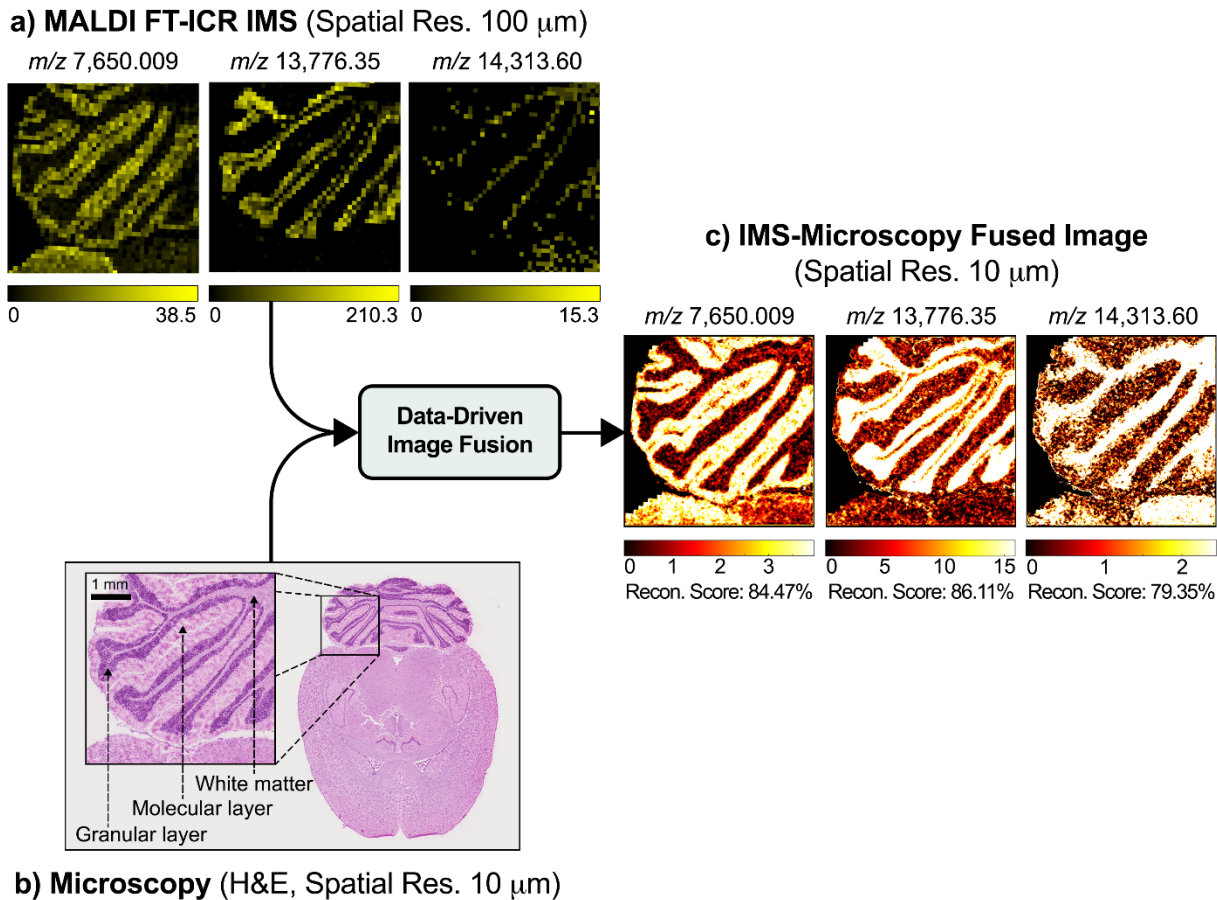


**Figure 2.12:** Data-driven, multi-modal image fusion of a) FT-ICR IMS data acquired at 100- $\mu\text{m}$  spatial resolution with b) H&E microscopy measurements acquired at 10- $\mu\text{m}$  spatial resolution in order to predict c) protein ion distributions at 10- $\mu\text{m}$  spatial resolution. Three protein species with relatively good reconstruction scores (>75%) are exemplified here.

## Discussion

Modifications to the gas manifold of a 15T FT-ICR MS have enabled control of the gas flow and pressure in the MALDI source region. A systematic evaluation of the effect of source pressure on ion transmission efficiency through the ion funnel found that reducing the source pressure from 2.9 Torr to 750 mTorr improved the transmission efficiency of high  $m/z$  protein species by 10 to 100-fold. This improvement is attributed to a less dampened effective potential

for ion radial confinement at reduced pressures and has enabled the detection of protein standard ions up to  $m/z$  24,000. Other observations consistent with previous ion funnel reports, including a LMCO effect and differences in the transmission efficiencies of singly and multiply charged ions, are also noted. The newly optimized source conditions have been used in an imaging experiment to roughly double the mass range for which high quality protein ion images can be acquired from rat brain and kidney tissue. The high resolution accurate mass capabilities of FT-ICR MS have facilitated the identification of proteins detected in the imaging data. We have used a computational tool, FT-ICR IMS-microscopy image fusion, to mitigate the long acquisition time associated with FT-ICR protein imaging, required for the resolution of protein isotopic distributions, and produce protein images that have both high mass resolution and high spatial resolution.

## **Methods**

### *Mass Spectrometry*

All experiments were performed on a 15T solariX XR FT-ICR mass spectrometer equipped with an Apollo II dual MALDI/ESI source and a dynamically harmonized ParaCell (Bruker Daltonics, Billerica, MA). The MALDI source employs a Smartbeam II Nd:YAG laser system (2 kHz, 355 nm). Each protein standard mass spectrum was acquired by manually performing a random raster of a MALDI spot for 8,000 laser shots. Data were collected from  $m/z$  1,500 to 30,000 with a resolving power ( $m/\Delta m$ ) of  $\sim 48,000$  at  $m/z$   $\sim 17,000$  unless otherwise noted (using a 6.71 s time-domain transient length) and visualized using Compass DataAnalysis 5.0 (Bruker Daltonics, Billerica, MA). The most abundant isotopic mass was selected to determine the ion intensities for the protein standard experiments. The ion optics were tuned to maximize high  $m/z$  ion

transmission, including the funnel RF amplitude (285 V<sub>pp</sub>), source octopole (2 MHz, 525 V<sub>pp</sub>), collision cell (collision voltage: -8.0 V, cell: 1.4 MHz, 1900 V<sub>pp</sub>), time of flight delay (3.2 ms), and transfer optics (1 MHz, 410 V<sub>pp</sub>). The funnel RF amplitude setting is close to the upper software limit of this element. The source DC optics were kept constant for all experiments (Capillary Exit: 250 V, Deflector Plate: 200 V, Plate Offset: 100 V, Funnel 1: 150 V, Skimmer 1: 70 V). Gated trapping was used in the ICR cell to more efficiently trap high  $m/z$  species:<sup>119, 133, 134</sup> the initial front and rear trapping potentials were set to 2.5 V and ramped down to 1.5 V in 10 ms before ion detection. Ion detection was performed using a sweep excitation power of 50%.

The source region of the instrument is backed by a rough pump and uses atmospheric gas admitted from the open ESI source to maintain a pressure of ~2.9 Torr (~3.9 mbar) in the source region. In order to regulate the pressure and gas flow in the source region of the instrument, 3 minor modifications were made to the gas manifold (Figure 2.1). First, an isolation valve (KF25 aluminum bellows block valve from Agilent Varian, Santa Clara, CA) was inserted between the source rough pump and the vacuum housing. Second, a secondary rough pump (E2M28 rotary vane pump from Edwards, Burgess Hill, England) was added to the source region. The conductance of this secondary pump was also controlled using an isolation valve. A Pirani convection vacuum gauge (CVM211 Stinger from InstruTech, Longmont, CO) was added to accurately measure the pressure in the source region. However, the measured pressure is likely somewhat different than the actual pressure in the ion funnel, which can vary locally within the device.<sup>96</sup> Finally, the conductance through the ESI capillary was regulated by removing the ESI source and fitting a push-connection of flexible tubing over the end of the ESI capillary. The other end of this tubing was connected to a metering valve (Swagelok, Solon, OH) to regulate the gas flow into the source region. While the connection to the ESI capillary was not a perfect seal, the

fitting was sufficient to provide a minimum source pressure of ~250 mTorr (~0.33 mbar) when the metering valve was completely closed. For all experiments herein, altering the source pressure had a minimal effect on the pressure of the downstream collision cell and ICR cell.

### *Imaging Mass Spectrometry*

Transverse sections of rat brain and coronal sections of rat kidney were collected at 12  $\mu\text{m}$  using a Cryostar<sup>TM</sup> NX70 Cryostat (Thermo Fisher Scientific, San Jose, CA, USA) and thaw mounted onto indium tin oxide (ITO)-coated slides. Slides containing the tissue sections were washed to remove salts and lipids as previously described.<sup>135</sup> Briefly, the wash protocol consisted of: 70% ethanol (30s), 100% ethanol (30s), Carnoy's fluid (6:3:1 ethanol:chloroform:acetic acid, 2 min), 100% ethanol (30s), water (30s), and 100% ethanol (30s). Following the wash, samples were dried using a desktop vacuum desiccator for 30 minutes. A DHA matrix layer was then applied to the slides using a custom-built sublimation apparatus (110°C, 4.5 minutes, <70 mTorr).<sup>136</sup> Immediately prior to IMS analysis, a matrix recrystallization step was performed to improve protein sensitivity (using 1 mL of 1:1, TFA:H<sub>2</sub>O for 3 minutes at 37 °C).<sup>137</sup> Images were acquired at a pixel spacing of 100  $\mu\text{m}$  (for brain tissue) and 60  $\mu\text{m}$  (for kidney tissue) in both the x and y dimensions using a ~75- $\mu\text{m}$  laser beam (1,000 laser shots).<sup>138</sup> Data were collected from  $m/z$  1,000 to 30,000 using a 4.47 s time-domain transient length. This shorter length transient compared to the protein standard experiments detailed above decreased the time required for image acquisition and resulted in a resolving power of ~41,000 at  $m/z$  ~17,000. The resulting ion images were visualized using FlexImaging 5.0 (Bruker Daltonics, Billerica, MA) and images are displayed using root-mean-square (RMS) normalization. All ion images were visualized using interpolation except those displayed as part of the image fusion workflow. Following image acquisition, tissue

sections were stained using hematoxylin and eosin (H&E) and scanned using a SCN400 brightfield digital whole slide scanner (Leica Microsystems, Bannockburn, IL).

### *Data-driven Multi-modal Image Fusion*

The availability of both IMS and microscopy measurements (albeit with different pixel sizes), enables the use of data-driven image fusion as a means of cross-modal prediction.<sup>132</sup> Briefly, the mass spectra were normalized on the basis of their total ion current, and baseline corrected using a piecewise cubic approximation of the baseline at the 10% quantile of ion intensities, while employing a window size of 100 and a step size of 50. The spectra were subsequently peak-picked to produce an IMS data source of 1,156 peak ion images, consisting of 11,129 on-tissue pixels in total and 1,704 pixels within the highlighted tissue area. These steps were performed using the Bioinformatics Toolbox of MATLAB (MathWorks). The microscopy data source was an H&E stain of a tissue section serial to the section sampled by IMS and consists natively of the standard red, green, and blue intensity bands, which are subsequently expanded to 905 bands using the transformations described previously.<sup>132</sup> The microscopy source consists of 2,928,451 pixels, 166,848 of which fall within the highlighted area. The IMS and microscopy data sources were spatially registered to each other using a similarity transformation (allows translation, rotation, and scaling), as determined by manual selection of corresponding fiducials in MATLAB using the `cpselect()` and `cp2tform()` functions. The mapping step of the fusion process employed an integer 2-D Gaussian bell curve centered on the IMS pixel to map microscopy to IMS measurements.

The fusion process consists of a model building and evaluation phase followed by a prediction phase that then performs the actual estimation of higher-resolution distributions. The modeling phase empirically learns a partial least squares linear regression model from the linked IMS and microscopy measurements, yielding an IMS/microscopy model that captures how the ion



intensity of certain ion species changes when the values of one or more microscopy variables change. The reliability of this model in capturing relationships between observations in IMS and observations in microscopy is evaluated for each mass spectral peak individually using several figures of merit (*e.g.*, reconstruction scores).<sup>132</sup> Prediction to a higher spatial resolution is performed only for those ions that are identified to have high predictive capability. For example, in the workflow described here,  $m/z$  7,650.009, 13,776.35, and 14,313.60 all yielded good connection to the H&E microscopy, as reported by reconstruction scores of 84.47%, 86.11%, and 79.35%, respectively. For these ions, the prediction phase of the fusion workflow performed prediction to 10- $\mu\text{m}$  spatial resolution.

## CHAPTER III

### SPATIALLY TARGETED PROTEOMIC ANALYSIS FROM TISSUE USING LIQUID EXTRACTION SURFACE ANALYSIS

This chapter was adapted from the previous published Ryan et al., *Rapid Communications in Mass Spectrometry*, Copyright 2018 by Wiley

#### Overview

Liquid extraction surface analysis (LESA) can be used to generate spatially-directed protein identifications in an imaging mass spectrometry workflow. This approach involves the use of robotic micro-extractions coupled either directly to online liquid chromatography or collected for offline LC analysis. Robotic liquid surface extractions are reproducible across various tissue types, providing significantly improved spatial resolution, with respect to extractions, while still allowing for a robust number of protein identifications. A single 2  $\mu$ L extract allows for the identification of over 14,000 peptides with little sample preparation, increasing throughput for spatially targeted workflows. The utility of tissue surface extractions and liquid chromatography, offers a new and effective approach to provide spatial proteomics data in an imaging experiment.

#### Introduction

Since the emergence of MALDI IMS<sup>11</sup>, the field has seen tremendous growth in a diverse range of research areas including the proteomic study of diseased tissue<sup>139, 140</sup>, drug

development<sup>141, 142</sup>, and biomarker detection.<sup>143, 144</sup> IMS analysis relies on the systematic interrogation of a sample, generally a thin tissue section, to generate individual mass spectra at discrete x,y- positions. This process gives rise to the spatial mapping of thousands of proteins, lipids, and small molecules within a biological sample.<sup>145</sup>

Molecular identification in an IMS experiment is crucial in determining the physiological role of the detected analytes in the system being studied. Typically, protein IMS experiments have been carried out using TOF instruments due to the platform's high sensitivity over a broad mass range, high data acquisition speeds, and relatively low cost. However, identifying proteins during MALDI-TOF IMS analyses can be challenging. Ideally, protein ions would be analyzed and sequenced by tandem mass spectrometry (MS/MS or MS<sup>n</sup>) directly from tissue. Generating useful fragmentation data becomes difficult at the higher  $m/z$  values ( $> \sim 3000$ ). A second approach for identification during an imaging experiment is the use of high resolution accurate mass measurements to unambiguously identify the empirical chemical formula for the ion of interest. However, collecting accurate mass measurements using MALDI-TOF platforms is difficult because of their limited mass accuracy (typically  $>20$  ppm) and lower mass resolving power, particularly for high  $m/z$  ions (i.e.,  $> 3000$ ).<sup>146</sup> Recently, high resolving power, high mass accuracy FT-ICR MS has been used to help link identifications through accurate mass measurements to LC-MS/MS proteomics data and TOF-based imaging experiments.<sup>15, 16, 40, 41</sup> For example, in recent studies, we were able to detect intact proteins up to 20 kDa, with resolving powers of  $\sim 75,000$  at  $m/z$  5,000 and mass accuracies  $< 5$ ppm.<sup>41</sup> Although progress has been made, the identification of proteins from tissue still remains a difficult task.

Due to the practical issues associated with fragmenting ions directly from tissue, protein identifications for MALDI IMS experiments are often achieved by performing secondary LC-based experiments to complement the IMS data.<sup>147</sup> By identifying analytes in a secondary experiment, identifications can be correlated back to the imaging data through the matching of intact molecular weights.<sup>35, 148, 149</sup> These complimentary experiments typically fall into 3 categories: 1) bulk tissue homogenization and protein extraction, 2) enzymatic digestion performed directly on tissue followed by MS/MS of the resulting peptides, and 3) spatially-targeted surface extractions of peptides or proteins. In the bulk homogenization experiment, the entire tissue or tissue section is homogenized, proteins are extracted and further subjected to bottom-up LC-MS/MS or top-down approaches.<sup>150</sup> Although the more common approach, bottom-up identifications are often difficult to correlate back to IMS data of intact proteins because the intact mass information, and post translational information is often lost during the bottom-up experiment. Also, all spatial information is lost during the homogenization process. Another approach is to perform on-tissue enzymatic digestions. An enzyme is applied to the sample in a way that minimizes analyte delocalization on the tissue surface, and proteins are sequenced directly using MALDI MS/MS.<sup>151</sup> These experiments suffer from low throughput as they require additional sample manipulation, relative to intact protein analysis, and each peptide is usually sequenced individually. These bottom-up workflows are also susceptible to missing post translational modifications (PTM) information due to mass mismatches with the IMS data and missing peptides. Finally, spatially-directed approaches, such as enzyme-loaded hydrogels and liquid extraction surface analyses (LESA), allow for the interrogation of discrete regions of the tissue surface, retaining the spatial integrity of an IMS analysis. Hydrogels, small gel polymers that are loaded with trypsin and placed on a tissue for digestion and extraction of peptides and have

been shown to be an efficient method of generating protein identifications but are difficult to manipulate due to their small size.<sup>72, 74, 152</sup> LESA workflows involve the dispensing of small volumes of solvent onto the tissue surface, allowing for the diffusion of analytes into the liquid which can be followed by traditional proteomic workflows providing for a sensitive, high-throughput approach to performing spatially targeted proteomics experiments.<sup>153</sup>

Liquid micro-extractions between a tissue surface and solvent droplet have been shown to produce robust LC-based proteomics results.<sup>154</sup> Schey et al. manually pipetted 1  $\mu$ L volumes of solvent onto a tissue surface and detected upwards of 100 intact protein signals by simply aspirating and re-dispensing the solvent on the tissue surface multiple times and then subjecting the extraction to top-down LC-MS/MS.<sup>75</sup> This approach is useful when attempting to study a tissue sample in a spatially targeted manner as the sample is kept intact while targeting discrete regions for analyses. A semi-automated approach uses a robotic pumping and positioning system to sample the surface of a substrate with greater accuracy and precision.<sup>155-160</sup> It's ease of use, reproducibility, automated functionality, and ability to interrogate discrete regions of a sample has been demonstrated for analyzing several classes of biomolecules from a range of surfaces, including tissue, dried blood spots, food surfaces, and latent fingerprints.<sup>161-164</sup> Previous studies have shown the capabilities and application of LESA, which utilized disposable capillary tips and enabled offline proteomics analysis of tissue extracts.<sup>155-158, 161-164</sup> Recently, this liquid extraction technology has been modified to replace the disposable capillary with a glass capillary (LESAPLUSLC) allowing for increased droplet resolution on the sample surface. The capillary outlet is fed into a 6-port valve where the sample can be injected onto a column for online LC-MS analysis.<sup>165</sup>

Herein, we report the coupling of robotic surface micro-extractions from thin tissue sections directly to LC-MS and LC-MS/MS using a glass capillary setup. Extractions are completed and taken offline for bottom-up MS analysis to assess the extraction process and determine its efficiency and robustness. This methodology provides improved reproducibility and droplet resolution when compared to previous methods using hand pipetting, and has been incorporated directly into online LC-based workflows. The enhanced micro-extraction process allows for the use of both bottom-up and top-down approaches, with a higher throughput than previous IMS protein identification workflows.

## Results

### *Surface Extraction Performance*

In order to visualize the effect of solvent composition on droplet resolution, various combinations of solvents were tested using an increasing volume of extraction solvent while dispensing onto water sensitive paper using the LESApplusLC platform (Figure 3.1 and Table 3.1). Three replicates were measured to assess the reproducibility of the droplet diameters. For 100% H<sub>2</sub>O, the average extraction volume diameter on water sensitive paper is below 600  $\mu\text{m}$  for the smallest extraction volume (0.5  $\mu\text{L}$ ), ~70% smaller than previous efforts using manual pipetting.<sup>75</sup> We also see an improvement in droplet resolution compared to the older, air-infused mandrel for the LESA experiments. The prior setup yielded an average spot size of  $2.2 \pm 0.04$  mm dispensing 1:1 ACN:H<sub>2</sub>O (~50% decrease in resolution). However, the spot size increases significantly with increasing percentages of organic solvents and extraction volume. LESA droplet sizes were also assessed on tissue using hematoxylin stain (Table 3.1). The values measured from the on-tissue

experiment are slightly larger than their water sensitive paper counterparts. This is mainly due to the water-sensitive paper being more hydrophobic than the tissue, allowing the surface tension of the liquid to maintain a smaller droplet profile. Even though the dispensing/aspiration step was held for twice as long as the water sensitive paper tests in order to allow for the stain to penetrate the cells, no change in diameter was observed using the increased dispensing time for the on-tissue measurements. The spot size measurements from tissue were 1.23 mm (5.6% RSD), 1.78 mm (4.5% RSD), 2.29 mm (2.2% RSD), and 2.55 mm (3.2% RSD) for 0.5, 1.0, 1.5, and 2.0  $\mu\text{L}$  extraction volumes, respectively. These results demonstrate the reproducibility of a LESA experiment, and improvements compared to similar techniques, with regards to droplet resolution.

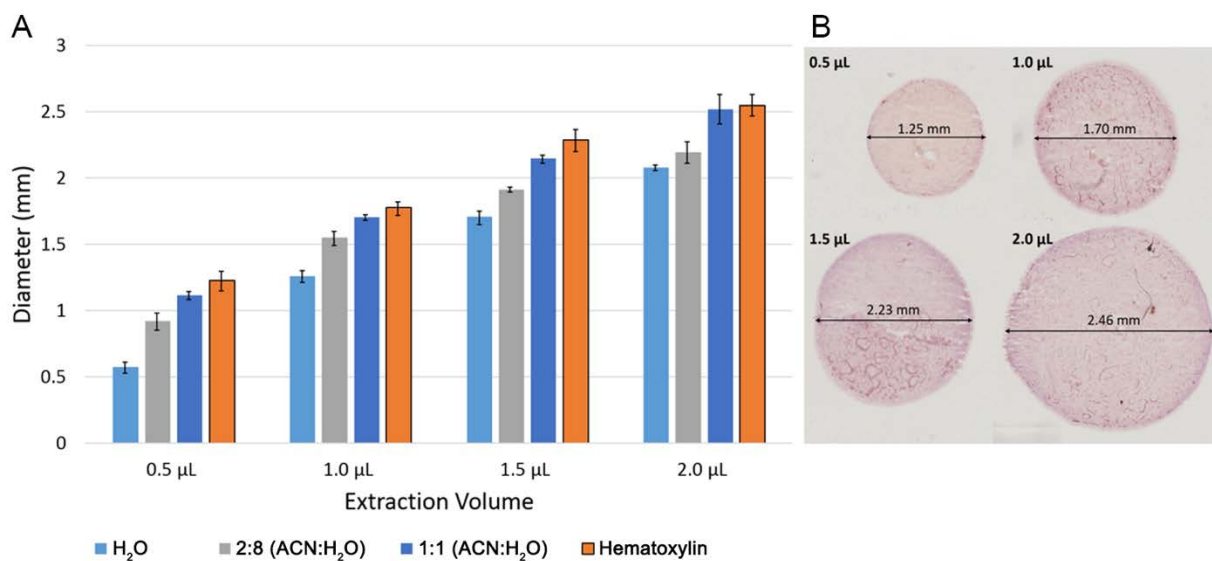


**Figure 3.1:** A) The measured droplet resolution of the LESAplusLC system on water-sensitive paper decreases as the volume dispensed increases and as the relative organic fraction of the solvent increases. B) The measured droplet resolution of the LESAplusLC system on rat brain tissue (cerebellum) using hematoxylin stain to visualize the solvent diffusion during extraction. For both experiments, droplet diameter measurements were made using bright field microscopy.

Droplet Resolution Measured from Water Sensitive Paper			
Volume Dispensed	Solvent (ACN:H <sub>2</sub> O)	Average Measured Diameter (mm)	Percent Relative Standard Deviation
0.5 µL	0:10	0.57	6.3
0.5 µL	2:8	0.92	7.0
0.5 µL	1:1	1.12	2.8
1.0 µL	0:10	1.26	3.1
1.0 µL	2:8	1.55	3.2
1.0 µL	1:1	1.71	1.3
1.5 µL	0:10	1.71	3.2
1.5 µL	2:8	1.91	1.0
1.5 µL	1:1	2.15	1.3
2.0 µL	0:10	2.08	1.2
2.0 µL	2:8	2.20	3.2
2.0 µL	1:1	2.52	6.7
Droplet Resolution Measured from Tissue			
0.5 µL	Hematoxylin	1.23	5.6
1.0 µL	Hematoxylin	1.78	4.5
1.5 µL	Hematoxylin	2.29	2.2
2.0 µL	Hematoxylin	2.55	3.2

**Table 3.1:** Droplet resolution of the LESApplusLC system as measured from water sensitive paper and tissue sections (rat brain cerebellum). Measurements were made varying solvent composition and volume dispensed (n=3).

In order to determine the reproducibility of the proteomic extraction from the tissue using the glass capillary mandrel, extractions were performed from rat brain cerebellum following on-tissue proteolytic digestion using trypsin. A single, 2 µL volume was dispensed/aspirated 5 times (75 seconds total) onto the tissue surface, and subjected to offline, bottom-up LC-MS/MS where an average of 1620 proteins were identified across the 5 replicates. These results showed that the extraction was extremely reproducible with a relative standard deviation of 2.7% (1<sup>st</sup> Replicate: 1560 unique proteins, 2<sup>nd</sup> Replicate: 1661 unique proteins, 3<sup>rd</sup> Replicate: 1615 unique proteins, 4<sup>th</sup> Replicate: 1603 unique proteins, 5<sup>th</sup> Replicate: 1662 unique proteins) between the 5 samples. It is also important to maintain sensitivity at decreasing spot size in order to allow for the interrogation of smaller foci. The overall sensitivity and reproducibility of the LESApplusLC platform was



assessed by measuring the total number of proteins identified and peptides observed from tissue as a function of extraction volume. Figure 3.2 highlights the results from triplicate surface extractions that were completed using 2.0, 1.5, 1.0, and 0.5  $\mu\text{L}$  volumes of 1:1 ACN:  $\text{H}_2\text{O}$  (0.5% FA) from the cerebellum of a rat brain that had been digested overnight using trypsin. This solvent composition was selected for these experiments based on previous tissue extraction experiments in our lab. The total number of peptides observed across the interrogated volumes, from largest to smallest, were  $8475 \pm 331$  (2.0  $\mu\text{L}$ , RSD 3.9%),  $8361 \pm 361$  (1.5  $\mu\text{L}$ , RSD 4.3%),  $7791 \pm 568$  (1.0  $\mu\text{L}$ , RSD 7.3%), and  $4837 \pm 933$  (0.5  $\mu\text{L}$ , RSD 19.3%) peptides. The total number of protein identifications were found to be  $1165 \pm 55$  (RSD 4.7%),  $1175 \pm 43$  (RSD 3.7% RSD),  $1119 \pm 48$  (RSD 4.3%), and  $860 \pm 104$  (RSD 12.1%) as LESA volumes are varied from 2.0-0.5  $\mu\text{L}$ . The relative standard deviations across both the peptide and protein replicates were found to be quite low for most volumes (RSD < 5%), with even the smallest droplet size experiments (0.5  $\mu\text{L}$ ) having an RSD of just over 12%.

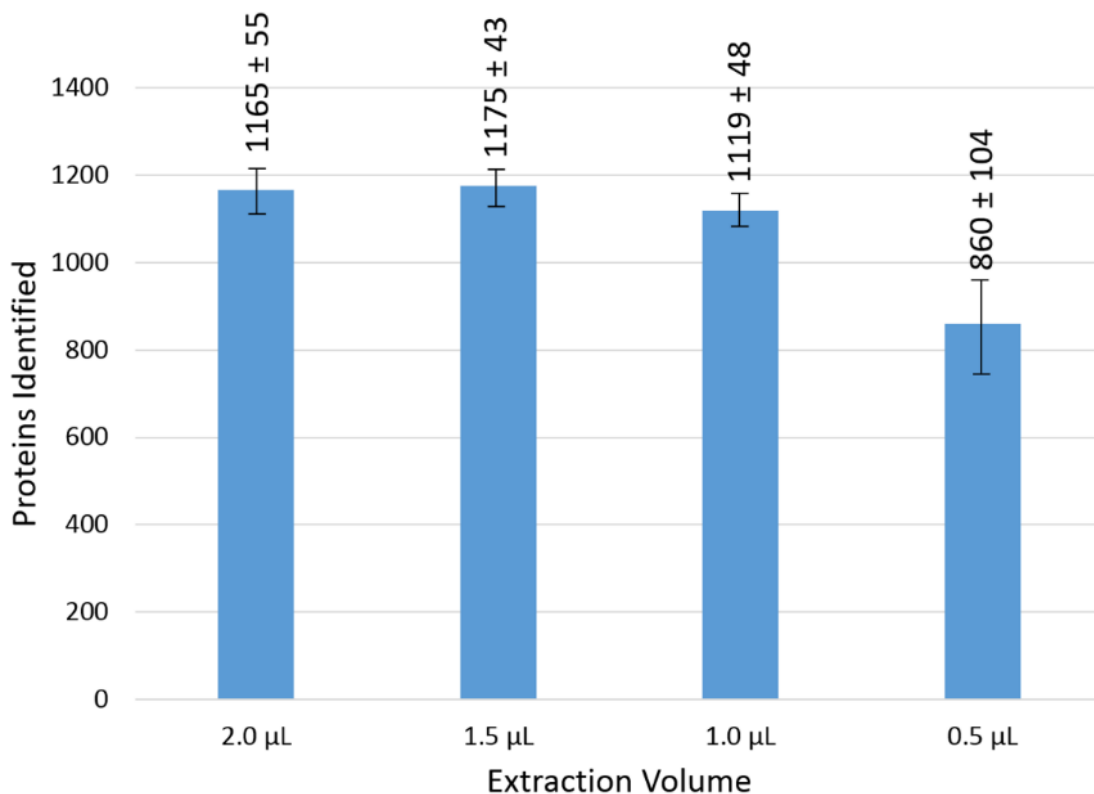


**Figure 3.2:** The number of unique proteins identified from digested rat brain cerebellum decreases as the volume dispensed on tissue is decreased, and is reproducible across volumes dispensed (n=3).

One of the advantages of utilizing an automated liquid surface extraction platform is the ability to increase throughput, minimizing sample preparation time and allowing for multiple extraction experiments to be completed in a single experiment. Comparing the LESA experiment to a similar, spatially-targeted technology such as hydrogels highlights the increase in throughput achieved. Whereas the typical hydrogel experiment takes ~2-2.5 days to complete, the LESA workflow takes ~1 day for bottom-up and ~2 hours for top-down analysis. A hydrogel experiment requires the casting of the gel (~16 hours), reswelling and gel placement (~1-2 hours), digestion (~14 hours), and extraction and LC-MS/MS analysis (~1-2 hours). The bottom-up LESA experiment can be completed in ~16 hours total. This includes the overnight digestion and LC-

MS/MS runs. The number of identifications are comparable to other spatially targeted approaches such as hydrogels. A hydrogel fabricated with a diameter of 1.66 mm has been shown to be capable of identifying 1052 proteins, while the LESA experiment at 1.0  $\mu\text{L}$  ( $\sim 1.71$  mm diameter measured previously) identified 1119 proteins.<sup>74</sup> The top-down experiments can be completed in as little as 1-2 hours, where the majority of the time is devoted to LC-MS/MS analysis, as the tissue washes and extractions only take  $\sim 10$  minutes to complete. For both bottom-up LESA methodologies, the analyte extraction steps require minimal time ( $\sim 10$  minutes) relative to the digestion (overnight) and LC-MS/MS ( $\sim 1-2$  hour) steps. This improved throughput allows multiple LESA experiments to be performed rapidly, enabling the generation of multiple extractions and analyses from a single tissue section.

LESA also has the advantage of allowing for sequential surface extractions to effectively 'build-up' analyte concentrations enabling both detection and structural identification by MS/MS even for low abundance species. This is particularly important for tissue analysis where the abundance of analytes can vary orders of magnitude across the surface. To determine the total amounts of extractable proteins gathered in sequential liquid surface extractions, peptides were extracted from the cerebral cortex of a trypsin-digested rat brain. A single 2  $\mu\text{L}$  extraction was gathered from the cerebral cortex and collected for offline LC analysis. Following this, the tissue was allowed to dry and another extraction was then collected from the same spot and analyzed separately. This process was repeated 5 times and the total peptide and protein identification counts were compared across each subsequent extraction (Figure 3.3). It is evident that after the initial extraction, the losses in both peptides observed and proteins identified are substantial. Between the 1<sup>st</sup> and 2<sup>nd</sup> extractions there is a decrease of approximately 30% and 42% in the peptides and proteins identified, respectively. By the 5<sup>th</sup> extraction a total decrease of 96% (peptides) and 98%

(proteins) from the 1<sup>st</sup> extraction is observed. Between the 1<sup>st</sup> and last extraction, there are no new species being detected, only a loss in identifications of proteins detected in the prior runs. As there are no new species being detected, the results suggest that after the 2<sup>nd</sup> extraction from the same spot the results are diminishing, and combining subsequent extractions after this is unnecessary. However, the ability to perform multiple extractions at the same spot is important for improving sensitivity and generating sufficient signal to produce quality MS/MS data from liquid surface extractions.

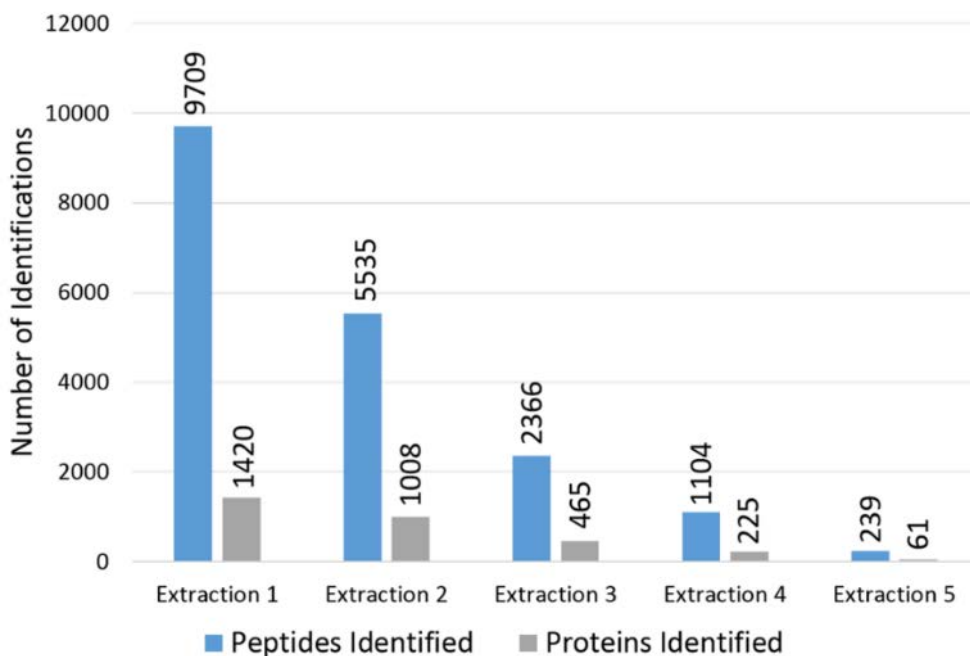


**Figure 3.3:** Five LESA extractions gathered sequentially from the same spot on trypsin-digested rat brain that show a decrease in unique protein identifications and peptides identified through sequential extractions.

### Correlating IMS with LESApplusLC Protein Experiments

Coupling LESApplusLC with LC-based experiments provides a high throughput method for generating spatially-targeted proteomics data for the various proteins and proteoforms observed in imaging MS experiments by minimizing sample preparation and time between experiments. In order to determine the efficacy of coupling LESA directly to LC-MS/MS to analyze intact proteins from tissue, full body tissue sections of mouse pup were prepared. Full body tissue sections serve as an excellent sample to test this spatially-targeted workflow because there are many large heterogeneous substructures in the tissue that can be easily targeted for analysis using the LESApplusLC system without the risk of collecting data from overlapping regions.

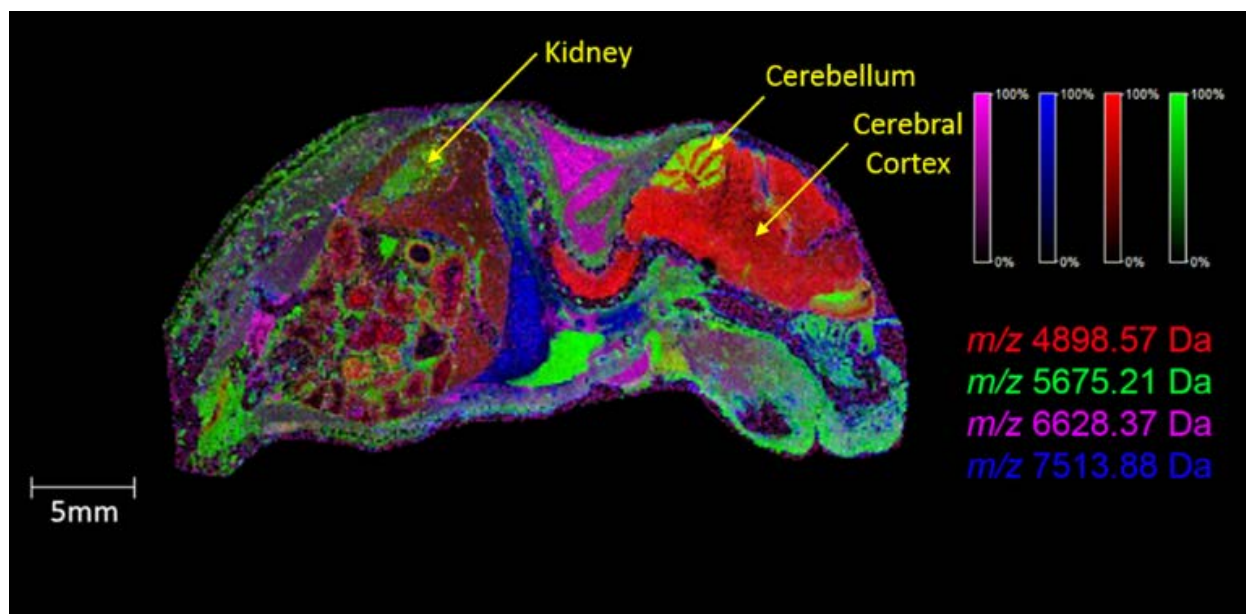


**Figure 3.4:** A sagittal section of mouse pup was imaged at 125  $\mu\text{m}$  in order to determine regions rich in protein signal. An overlay of four ions,  $m/z$  4898.57,  $m/z$  5675.21,  $m/z$  6628.37 and  $m/z$  7513.88, were selected to detail the various substructures of the mouse pup tissue section. Based on intensity and localization of protein signals, the kidney, cerebellum, and cerebral cortex were chosen for interrogation by LESA.

A full body protein image from a mouse pup was acquired on a 15T FT-ICR MS at 125  $\mu\text{m}$  spatial resolution. The data showed a number of unique protein distributions, including  $m/z$  4,898.57,  $m/z$  5675.21,  $m/z$  6,628.37, and  $m/z$  7,513.88 (Figure 3.4). MALDI FT-ICR protein data provide the spectral quality necessary to fully resolve the isotopic envelopes and provide high mass accuracy for the observed ions. Based on these results, the cerebellum, cerebral cortex, and kidney were chosen for interrogation using spatially targeted surface extractions. Adjacent serial tissue sections of the mouse pup were used for LESApplusLC extractions for both bottom-up and top-down experiments. For the bottom-up analysis, two separate, 2  $\mu\text{L}$  surface extractions were combine for each target area. The aliquots were dried down and reconstituted into 10  $\mu\text{L}$  of  $\text{H}_2\text{O}$  (0.5% FA) prior to analysis. The results are presented in Figure 3.5 and Table 3.2 using a Venn diagram to compare the total number of protein identifications and a table highlighting some of the proteins identified that are unique to the area sampled. Both the cerebellum and cerebral cortex extractions yielded a large number of identifications proteins respectively, many of which were identified in both substructures of the brain (1536). Interestingly, the kidney produced far fewer protein ID's than the other two areas sampled.

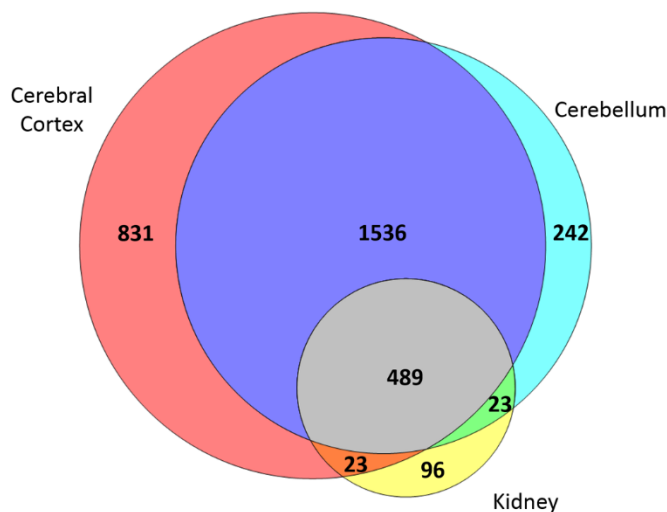


**Figure 3.5:** Proteins identified from 3 regions of a mouse pup tissue section by combining 2 liquid surface extractions from the same spot. In total, 2879 proteins were identified from the cerebral cortex, 2290 proteins were identified from the cerebellum, and 602 proteins were identified from the kidney. The 3 regions tested displayed overlaps in the proteins identified as highlighted in the Venn diagram.

	Accession Number	Description
Kidney	Q91Y97	Fructose-bisphosphate aldolase B
	Q8CGP1	Histone H2B type 1-K
	Q8C196	Carbamoyl-phosphate synthase [ammonia]
	Q9JIL4	Na(+)/H(+) exchange regulatory cofactor NHE-RF3
	Q9QXD1	Peroxisomal acyl-coenzyme A oxidase 2
	P51667	Myosin regulatory light chain 2
	Q9QXD6	Fructose-1,6-bisphosphatase 1
	P52825	Carnitine O-palmitoyltransferase 2, mitochondrial
	Q64442	Sorbitol dehydrogenase
	P70694	Estradiol 17 beta-dehydrogenase 5
Cerebellum	Q8VHQ9	Acyl-coenzyme A thioesterase 11
	Q924X2	Carnitine O-palmitoyltransferase 1, muscle isoform
	Q62203	Splicing factor 3A subunit 2
	Q3UZA1	CapZ-interacting protein
	Q3TMP8	Trimeric intracellular cation channel type A
	Q9Z1E4	Glycogen [starch] synthase, muscle
	P84244	Histone H3.3
	Q9CY02	Alpha-hemoglobin-stabilizing protein
	P57722	Poly(rC)-binding protein 3
	Q9D783	Kelch-like protein 40
Cerebral Cortex	O35143	ATPase inhibitor, mitochondrial
	Q5QNQ9	Collagen alpha-1(XXVII) chain
	P68500	Contactin-5
	P62889	60S ribosomal protein L30
	O54901	OX-2 membrane glycoprotein
	Q91VJ2	Protein kinase C delta-binding protein
	O35668	Huntingtin-associated protein 1
	P55937	Golgin subfamily A member 3
	Q9WU84	Copper chaperone for superoxide dismutase
	Q91YE6	Importin-9

**Table 3.2:** Selected proteins identified from LESApplusLC extracts that are unique to the cerebral cortex, cerebellum, and kidney in mouse pup full body tissue sections.

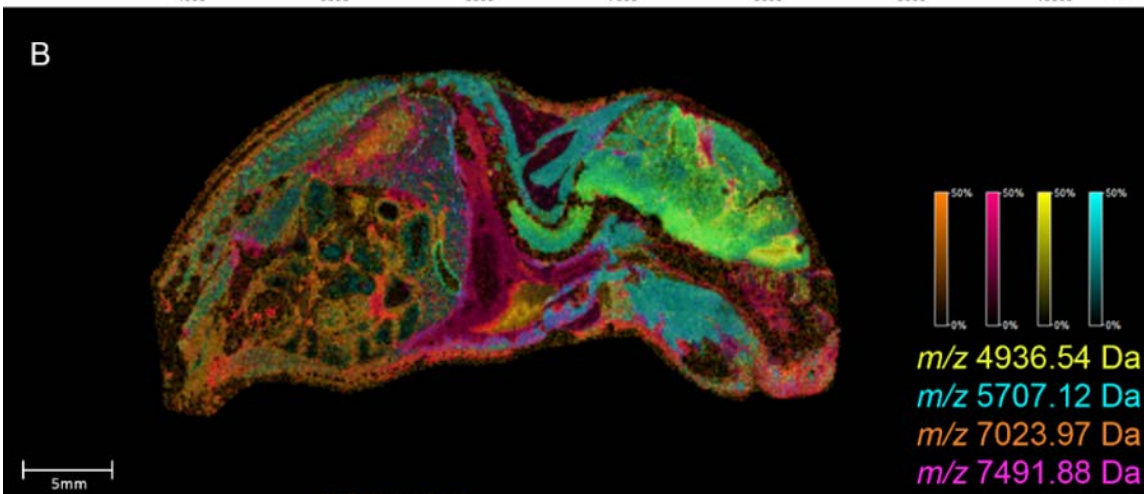
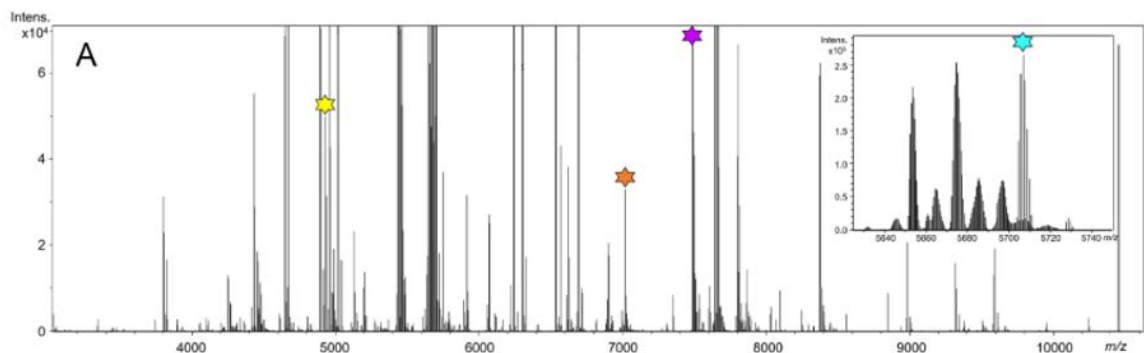
Spatially targeted liquid surface extractions were also used to generate top-down data from full body mouse pup tissue sections. Here, two separate 2  $\mu$ L surface extractions were combined for each target area prior to offline LC-MS/MS analysis. Top-down results were initially processed

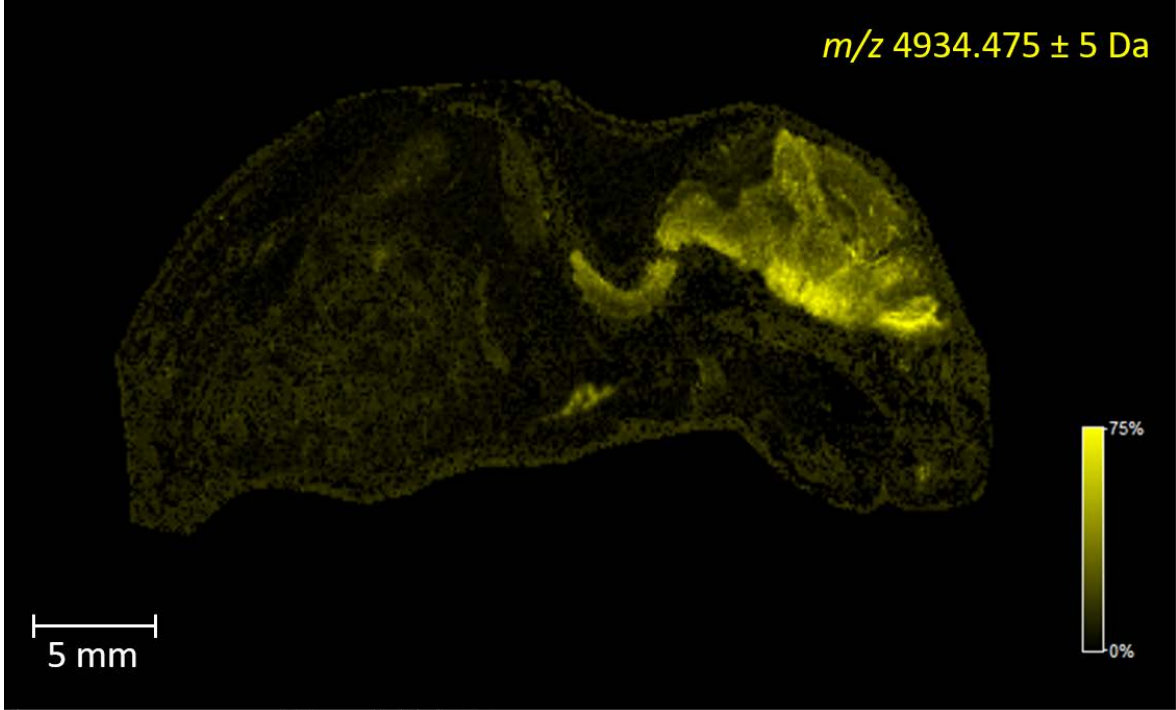
using the proteomics search engine Byonic optimized for ETD data. The results from these searches identified 27, 33, and 38 intact proteins from the kidney, cerebral cortex, and cerebellum, respectively, out of a total of 81, 69, and 72 intact protein species detected during LC-MS/MS analysis. Based on these results, selected proteins were then chosen for de novo manual interpretation guided by the database results to improve overall sequence coverage (Figure 3.6). Proteins detected in the imaging experiment were correlated to identifications from the top-down data by matching the intact accurate masses of the two experiments to within 2 ppm. The ion at  $m/z$  4,936.540 was determined to be N-term Acetylated Thymosin  $\beta$ 10 (0.36 ppm), a protein that has been shown to bind and sequester G-actin (Figure 3.6D).<sup>166</sup> Thymosin  $\beta$ 10 is known to be abundant in brain tissue and was found localized mainly to cerebral cortex (Figure 3.6C).<sup>167</sup> The ion at  $m/z$  5707.118 was determined to be ATP synthase subunit  $\epsilon$  (-1.08 ppm). ATP Synthase is a general mitochondrial protein responsible for converting ADP to the ATP (Figure 3.6F) and can be localized to many different tissue types.<sup>168, 169</sup> This protein was found to be localized to all 3 targeted regions (Figure 3.6E). The ion observed at  $m/z$  7023.974 in the MALDI IMS data was identified as the N-terminally acetylated form of Histone H2A (-0.56 ppm) (Figure 3.6H) in its +2 charge state. This ion was found to be localized in the cerebellum and kidney (Figure 3.6G). Histone H2A plays an important role in the folding of DNA in chromatin<sup>170</sup> and is known to be elevated in tissue that has undergone trauma or disease.<sup>171</sup> Here it was found localized to the cerebellum and kidney regions. The dimethylated form of hemoglobin subunit A was determined to be the ion at  $m/z$  7491.884 (-1.41 ppm), in its +2 charge-state, and can be seen localized to the kidney (Figures 3.6I and 3.6J). Subunit A is one of the 4 major subunits that make up hemoglobin, an important oxygen-transporting metalloprotein found in red blood cells, which are produced in the kidney.<sup>172, 173</sup> The mass range of the proteins identified span from 4,500 to 18,000 Da. From



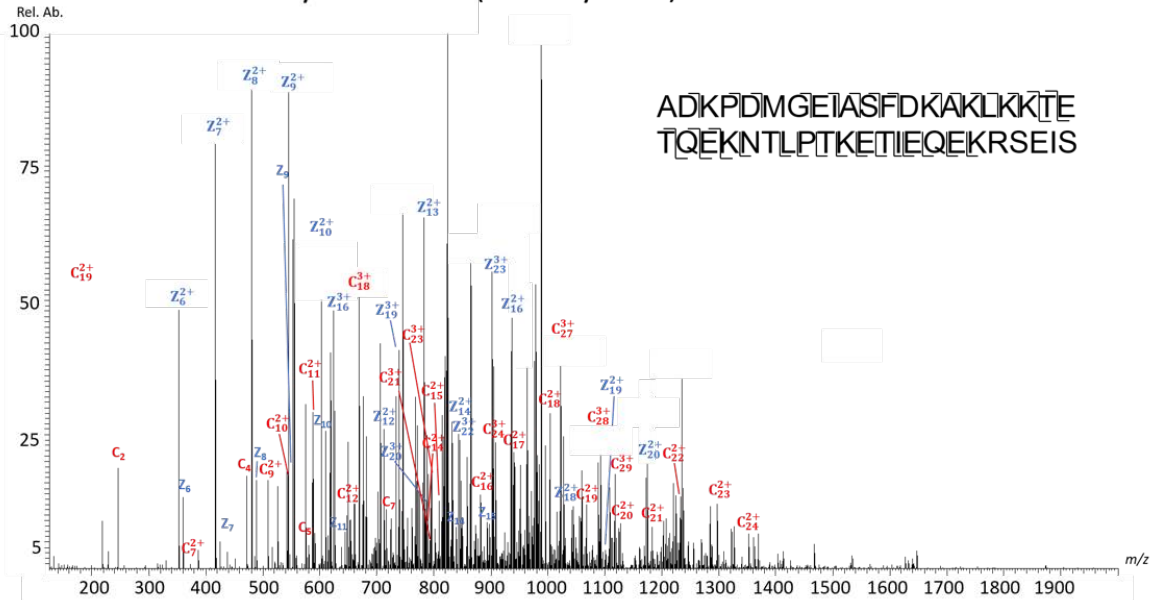
the 4 proteins identified by top-down sequencing, 3 were found to be correlated to the 3 regions subjected for bottom-up mass spectrometry in the prior section. Thymosin beta-10 was not found to be in any of the bottom-up extractions.

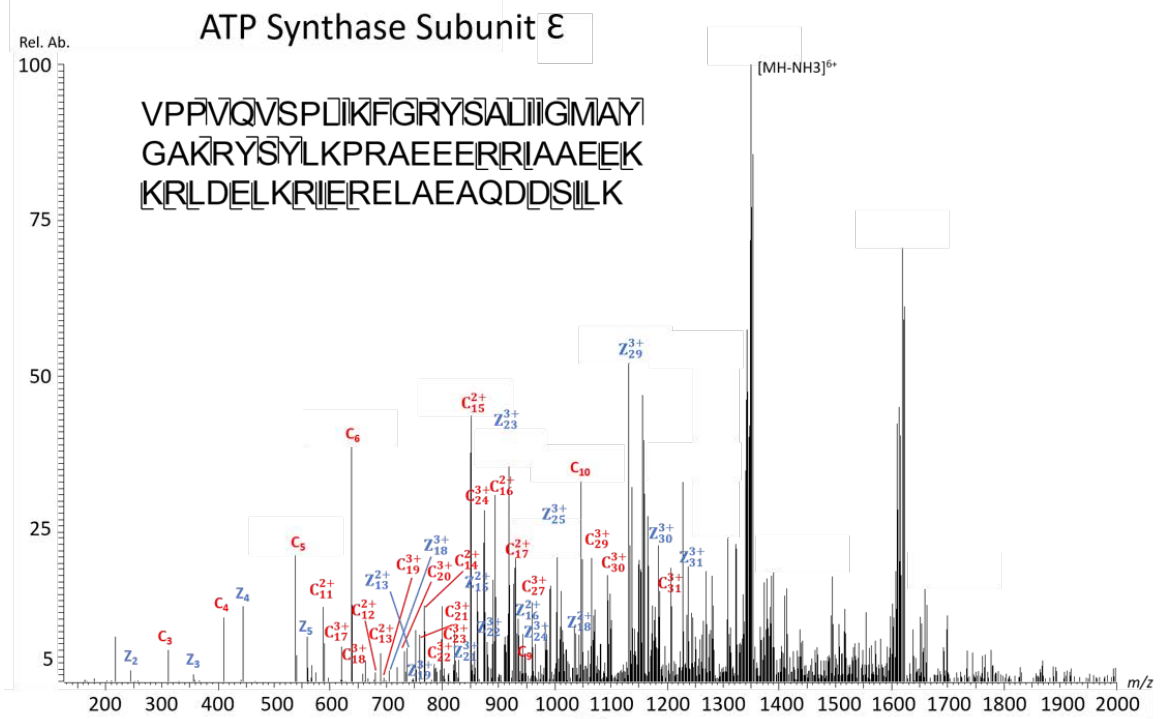
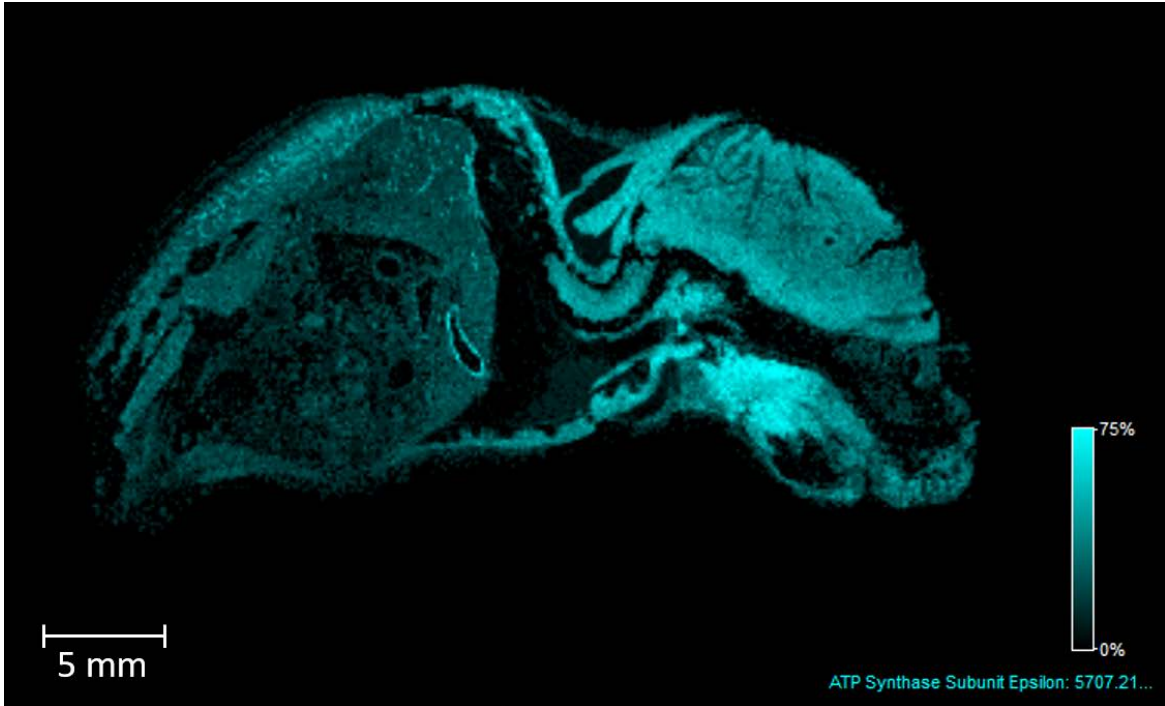
A unique advantage of the LESApplusLC system is the ability to perform online LC-MS experiments with a surface extraction. This feature maximizes throughput and minimalizes potential sample loss during preparation steps. In order to test the performance of this methodology, intact proteins were extracted from the same three target areas mentioned above (cerebellum, cerebral cortex, and kidney) within the full body mouse pup tissue section and subjected to online LC-MS in triplicate. A single 2  $\mu$ L extract was gathered by dispensing the extraction volume five times (15 s each) onto the tissue surface and then automatically injecting it onto the sample loop directly. The total number of proteins detected for each run ( $S/N > 3$ ) was determined using the deconvoluted average mass spectra over the entire LC experiment (select chromatograms for each target area are depicted in Figure 3.7). From the cerebellum a total of  $60 \pm 6$  proteins were detected while the kidney and cerebral cortex yielded  $57 \pm 13$ , and  $52 \pm 15$  respectively. Though the relatively slow scan time of the FT-ICR prevented LC-MS/MS identification, the number of protein species detected are comparable to previous methods using hand pipetting.<sup>75</sup> Additionally, although previous studies have demonstrated online LC-based analysis from liquid surface extractions using home-built systems,<sup>159, 160</sup> this is the first example of this capability being demonstrated for proteins using the commercial LESApplusLC platform. Future studies will examine implementing this online workflow on a MS platform more amenable to top-down LC-MS/MS experiments.

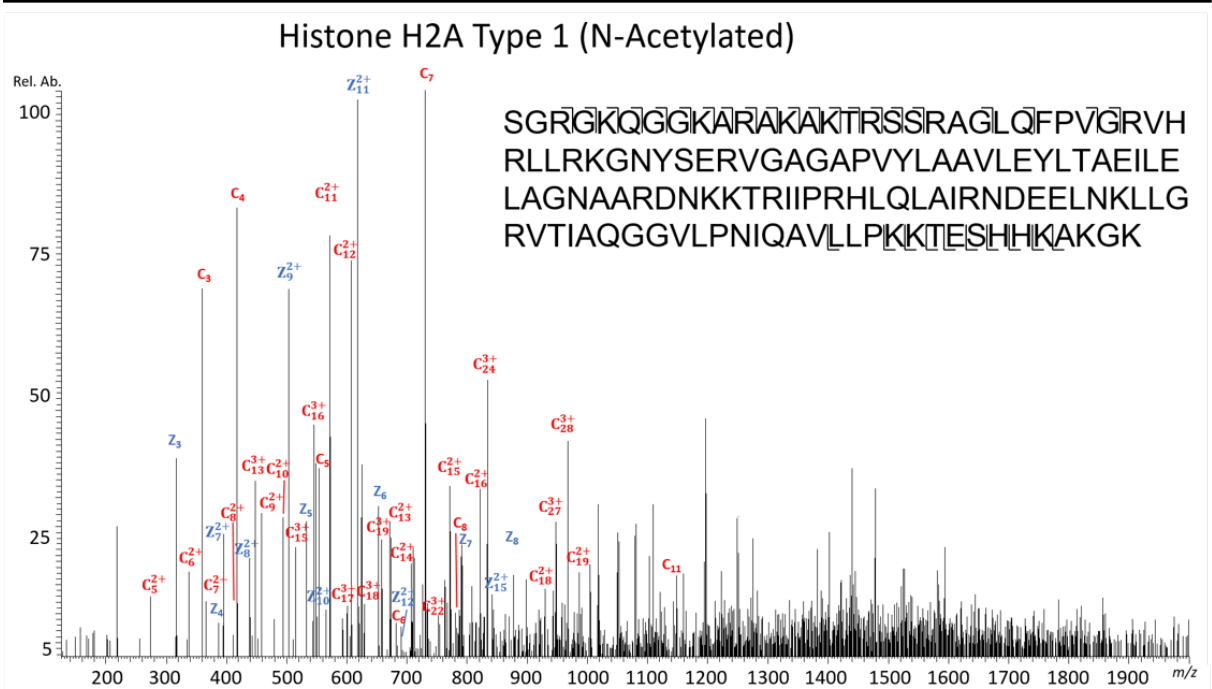
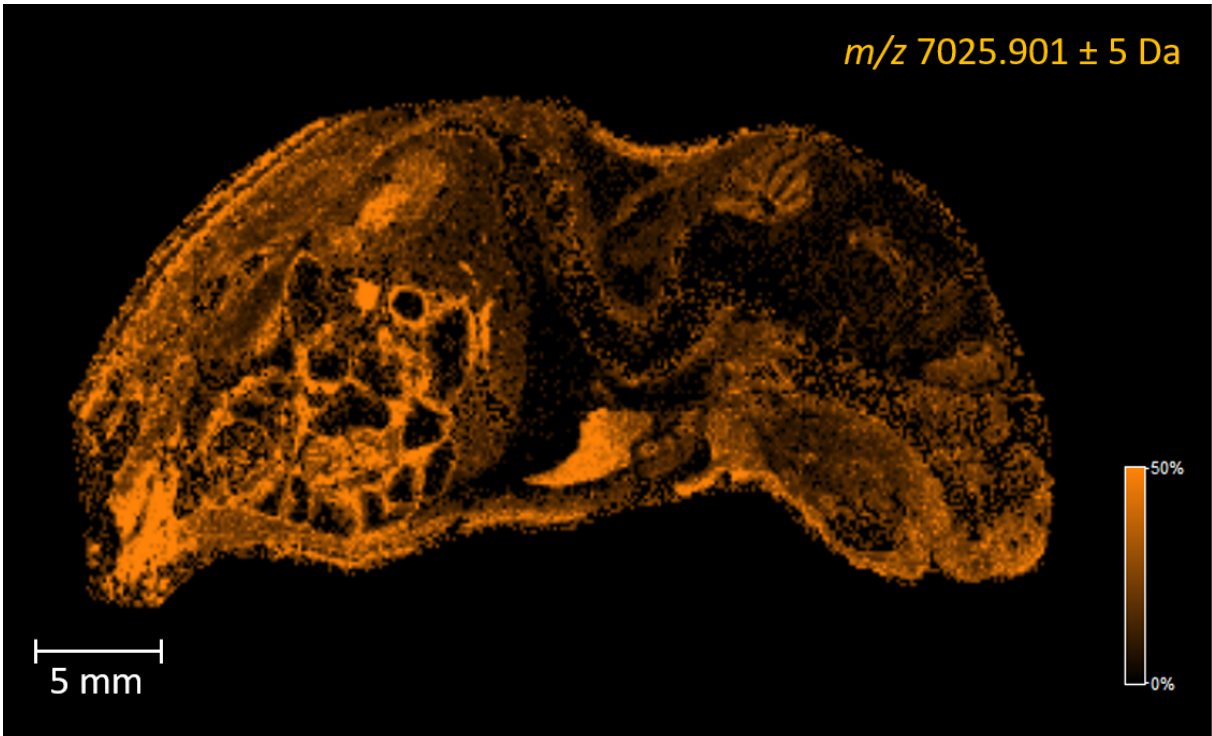




Thymosin B10 (N-acetylated)







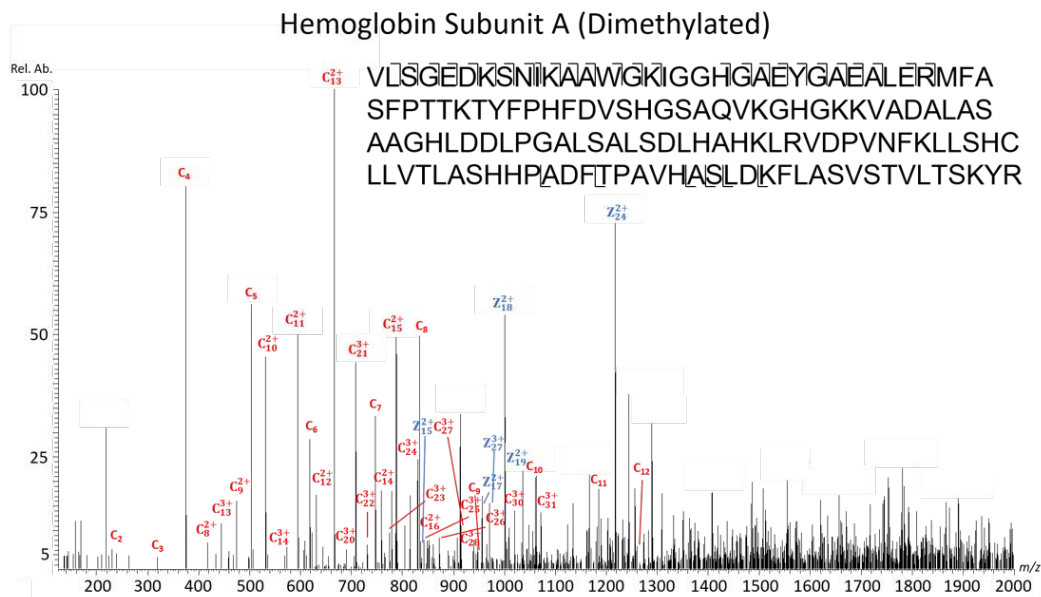
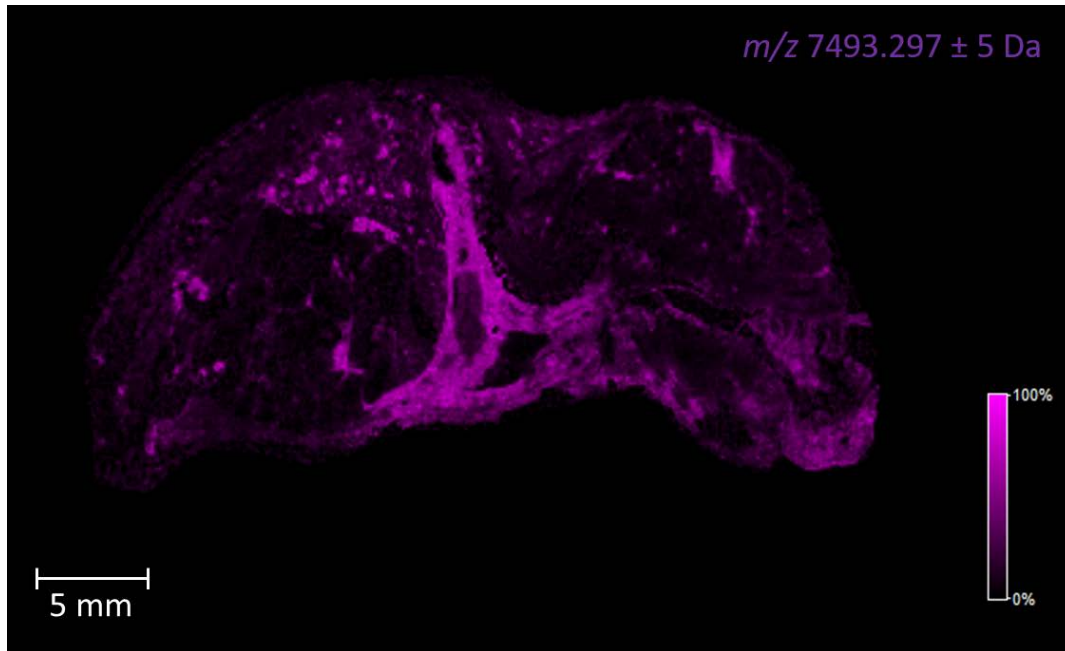


**Figure 3.6:** A & B) Spectral and imaging data from a 125  $\mu\text{m}$  spatial resolution MALDI protein image from a sagittal section of a mouse pup acquired on a 15T FT-ICR MS. Four ions were chosen to exemplify the many tissue substructures present as highlighted in the image overlay (B). The proteins sequenced below are highlighted by a star in the average mass spectrum of the protein image. C & D) The high resolution, top-down mass spectrum of  $m/z$  4,898.57 allows for its identification as N-acetylated Thymosin  $\beta$ 10. E & F) The high resolution, top-down mass spectrum of  $m/z$  5,675.21 allows for its identification as ATP synthase subunit  $\epsilon$ . G & H) The high resolution, top-down mass spectrum of  $m/z$  6,628.37 (+2) allows for its identification as N-acetylated histone H2A Type 1. I & J) The high resolution, top-down mass spectrum of  $m/z$  7,513.88 (+2) allows for its identification as dimethylated hemoglobin subunit A.

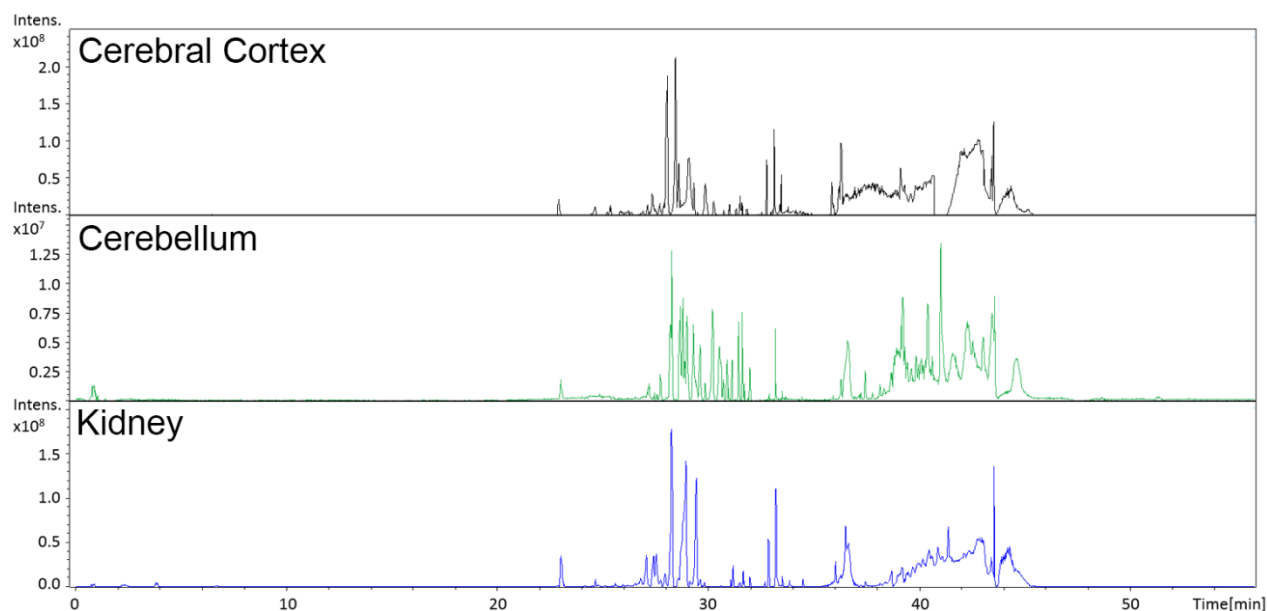


**Figure 3.7:** Total ion chromatograms (TIC) from the selected tissue regions from mouse pup analyzed by LESAplus coupled to online LC-FT-ICR MS.

## Discussion

This work has demonstrated the capabilities of robotically-controlled, spatially-targeted liquid surface extractions coupled to online and offline proteomics workflows for identifying proteins observed in imaging mass spectrometry experiments. A number of experimental characteristics were measured to assess the efficiency of the LESAplusLC extraction including extraction spot size, number of peptides detected, and number of proteins identified across multiple experiments. Utilization of a glass capillary for extractions allows for improved droplet resolutions ( $< 600 \mu\text{m}$  on water sensitive paper) and reproducibility (relative standard deviations of  $< 5\%$ ) for most experiments. Comparisons of spatially-targeted proteomic techniques such as hydrogel experiments, laser capture laser microscopy (LCM), and tissue homogenization have been discussed elsewhere.<sup>74</sup> In these studies, 1.5 mm LCM, 1.5 mm tissue punch/digestion,

and 1.67 mm hydrogel experiments yielded ~800-1000 protein identifications whereas the 1.0  $\mu$ L LESA experiment (1.71 mm on tissue) described herein yielded ~1120 protein identifications. Although a modest improvement in the number of protein identifications, the LESAplusLC workflow is a significant improvement in throughput relative to other approaches. Hydrogels, tissue punches, and LCM are all time-consuming experiments, while the automated LESA extraction can generate samples, ready for LC-MS/MS analysis, in ~10 minutes. Additionally, the tissue is preserved during LESA experiments, allowing for sequential extractions that effectively improve the sensitivity of the technique. Finally, direct coupling of LESAplusLC to HPLC allows for the generation of online LC-MS data directly from tissue with minimal sample preparation. Using only a single 2  $\mu$ L extraction, we were able to detect upwards of 60 proteins from various regions of tissue. Robotic liquid micro-extractions allow for a more reproducible approach to generating protein identifications to complement an IMS workflow. The combination of robotic extraction and online LC technologies allows for the rapid collection of spatially-targeted protein identifications that can be correlated to imaging MS data using accurate mass-matching. The spatial sampling precision, coupled with robustness and reproducibility, make the LESAplusLC technique more suitable for high-throughput spatial proteomic experiments than previous manual methodologies and will aid in the challenge of identifying proteins observed by MALDI IMS.

## **Methods**

### *Tissue Preparation*

One week old C57BL/6 control mice that had been stored at -80 °C were shaved over dry ice to remove as much hair as possible to avoid contamination during sample preparations and IMS.



Frozen rat brain was purchased from Pel-Freeze Biologicals (Rogers, AR, USA), and was stored at -80 °C until sectioning. In all cases, tissue was sectioned (12 µm thickness) at -15 °C using a CryoStar™ NX70 Cryostat (Thermo Fisher Scientific, San Jose, CA, USA), thaw mounted onto conductive indium-tin-oxide coated slides (Delta Technologies), and dried in a vacuum desiccator for at least 20 minutes prior to preparation for analysis. To maximize sensitivity for proteins and peptides, tissue sections underwent a washing protocol to remove lipids and salts. The wash steps included 70% ethanol (30s), 100% ethanol (30s), Carnoy's Wash (6:3:1 ethanol:chloroform:acetic acid), 100% ethanol (30s), water (30s), and 100% ethanol (30s) as described previously.<sup>174</sup> Animal husbandry and experimental procedures were conducted in agreement with Public Health Service policy and approved by the Vanderbilt University School of Medicine Institutional Animal Care and Use Committee.

### *MALDI IMS*

For imaging experiments, MALDI matrix (DHA) was applied to the sample using a robotic sprayer (TM Sprayer, HTX Technologies, Carrboro, NC, US) at a concentration of 15 mg/mL in 9:1, ACN:H<sub>2</sub>O. The sprayer nozzle was set to spray at 80 °C using a carrier solvent of 9:1 ACN:H<sub>2</sub>O at a flow rate of 0.1 mL/min and a drying sheath gas of dry nitrogen set to 10 psi. Four passes of matrix were applied using alternating offsets (1 mm) and directional rotations (90 degrees) with a 2 mm track spacing. The spray velocity was set to 1100 mm/min with a 2 s dry time between passes and 40 mm nozzle height. The matrix layer on the sample was recrystallized prior to MALDI analysis as previously described using 1.0 mL of 1:1, TFA:H<sub>2</sub>O at 37 °C for 3 minutes.<sup>20</sup> The image was acquired in positive ion mode at 125 µm spatial resolution on a Bruker Solarix 15T FT-ICR MS (Bruker Daltonics, Billerica, MA, USA). The instrument employs a Smartbeam II 2 kHz frequency tripled Nd:YAG (355 nm) laser, as well as an Apollo II dual MALDI/ESI ion

source. Each pixel was the sum of 2000 laser shots, using the smallest laser focus (~50  $\mu\text{m}$ ), while random-walking the target within the 125  $\mu\text{m}$  pixel. The mass spectrometer was externally calibrated prior to analysis using a protein mixture (insulin, cytochrome C, trypsinogen, and apomyoglobin). Data were collected from  $m/z$  1,385 - 20,000 with a time-domain file size of 512K (FID length: 1.6078 s), yielding a resolving power of ~42,000 at  $m/z$  5000. In order to generate an image with a higher mass range, the ion optics were tuned as follows: accumulation hexapole (1.4 MHz, 1700 Vpp), time-of-flight delay (2.1 ms), funnel RF amplitude (200 Vpp), transfer optics (2 MHz, 380 Vpp), and ICR cell (sweep excitation power: 40%).

#### *In Situ Tryptic Digestion*

Trypsin was dissolved into 333  $\mu\text{L}$  of ammonium bicarbonate (100 mM, pH~8.50), 67  $\mu\text{L}$  of acetic acid (100 mM), and 40  $\mu\text{L}$  of acetonitrile to a final concentration of 0.045  $\mu\text{g}/\mu\text{L}$ . The sample was sprayed at a temperature of 30  $^{\circ}\text{C}$  using the TM Sprayer for 8 total passes using alternating directional rotations and offsets. The sprayer used a flow rate of 0.0075 mL/min, with a 2 mm track spacing, a nozzle height of 40 mm, and a velocity of 700 mm/min using a syringe pump.<sup>149</sup> Immediately following trypsin application, samples were left to digest overnight at 37  $^{\circ}\text{C}$  in a covered dish that contained 3 mL of 100 mM ammonium bicarbonate.

#### *Tissue Extractions*

Tissue extractions were completed using the TriVersa NanoMate (Advion, Inc., Ithaca, NY, USA) modified to include a glass capillary (LESAPLUSLC) for improved spatial resolution and online integration with LC-based experiments.<sup>165</sup> Scanned images of thaw-mounted samples were uploaded to the ChipSoft Software (Advion, Inc., Ithaca, NY, USA) to allow histological regions of interest to be selected for analysis. For online LC-MS analysis of intact proteins, extractions

were completed by aspirating 3  $\mu\text{L}$  of extraction solvent (1:1 ACN:H<sub>2</sub>O with 0.5% FA) and dispensing 2  $\mu\text{L}$  on tissue. The dispensed extraction solvent was left on tissue for 15 s prior to re-aspiration back into the capillary. This process was repeated 5 times, after which the capillary was moved back to the solvent well to draw enough solvent to load the sample into the sample loop (~6  $\mu\text{L}$  volume) on a 6-port HPLC valve. All extractions were completed by dispensing the volume from the capillary at a height of 0.5 mm above the surface of the sample. For top-down experiments not directly coupled to the LC, extractions were completed in the same manner but deposited into a single well of a 96-well plate that contained 15  $\mu\text{L}$  of H<sub>2</sub>O (0.5% FA). The contents of that well were then injected onto the column immediately for LC-MS analysis (see below for details).

For peptide extractions, on-tissue tryptic digestion was performed as described above. For all bottom-up offline experiments, a combination of 1:1 ACN:H<sub>2</sub>O (0.5% FA) was used as the extraction solvent. Extractions were all completed using an initial aspirated volume of 3.0  $\mu\text{L}$  while varying the total amount dispensed on tissue. Instead of being pulled into the 6-port valve for the dispensing/aspirating, the aliquots were deposited into a single well of a 96-well plate that contained 100  $\mu\text{L}$  of H<sub>2</sub>O (0.5% FA). Samples were dried down using a desktop vacuum centrifuge (Thermo Fisher Scientific, San Jose, CA, USA) and stored at -80 °C until analysis. For the droplet resolution experiments, hematoxylin stain was used for the extraction solvent as the liquid can penetrate the cell nucleus, allowing for visualization of solvent diffusion and measurement of extraction spot size on rat brain tissue. Extraction solvents were able to interact with the surface for 30 seconds and repeated twice to ensure the stain had enough time to penetrate the cells. Additionally, extraction spot size measurements were made by dispensing varying volumes of solvent onto water sensitive paper (Rittenhouse, St. Catherines, Ontario, CA). Following spot size

experiments, the tissue sections or water sensitive paper were left to dry under vacuum and spot size measurements were made using an optical microscope (Olympus, Center Valley, PA, USA).

#### *Online LC-MS*

For the online LC-MS experiments, proteins were eluted using an analytical column which was packed with 20 cm of C4 reverse phase material (Halo Protein C4, 3.4  $\mu\text{m}$ , 400 $\text{\AA}$ ) with a laser-pulled emitter tip. Proteins were loaded on the capillary reverse phase analytical column (360  $\mu\text{m}$  O.D. x 150  $\mu\text{m}$  I.D.) using a Waters nanoACQUITY UPLC (Waters Corporations, Milford, MA, USA) where mobile phase A consisted of 0.1% formic acid, 99.99% water, and mobile phase B consisted of 0.1% formic acid, 99.99% acetonitrile, eluting at 0.600  $\mu\text{L}/\text{min}$ . Ions were generated using a Bruker Captive Spray nanoelectrospray source (Bruker Daltonics, Billerica, MA, USA) and directed into a Bruker SolariX 15T FT-ICR MS (Bruker Daltonics, Billerica, MA, USA). The mass spectrometer was set to scan from  $m/z$  230-2,000, with a file size of 1M yielding a resolving power of 150,000 at  $m/z$  400 (FID length: 0.5243 s). Ion optics were tuned as follows: accumulation hexapole (2 MHz, 1200 Vpp), time-of-flight delay (0.8 ms), funnel RF amplitude (280 Vpp), transfer optics (4 MHz, 290 Vpp), and ICR cell (sweep excitation power: 18%).

#### *Bottom-Up Tandem Mass Spectrometry*

Bottom-up mass spectrometry was employed to identify proteins from targeted regions detected during IMS analysis of the mouse pup and to characterize the efficiency of various extraction conditions on brain tissue. For the mouse pup experiment, tryptic peptides from the tissue extracts were injected and gradient eluted on a pulled tip emitter column (360  $\mu\text{m}$  O.D. x 100  $\mu\text{m}$  I.D. x 35 cm) packed in-house with C18 material (Waters BEH C18, 1.7  $\mu\text{m}$ , 130  $\text{\AA}$ ). The column was heated to 60  $^{\circ}\text{C}$  with a flow rate of 400 nL/min during operation using an Easy-nLC

1000 UHPLC (Thermo Scientific, San Jose, CA, USA), where the mobile phase A consisted of 0.1% formic acid, 99.9% water, and mobile phase B consisted of 0.1% formic acid, 99.9% acetonitrile. Peptides were eluted on the reverse phase column using a linear gradient of 2-20% B for 100 minutes, followed by 20-32% B for 20 minutes, and lastly 32-95% B for 1 minute. An Orbitrap Fusion Tribrid mass spectrometer (Thermo Scientific, San Jose, CA, USA) was used to mass analyze the eluting peptides. MS1 scans were acquired using the Orbitrap at 120k resolution, a mass range of 400-1600  $m/z$ , an automatic gain control (AGC) target of  $1.0 \times 10^6$ , and a maximum injection time of 100 ms. The top 17 most abundant ions measured in the MS1 scans were then mass isolated using a quadrupole mass filter at 2  $m/z$  window width to undergo fragmentation in the HCD cell using 35% normalized collision energy. The fragmented ions are subsequently mass analyzed in the linear ion trap using an AGC target of  $1 \times 10^4$ , a maximum injection time of 35 ms, and the normal scanning rate setting. Dynamic exclusion of 30 s was used for all MS2 scans. For identification of peptides, tandem mass spectra were searched using Protalizer software (Vulcan Analytic, Birmingham, Alabama, USA) against a rat database created from the UniprotKB protein database ([www.uniprot.org](http://www.uniprot.org)). Variable modifications such as carbamidomethyl, phosphorylation, methionine oxidation, and deamidation were included in the database search. Proteins were identified with at least 2 unique peptides per protein, with a false discovery rate of 1%.

For the extraction characterization experiments, an analytical column was packed with 22 cm of C18 reverse phase material (Jupiter, 3  $\mu\text{m}$  beads, 300Å, Phenomenox) directly into a laser-pulled emitter tip (Sutter Instrument Company, Novato, CA, USA). Peptides were loaded on the capillary reverse phase analytical column (360  $\mu\text{m}$  O.D. x 100  $\mu\text{m}$  I.D.) using a Dionex Ultimate 3000 nanoLC and autosampler. The mobile phase solvents consisted of 0.1% formic acid, 99.9% water (solvent A) and 0.1% formic acid, 99.9% acetonitrile (solvent B). Peptides were eluted with

a gradient at a flow rate of 350 nL/min. The 95 minute elution was performed as follows: 1-3 min, 2% B (sample loading from autosampler); 3-78 min, 2-40% B; 78-84 min, 40-90% B; 84-86 min, 90% B; 86-87 min, 90-2% B; 87-95 min (column re-equilibration), 2% B. A Thermo Q Exactive Plus Orbitrap mass spectrometer (Thermo Scientific, San Jose, CA, USA), equipped with a nanoelectrospray ionization source, was used to analyze the eluting peptides. The instrument method consisted of MS1 using an MS AGC target value of  $3 \times 10^6$ , followed by up to 15 MS/MS scans of the most abundant ions detected in the preceding MS scan. A maximum MS/MS ion accumulation time of 80 ms was used with a MS<sup>2</sup> AGC target of  $1 \times 10^5$  and an intensity threshold of  $2.5 \times 10^4$ . Dynamic exclusion was set to 30s, HCD collision energy was set to 27 normalized collisional energy, and peptide match and isotope exclusion were enabled. Peptides were identified using Protalizer (Vulcan Analytic, Birmingham, Alabama, USA) as described above.

#### *Top-Down Tandem-Mass Spectrometry*

For top-down tandem mass spectrometry of the extractions not directly coupled to the LC from the three targeted regions of mouse pup, extracted proteins were diluted 5-fold in 0.1% formic acid and were loaded onto a reverse-phase capillary trap column using a helium-pressurized cell. The trap column (360  $\mu\text{m}$  OD x 150  $\mu\text{m}$  ID) was fritted with a filter end-fitting (IDEX Health & Science) and packed with 4 cm of C4 reverse phase material (Halo, 400 Å). An M-520 microfilter union (IDEX Health & Science) was used to connect the trap column to a capillary analytical column (360  $\mu\text{m}$  OD x 100  $\mu\text{m}$  ID), which was equipped with a laser-pulled emitter tip and packed with 15 cm of C4 material. Using an Eksigent NanoLC Ultra HPLC, proteins were gradient-eluted at a flow rate of 500 nL/min, and the mobile phase solvents consisted of 0.1% formic acid, 99.9% water (solvent A) and 0.1% formic acid, 99.9% acetonitrile (solvent B). A 100-minute gradient was performed and eluted proteins were mass analyzed using an ETD-enabled LTQ Orbitrap Velos

mass spectrometer with a nanoelectrospray ionization source (Thermo Scientific, San Jose, CA, USA). The instrument was operated using a data-dependent method. A full scan spectrum of  $m/z$  400–2000 was acquired as the initial scan event per duty cycle. Following the full-scan, four data-dependent scan events were performed using ETD in the linear ion trap for the four most abundant ions in each MS scan. Dynamic exclusion was enabled allowing a repeat count of 1 within 20 seconds. ETD tandem mass spectra were acquired sequentially using the linear ion trap followed by the Orbitrap (resolving power 15,000 at  $m/z$  400) for mass analysis. An isolation width of 3  $m/z$  and an ETD reaction time of 90 ms were used for MS/MS analysis. The MS<sup>n</sup> AGC target value in the ion trap was set to  $2 \times 10^4$ , the MS<sup>n</sup> AGC target for Orbitrap scan events was  $8 \times 10^5$ , and the ETD reagent ion (fluoranthene) AGC target was set to  $1 \times 10^5$ . Protein Metrics Byonic (San Carlos, CA, USA) search engines were used to process the raw data against a rat protein database created from the UniprotKB protein database. Variable modifications including methionine oxidation, methylation, demethylation, and phosphorylation were used in the search and the false discovery rate was set to 1%. Database results were used to guide manual de novo sequencing. All proteins selected for de novo sequencing had Byonic identification scores  $>1,000$ .

## CHAPTER IV

### **MICROLESA: INTEGRATING AUTOFLUORESCENCE MICROSCOPY, IN SITU MICRO-DIGESTIONS, AND LIQUID EXTRACTION SURFACE ANALYSIS FOR HIGH SPATIAL RESOLUTION TARGETED PROTEOMIC STUDIES**

This chapter was adapted from the previous published Ryan et al., *Analytical Chemistry*,

Copyright 2019 by ACS

#### **Overview**

The ability to target discrete features within tissue using liquid surface extractions enables the identification of proteins while maintaining the spatial integrity of the sample. Previous approaches employing a standard liquid micro-extract was limited to interrogate tissue foci on the order of 600  $\mu\text{m}$  in diameter. In order to combat this limitation, a liquid extraction surface analysis (LESA) workflow, coined microLESA, was developed. This new workflow allows proteomic profiling from discrete tissue features ( $<150$   $\mu\text{m}$  in diameter) by integrating non-destructive autofluorescence microscopy and spatially targeted liquid micro-digestions with LESAs. Autofluorescence microscopy provides the visualization of tissue foci without the need for chemical stains on the section of tissue or the use of serial tissue sections. Tryptic peptides are generated from tissue foci by applying picoliter (pL) droplets of enzyme onto the surface prior to LESAs. The microLESA workflow reduced the diameter of the sampled area almost 5-fold compared to previous LESAs approaches. Experimental parameters were tested and optimized for



the enzymatic micro-digest, such as tissue thickness, trypsin concentration, and incubation duration. The microLESA workflow was applied to the study of fluorescently-labeled *Staphylococcus aureus* infected murine kidney in order to identify unique proteins related to host defense and bacterial pathogenesis. Proteins related to nutritional immunity and host immune response were identified by performing microLESA at the infectious foci and surrounding abscess. These identifications were then used to annotate specific proteins observed in infected kidney tissue by MALDI FT-ICR IMS through accurate mass matching.

## Introduction

The ability to determine the spatial distribution of a protein species, and their various proteoforms (e.g. post-translational modifications), in a tissue sample has proven useful in interrogating biological processes related to health and disease.<sup>59, 143, 175</sup> In many cases, this is done using MALDI MS by either collecting individual spectra from discrete foci as a histology guided profiling experiment<sup>140, 176</sup> or by imaging the tissue by rastering the sample to collect spectra at every pixel location.<sup>41, 149</sup> However, identification of proteins directly from tissue using MALDI can be challenging due to reasons discussed in earlier chapters, such as fragmentation efficiency. Traditionally, homogenized tissue extractions have been used to compliment MALDI MS experiments and provide identifications.<sup>50, 177</sup> These methods have proven to be effective and allow for relative and absolute quantification of the analytes extracted from tissue.<sup>178, 179</sup> Although bulk homogenization of the sample maximizes analyte extraction, the process leads to a complete loss of the spatial information making identification of protein signals from distinct foci difficult.

Spatially targeted protein identification strategies have been developed that extract material from tissue surfaces using spatially targeted means to correlate proteomic identifications with

specific tissue foci observed in spatially targeted MALDI experiments. Proteomic profiling of discrete tissue foci has been accomplished using different approaches: tissue punch biopsies,<sup>180, 181</sup> laser capture microdissection (LCM),<sup>182-184</sup> hydrogel extractions,<sup>74, 152</sup> and liquid micro-junctions.<sup>156, 157</sup> LESA was shown earlier to be an effective, high-throughput approach for spatially targeted protein identifications.<sup>185</sup> The LESA experiment utilizes small volumes of solvent (~0.5-3.0  $\mu\text{L}$ ) that can be manipulated on the tissue section surface to extract analytes. A glass capillary delivers and dispenses the solvent on the tissue while maintaining a liquid micro-junction between the tip, liquid, and sample allowing for the extraction of endogenous molecules into the solvent. Following surface contact, the liquid can be aspirated off the sample and collected for off-line workflows or directly injected into a mass spectrometer for analysis. Although efficient, the LESA droplet diameter on tissue of approximately 500-600  $\mu\text{m}$  and is the limiting factor in determining what foci can be interrogated. The ability to resolve small histological foci using MALDI has created the need to advance these complimentary molecular identification technologies to achieve similar spatial fidelity.

The deposition of small volume droplets (< 500 pL) of liquid (matrix or trypsin) is used routinely to profile discrete regions of tissue by MALDI MS.<sup>151</sup> This type of droplet-based deposition has been demonstrated to enable MS analysis of these tissue areas. For trypsin droplet deposition experiments, MALDI is typically used for analysis but LESA has also been demonstrated to be effective for extracting peptides from areas digested using LESA-based approaches. Prior research combined droplet-based trypsin deposition with liquid micro-extraction to decrease the area of the region to be subjected to enzymatic digestion.<sup>186</sup> This approach bypasses the typical limitations imposed by LESA (i.e. large extraction droplet diameter on tissue) by targeting tryptic peptides that are produced only in the tissue foci where the droplet-based micro-

digest has been performed. Although this represents an improvement over traditional LESA workflows, further development is needed to improve spatial resolution and precision so that spatially targeted proteomics experiments can be performed on specific tissue substructures and cell types.

*Staphylococcus aureus* is a widely studied Gram-positive bacterium that is responsible for over 40,000 deaths annually.<sup>187, 188</sup> *S. aureus* infections often lead to the generation of purulent, inflammatory foci known as an abscess. *S. aureus* infection and subsequent abscess formation is best described in 4 stages.<sup>189</sup> Initially, the opportunistic bacteria enters the body and eventual peripheral tissue while circulating through the bloodstream. A lesion is induced and a chemotactic response initiates the massive migration of host immune cells such as neutrophils, leukocytes, and other phagocytes.<sup>190</sup> The abscess begins to mature and grow in size, and present a central accumulation of pathogen. The regions surrounding the SAC are composed of necrotic tissue, a fibrin pseudocapsule, and a micro-colony associated meshwork.<sup>191</sup> These surrounding regions of the abscess are dynamic in nature, with both the host and bacteria fighting for survival. For example, the host has evolved mechanisms to hamper bacterial growth by sequestering metal vital for the development and progression of *S. aureus*, a process known as nutritional immunity.<sup>192</sup> Finally, growing abscesses will rupture causing secondary infections through the spread of bacteria. It is this final stage of the abscess formation where the bacteria begin to infect new sites, and without antimicrobial intervention, the host often dies from the infection.<sup>189</sup>

MALDI IMS has been applied to study the site of a *S. aureus* infection, as it allows for the ex vivo analysis of key molecules involved in the infections progression, and their distribution to specific cellular areas.<sup>193</sup> For example, using MALDI IMS the metal-chelating heterodimer calprotectin, consisting of the subunits S100A8 and S100A9, was found to localize to the site of

infection where it binds and removes metals which are essential to the bacteria's growth and disease progression.<sup>139</sup> The major hurdle in imaging proteins from the infectious foci is identifying the resulting peaks in the average mass spectrum. Commonly, orthogonal approaches such as tissue homogenization or LESA are used to gather spatially targeted identifications. Although useful, these approaches severely limit what foci can be targeted. Bacterial colonies are on the order of 10-20  $\mu\text{m}$  in diameter, and are very difficult to visualize through traditional microscopy without any prior histological staining.<sup>194, 195</sup> Through the incorporation of fluorescently-labeled bacteria the user can better visualize these bacterial colonies at the site of infection, which would normally be difficult to target using AF alone due to a lack of contrast with the surrounding fluorescing regions of the abscess.<sup>196</sup> Using the microLESA workflow and labeled bacteria, we can more accurately target these small colonies and the necrotic tissue surrounding them in order to get a better picture of the pathogenic progression as it is occurring in tissue.

Herein, we report a new workflow combining LESA with histology directed micro-digestions on tissue targeting specific histological structures based on high resolution, non-destructive AF microscopy. Autofluorescence (AF) microscopy has recently been demonstrated to improve accurate microscopy-IMS registration<sup>197</sup> and histological targeting<sup>198</sup> in MALDI IMS workflows. Tissue AF is the fluorescence of endogenous fluorophores in the tissue sample. AF microscopy is a high contrast, high resolution morphologically rich microscopy modality. Because AF does not require any tissue processing or staining and so does not modify the molecular make-up of tissue allowing for downstream targeted molecular analysis. This enables histological determination of tissue regions-of-interest (ROI) to be defined on the same tissue section prior to spatially targeted proteomics, bypassing complicated registration procedures between serial tissue sections. A piezoelectric spotting system with a robotic stage was used for spotting micro-digestion

solutions after ROI identification on the AF image; a new workflow referred to as microLESA herein. Optimization of digestion sensitivity, trypsin concentration, digest spot size, and digestion time are all reported. The microLESA workflow was applied to study the host-pathogen interface in mouse kidney that was infected with *Staphylococcus aureus*. In this work we show advanced proteomic targeting of small histological structures (100  $\mu\text{m}$ ) guided by a non-destructive AF microscopy.

## Results

The microLESA workflow, depicted in Figure 4.1, utilizes both autofluorescence microscopy and liquid micro-digestions in order to target discrete features on the tissue surface for enzymatic digestion. Once digested, peptides are extracted using a traditional LESA. In order to achieve a robust digest, experimental parameters such as trypsin concentration and tissue thickness, were optimized.

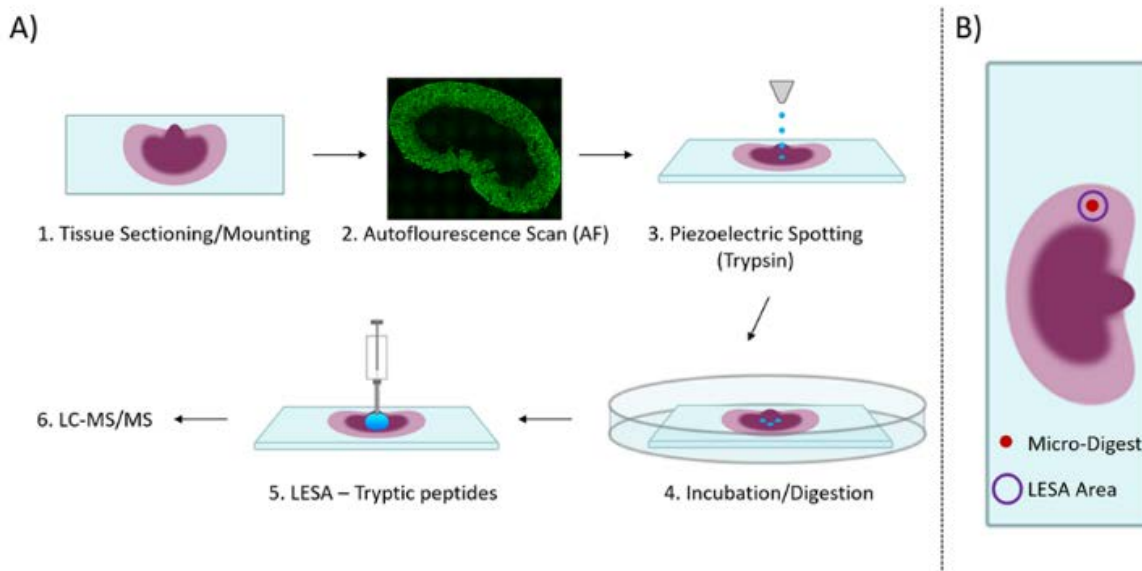
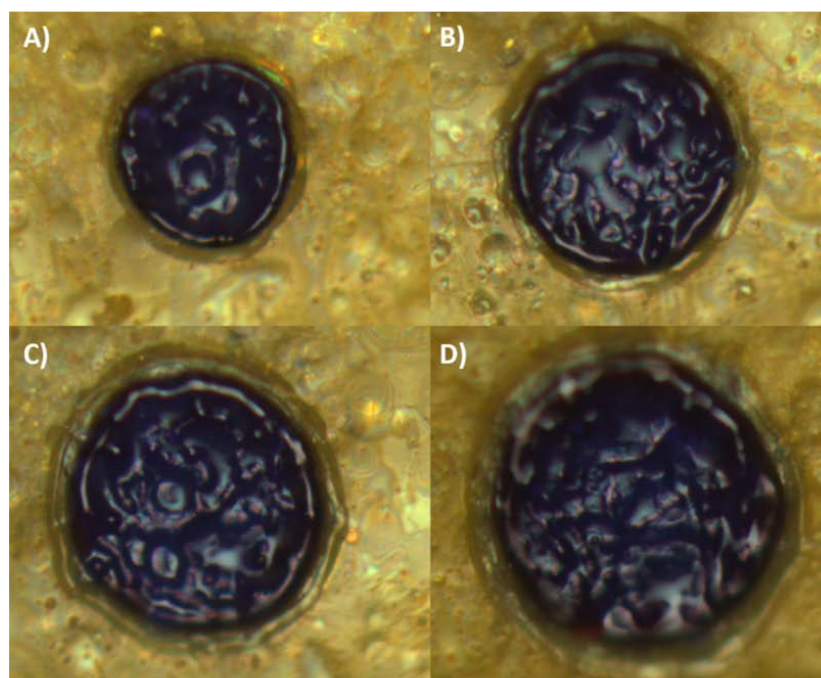


**Figure 4.1:** Overview of microLESA workflow. 1A) Briefly, the tissue is sectioned and mounted onto a microscope slide. An autofluorescence microscopy image is acquired to identify foci for

trypsin spotting. Trypsin is dispensed onto the tissue surface and incubated at 37 °C. Digested peptides are then extracted from the tissue using a traditional LESA. 1B) The digested area on tissue is dictated by the area of the micro-digest of trypsin, represented by a solid red circle. The digested peptides are collected from tissue using a traditional LESA (purple circle) that is larger than the digested area (red circle).

#### *microLESA: Achievable Spatial Resolution*

To quantify this observation, a series of dispensing conditions were tested, varying the amount of drops dispensed in one annotated region. The results of this experiment are depicted in Figure 4.2. A trypsin solution (0.075  $\mu\text{g}/\mu\text{L}$ ) was deposited onto water sensitive paper while varying the number of drops during each dispense event. As shown in Figure 4.2, when a single 220 pL drop was dispensed 21 separate times (60 s between droplets) the final trypsin spot on surface was  $\sim 112 \mu\text{m}$  (RSD 4.33%). It is noted that 21 drops was chosen to mimic the total volume of trypsin used for prior studies ( $\sim 4.5 \text{ nL}$ ).<sup>199</sup> This trypsin micro-digest spot size is 5x smaller than previously reported LESA spot size.<sup>185</sup> An increase in trypsin spot diameter was observed as the number of droplets during a single dispensing event increased. For example, when dispensing 7 drops during a single event the trypsin spot increased  $\sim 95\%$  in diameter ( $\sim 220 \mu\text{m}$ , RSD 3.82%), as seen in Figure 4.2. Although the throughput of the spotting experiment is increased by dispensing more droplets at once, minimizing the droplet diameter was of greater importance for the remaining experiments, and a single drop per dispensing event was employed throughout the remainder of this study.



Run	Deposition Method	Average Diameter ( $\mu\text{m}$ )	Standard Deviation ( $\mu\text{m}$ )	Relative Standard Deviation
A	1 x 21	112.48	4.87	4.33
B	3 x 7	161.50	2.55	1.58
C	5 x 5	195.63	8.12	4.15
D	7 x 3	218.35	8.34	3.82

**Figure 4.2:** The measured droplet diameters (volume  $\sim 220$  pL) of trypsin micro-digests from water-sensitive paper. The total amount of droplets dispensed at a single time was varied from 1 to 7, while still varying the total number of dispensation runs within a sample set to equate to the same total volume dispensed on a given spot (*i.e.* 1 spot dispensed 21 individual times yields the same total volume dispensed as 7 spots, dispensed 3 total times). Each run was completed 5 separate times ( $N = 5$ ) and bright field microscopy was used for measurement.

#### *Micro-digestion Trypsin Concentration and Digest Sensitivity*

To determine an optimal trypsin concentration for the micro-digest, varying trypsin concentrations (0.75, 7.5, and 75  $\text{ng}/\mu\text{L}$ ) were tested by digesting rat liver hepatocytes. Each concentration of

trypsin was tested in triplicate by dispensing single ~250 pL droplets until a total volume of 2.5 nL was deposited, per digest spot. A rat liver tissue section was divided into 3 regions, one for each trypsin concentration. Tissue regions had 3 separate digest regions for technical replicates, each containing 3 individual micro-digest spots (depicted in Figure 4.3). LESA was used to extract peptides from each digest region. Bottom-up proteomics analysis of the digests with varying trypsin concentrations (0.75, 7.5, and 75 ng/μL) resulted in  $61 \pm 11$  (RSD 17.3%),  $308 \pm 40$  (RSD 12.8%), and  $614 \pm 6$  (RSD 0.9%) unique protein identifications respectively. Moving an order of magnitude in concentration, 75 down to 7.55 ng/μL, led to a ~50% loss in the total number of protein identifications, and thus the remaining experiments were completed with trypsin concentrations of 7.5 ng/ μL. Due to the volume of trypsin needed for the instrument to dispense, moving an order of magnitude higher to 750 ng/μL makes the experiment cost prohibitive.

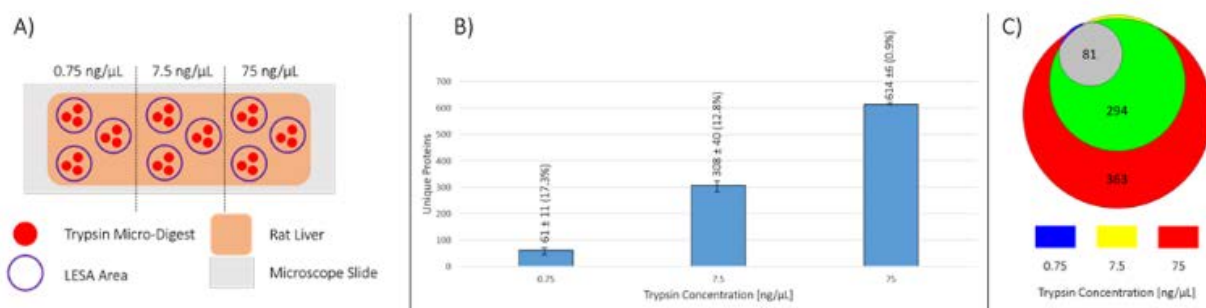


**Figure 4.3:** Optimization of trypsin concentration for microLESA digestion. A) A section of rat liver was divided into 3 regions. For each microLESA extract gathered (purple circle outline), 3 separate dispensing's of trypsin were deposited (red filled circle). Each concentration was tested in triplicate, extracting digested peptides from the 3 digested spots. B) The number of unique proteins identified as a function of trypsin concentration increased as the concentration increased. C) The spread between the protein identifications is depicted, with the majority of the proteins ID in the 0.75 and 7.5 ng/μL samples being identified in the 75 ng/μL samples.

Aside from the concentration of trypsin deposited onto a tissue surface, varying the number of digest spots to be targeted by a single LESA will also affect the total protein counts (*i.e.* increasing



the number of digest spots within one traditional LESA spot). To evaluate the importance of this parameter, the number of digestion spots per LESA extract was varied from 1 to 5 (Figure 4.4). Digestion spots, each with a total volume of ~2.5 nL, were deposited onto rat liver hepatocytes for analysis. From a single digestion spot, 372 unique proteins were identified from the liver. This is of great importance to note, as not all tissue foci of interest will be located on the surface, in groups, for digestion. It is useful to know that a large number of proteins are identifiable, relative to the area interrogated, by digesting one single spot on tissue. The number of identifications scaled linearly ( $R^2$ : 0.921,  $m$ : 88.1) to a total of 755 unique protein ID's gathered from 5 digested areas, a 2-fold increase from the single digestion.

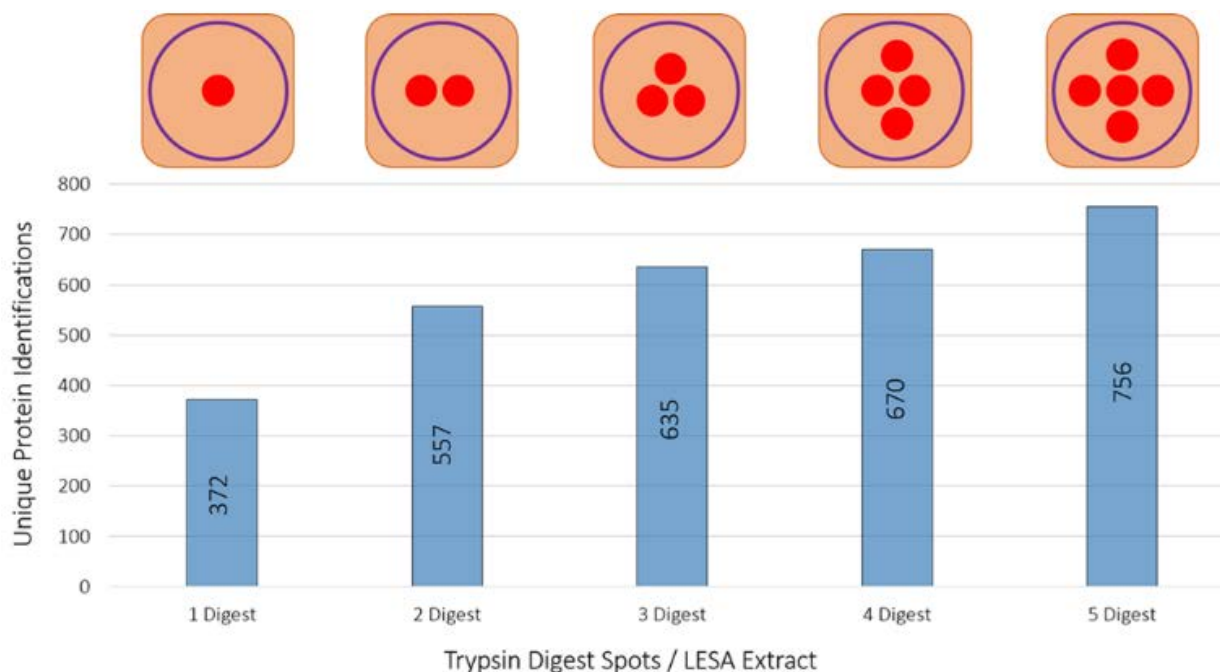


**Figure 4.4:** The total number of unique proteins identified as a function of digest areas per LESA extract. Trypsin was deposited onto rat liver (total volume of ~2.5 nL per digest spot) and the total number of digest spots per LESA extraction area was increased from 1 to 5.

*Micro-Digestion Incubation Time and Tissue Thickness*

The LESA extraction takes only a few minutes to complete and requires minimal sample preparation steps. The major factors limiting throughput in the microLESA experiment are the chromatography and the time allotted for the digestion to occur. To determine optimal trypsin spot incubation times, 12  $\mu\text{m}$  sections of rat liver underwent the microLESA workflow using 30 minutes, 1 hour, 2 hour, and 5 hour (incubation temperature: 37  $^{\circ}\text{C}$ ) incubation times. Following digestion, two separate 2  $\mu\text{L}$  LESA extracts of the peptides from each digest region were combined and subjected to offline LC-MS/MS. The 30 minute digestion produced  $528 \pm 99$  (RSD 18.7%) unique protein identifications. This number was somewhat lower in the number of proteins identified as well as higher in variability between the sample sets than the other conditions. For example, 1 hour and 2 hour incubations resulted in  $732 \pm 8$  (RSD 1.1%) and  $714 \pm 22$  (RSD 3.1%) unique protein identifications respectively. The 5 hour time point was also high in variability, generating  $568 \pm 159$  (RSD 27.9%) unique protein identifications. Because long digestion times did not yield a greater number of protein identifications 1-2 hour digestions were determined to be optimal for microLESA experiments. Tissue thickness was also tested by applying the microLESA workflow to extract peptides from rat liver tissue sections that varied in thickness from 8-30  $\mu\text{m}$ . It was determined that the thickness of the tissue section has no effect on the number of proteins identified. The results from this experiment are displayed in Figure 4.5.

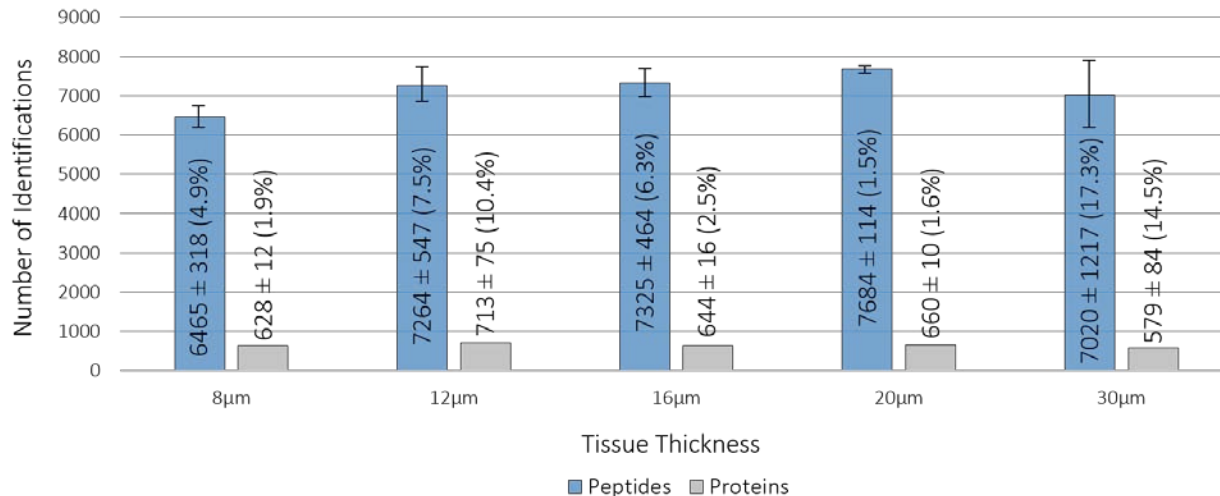


**Figure 4.5:** The tissue thickness as a function of unique proteins and peptides identified was studied using micro-digests combined with a LESA extract. Three digestion spots per extract were analyzed using LC-MS/MS. The results show there is no statistical change in the number of peptide and protein identifications between the sample sets (ANOVA: p-value 0.289 for peptides identified and p-value 0.0919 for unique proteins identified). These results suggest that the digestion may only be occurring on the surface of the tissue.

#### *Elucidating the Proteomic Drivers of Host-Pathogen Interactions*

As a proof-of-concept, kidney tissue from a mouse infected with GFP+ labeled *S. aureus* bacteria was subjected to the microLESA workflow and MALDI IMS. The fluorescence image (tissue autofluorescence and fluorescently labelled bacteria) of the kidney is depicted in Figure 4.6. The autofluorescence signal makes evident the many abscesses present within the tissue (labeled, Figure 4.6). Because within this plane of the tissue the largest bacterial colonies were observed in the bottom abscess, this region was chosen for microLESA. Five ROIs were chosen for trypsin spotting covering both the bacterial colonies and surrounding necrotic regions within the abscess. Following incubation, LESA was performed three times to ensure all digested peptides were extracted for LC-MS/MS analysis resulting in ~2,700 unique protein identifications. Mouse immune response proteins were identified, such as neutrophil response factors like the S100A9

protein (Protein ID: P31725) which is known to localize to the abscess during infection to sequester  $Mn^{2+}$  and  $Zn^{2+}$ .<sup>200</sup> Also identified are neutrophil secretory proteins such as neutrophil elastase (Protein ID: Q3UP87), a serine protease responsible for killing bacteria but can be inhibited by serine protease inhibitors released from *S. aureus* during infection.<sup>201</sup> Upwards of 65 unique *S. aureus* specific proteins were identified. Staphylococcal complement inhibitor (Protein ID: A6QIG6) is known to counteract the host immune response by reducing phagocytosis following opsonization and blocks all the downstream effector functions by selectively binding and inhibiting C3 convertases which play a role in the complement system activated during inflammation.<sup>202</sup> Also identified from the colony digests is the protein Iron-regulated surface determinant protein B (IsdB, Protein ID: A6QG30). It is known that *S. aureus* needs iron in order to replicate and continue to grow, but the host immune response is primarily aimed at sequestering and removing all iron at the site of infection in order to limit growth and kill the invading pathogens. IsdB is part of the iron-regulated surface determinant system responsible for binding heme, bringing it through the cell wall and membrane of the bacteria where it can then be degraded to free iron to be used as a nutrition source for the bacteria.<sup>203</sup> The identification of proteins involved in bacterial growth and survival directly from infected tissue is crucial in understanding the evolution and progression of a *S. aureus* infection. A list of selected *S. aureus* and neutrophil-specific proteins identified from the abscess using the microLESA workflow are presented in Table 4.1.

**Table 4.1:** Unique protein identifications from the abscess of a *S. aureus* infected murine kidney. Proteins identified from the bacterial colonies present in the abscess are listed, as well as proteins secreted by neutrophils to fight the infection. Proteins were identified with at least 2 peptides per protein, with a false discovery rate of 1%.

<b>Staphylococcus Aureus Protein Identifications</b>	
Q2FGF0  UPF0365 protein	Q2FFF8  Staphylococcal complement inhibitor
Q2FH00  Alanine dehydrogenase 1	Q2FFJ6  Aspartyl/glutamyl-tRNA(Asn/Gln) amidotransferase subunit B
Q2FH01  L-threonine dehydratase catabolic TdcB	Q2FFQ5  Foldase protein PrsA
Q2FHG3  Ribonuclease J 2	Q2FFV5  Phosphoenolpyruvate carboxykinase (ATP)
Q2FHG9  Translation initiation factor IF-2	Q2FG18  30S ribosomal protein S4
Q2FHI1  Elongation factor Ts	Q2FG27  Acetate kinase
Q2FHI2  30S ribosomal protein S2	Q2FG28  Putative universal stress protein
Q2FHI3  GTP-sensing transcriptional pleiotropic repressor CodY	Q2FG40  Pyruvate kinase
Q2FHR7  Carbamate kinase 1	Q2FG54  Threonine--tRNA ligase
Q2FHS7  FPRL1 inhibitory protein	Q2FG61  Trigger factor
Q2FHT6  Thioredoxin	Q2FGD8  30S ribosomal protein S20
Q2FHV1  Iron-regulated surface determinant protein A	Q2FGE3  Chaperone protein DnaK
Q2FHV2  Iron-regulated surface determinant protein B	Q2FJG3  Nucleoid-associated protein SAUSA300_0453
Q2FIB3  Glucose-6-phosphate isomerase	Q2FJN4  Alkyl hydroperoxide reductase C
Q2FIG2  UPF0337 protein SAUSA300_0816	Q2FJP8  ribosomal protein S6
Q2FIK4  Extracellular matrix protein-binding protein emp	Q2FK15  Ribitol-5-phosphate cytidyltransferase 1
Q2FIL7  Enolase	Q2FK29  L-lactate dehydrogenase 1
Q2FIS2  Lipoteichoic acid synthase	Q2FK44  Formate acetyltransferase
Q2FJ31  Alcohol dehydrogenase	Q2FK96  Heme oxygenase (staphylobilin-producing) 2
Q2FJ87  Uncharacterized epimerase/dehydratase SAUSA300_0538	Q2FDQ4  Fructose-bisphosphate aldolase class 1
Q2FJ92  Elongation factor Tu	Q2FDQ7  L-lactate dehydrogenase 2
<b>S100 Protein Identifications</b>	
P31725  Protein S100-A9	P97816  MOUSE Protein S100-G
P50543  Protein S100-A11	P27005  Protein S100-A8
P07091  Protein S100-A4	P97352  Protein S100-A13
<b>Neutrophil Protein Identifications</b>	
Q09014  Neutrophil cytosol factor 1	O70138  Neutrophil collagenase
O70145  Neutrophil cytosol factor 2	P11672  Neutrophil gelatinase-associated lipocalin O

O08692  Neutrophilic granule protein	P97369  Neutrophil cytosol factor 4
Q3UP87  Neutrophil elastase	

Protein identifications from microLESA extracts were used to annotate specific proteins observed in MALDI IMS data acquired from a serial section of *S. aureus* infected mouse kidney, demonstrating the utility of integrating microLESA into MALDI IMS workflows. Protein IMS was completed at 60  $\mu\text{m}$  spatial resolution on a modified 15T FT-ICR MS (reduced source pressure: 950 mTorr). The resulting image consisted of protein distributions ranging from ~3-29 kDa, with a number of signals localizing to the abscesses. Both S100A8 and S100A9, the proteins that non-covalently bind to form the heterodimer calprotectin, were found localized intensely to the abscess regions. MALDI FT-ICR IMS provided the mass accuracy necessary to determine that S100A9 is both acetylated and methylated (mass accuracy: 1.13 ppm). Calprotectin is a metal-chelating host protein complex that accounts for an estimated 60% of the cytosolic protein content of neutrophils.<sup>204</sup> Because bacteria require elemental nutrients for survival, metal sequestration is a primary mechanism for resisting bacterial pathogen proliferation within vertebrates, a process known as nutritional immunity.<sup>192, 205</sup>

N-acetylated cytochrome C oxidase subunit 6C (Cox6c) was also identified by microLESA and observed by IMS. Cox6c is one of the subunits of the large cytochrome c oxidase complex that is part of oxidative phosphorylation in mitochondria.<sup>206, 207</sup> The ability to identify proteins while maintaining spatial fidelity is critical for providing biological context to IMS results. MicroLESA provides a higher throughput, targeted approach to generate these identifications that when combined with IMS produce integrated data sets with both high spatial and molecular content.

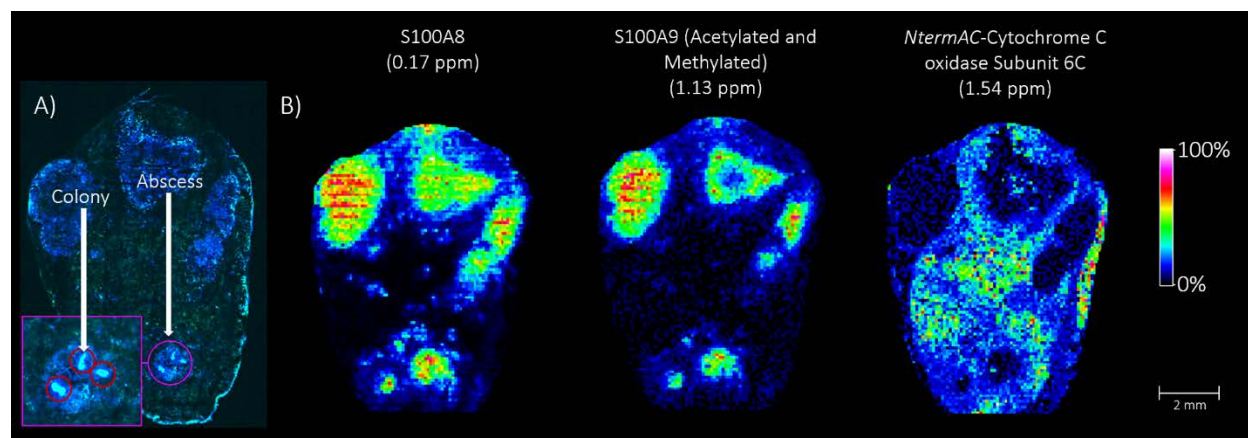


**Figure 4.6:** Autofluorescence microscopy and MALDI IMS images of fluorescently-labeled *S. aureus* infected mouse kidney tissue. A) Autofluorescence microscopy images were acquired to visualize the abscess and bacterial colonies targeted for digestion. The interrogated abscess is circled in purple and a ‘zoomed-in’ capture highlights the colonies that were targeted for digestion (Red circles) using the microLESA workflow. B) MALDI FT-ICR IMS was used to investigate the distribution of intact proteins present in the tissue. Selected proteins are presented which were identified using the data collected from the microLESA experiment, correlating the identifications by accurate mass matching.

## Discussion

A new workflow, termed microLESA, is presented that allows for the proteomic analysis of discrete tissue foci. The new workflow incorporates autofluorescence microscopy to generate high resolution, non-destructive images that allow for the visualization of target features on the same section of tissue that will undergo digestion. The use of a Piezo electric spotter allows for the deposition of small volumes of liquid. Dispensing trypsin in a solution of ammonium bicarbonate, we were able to get a droplet diameter of approximately 110  $\mu\text{m}$ , reproducibly. Analytical figures of merit for the microLESA workflow were also investigated. These

characteristics included: incubation duration, tissue thickness, and trypsin concentration. Autofluorescence enabled the gross morphology of the kidney tissue to be visualized, including abscesses and surrounding regions of a *S. aureus* infected murine kidney. *S. aureus* is unique as it can infect virtually any organ once it enters the bloodstream. The abscess architecture, although broadly defined, is still poorly understood *in vivo*. MALDI IMS enables the visualization of molecules vital for the host and pathogens survival; however, issues inherent to MALDI make their identification a challenge. As a case-study, we demonstrated the capabilities of this microLESA workflow to study abscess architecture. The resulting proteomics experiments produced thousands of protein identifications including a large number of bacterial proteins and proteins associated with host immune response. By integrating these data with imaging mass spectrometry, this workflow provides a way to effectively annotate species observed by MALDI IMS and delivers a more complete spatial proteomics description of a sample.

## Methods

### *Micro-Digestions and Autofluorescence Microscopy*

For the microLESA experiments, trypsin was dissolved in a 12:88 *v/v* solution of acetic acid (100 mM) and ammonium bicarbonate (100 mM) to a final concentration of 75 ng/ $\mu$ L, except for the trypsin concentration optimization experiments (detailed in results section). A Piezoelectric spotting system (sciFLEXARRAYER S3, Princeton, NJ, USA) was utilized with a piezoelectric dispenser capillary nozzle (PDC 50, type 3) for trypsin deposition. For all experiments, either bright field or AF microscopy images were acquired (Eclipse 90i, Nikon Instruments Inc. Melville, NY, USA) prior to any spotting. For microLESA of *S. aureus* infected murine kidney, an AF image



was acquired prior to spotting using FITC and DAPI filters (FITC excitation  $\lambda$ : 465-495 nm, emission  $\lambda$ : 515-555 nm, and DAPI excitation  $\lambda$ : 340-380 nm, emission  $\lambda$ : 435-485 nm). All microscopy images were collected with either a 4 or 10x objective, generating images with a resolution of 2.29 and 0.92  $\mu\text{m}/\text{pixel}$ , respectively. Microscopy exposure times were set to 200 ms for both filters. ROIs for trypsin spotting were annotated from a custom-built fiducial microscope slide, on microscopy images using ImageJ, and converted into relative coordinates for the piezoelectric spotter using an in-house developed Python script. The spotter was optimized to generate  $\sim 250$  pL droplets while dispensing trypsin. Briefly, the spotting system uses a camera to recognize a point of origin on the sample for which to spot from. An arbitrarily chosen fiducial was utilized prior to any ROI generation and used as the origin for which all spots would be deposited from. For all spotting runs, the piezo was initially tuned while dispensing pure water, then while dispensing a solution of trypsin, and in between all trypsin depositions to ensure a stable droplet. The PDC 50 was tuned to these approximate settings: 70-90 V, 40-60  $\mu\text{s}$ , a frequency of 500 Hz, and an LED delay of 200  $\mu\text{s}$ . These settings generated stable spot volumes of approximately 250 pL using a PDC 50 nozzle with relative standard deviations under 10%. Following trypsin deposition, slides were incubated at 37  $^{\circ}\text{C}$  for 2 hours except for the incubation optimization experiments.

#### *Micro-Digestions: Spotting specific ROI's with Trypsin*

In order to spot any liquid to specific ROI's on a tissue section, a custom-designed fiducial slide was used to register the spotting system. Briefly, the spotting system uses a camera to recognize a point of origin on the sample for which to spot from. An arbitrarily chosen fiducial was utilized prior to any ROI generation and used as the origin for which all spots would be deposited from. For all spotting runs, the piezo was initially tuned while dispensing pure water, then while dispensing

a solution of trypsin, and in between all trypsin depositions to ensure a stable droplet. The PDC 50 was tuned to these approximate settings: 70-90 V, 40-60  $\mu$ s, a frequency of 500 Hz, and an LED delay of 200  $\mu$ s. These settings generated stable spot volumes of approximately 250 pL using a PDC 50 nozzle with relative standard deviations under 10%.

### *Liquid Extraction Surface Analysis (LESA)*

Liquid surface extractions were completed using a TriVersa NanoMate (Advion Inc., Ithaca, NY, USA) with the LESApplusLC modification. Images of digested tissue were scanned using a flatbed scanner, uploaded, and annotated using the Advion ChipSoft software. LESA was performed by aspirating 5  $\mu$ L of extraction solvent (2:8 acetonitrile:water, with 0.1% formic acid) into the glass capillary. The capillary was then lowered to a height of approximately 0.5 mm above the tissue surface, and 2.5  $\mu$ L of solvent was dispensed onto the tissue surface. The liquid junction was maintained for 10 seconds and a volume of 3.0  $\mu$ L was re-aspirated back into the capillary. The initially drawn 5  $\mu$ L volume was then dispensed into a 96-well plate containing 200  $\mu$ L of water/0.1% formic acid. For each digested ROI, two LESA extracts were gathered from the region and combined. To prevent sample carryover, three wash cycles were completed between each ROI set. All extracts were dried down under vacuum and stored at -80 °C until LC-MS/MS analysis. Control and blank samples were gathered from undigested rat liver and a plain glass slide to account for endogenous peptides present, prior to digestion.

### *Animals and Bacterial Strains*

To create a stable GFP+ strain of *S. aureus* for subsequent murine infections and fluorescence microscopy, the region containing the *sarA* promoter driving sfGFP was first amplified out of pCM11 using primers 5'-

GTTGTTTCTAGACTGATATTTTTGACTAAACCAAATG-3' and 5'-  
GTTGTTGAGCTCTTAGTGGTGGTGGTG-3' (restriction sites underlined). The resulting PCR  
amplification product was then ligated into the XbaI and SacI site of pJC1111<sup>208</sup> to create pNP1.  
pNP1 was then chromosomally integrated into the SaPII site of *S. aureus* as previously  
described.<sup>209</sup> The region encompassing the chromosomal SaPII integration was then transduced  
into *S. aureus* strain LAC (AH1263) using phi80a. Integration of PsarA\_sfGFP at the SaPII site  
was confirmed using primers JCO717 and 719.<sup>209</sup> Frozen rat liver was purchased from Pel-Freeze  
Biologicals (Rogers, AR, USA), and stored at -80 °C until sectioning. All in-house animal  
experiments were performed with approval by the Vanderbilt Institutional Animal Care and Use  
Committee. Six to eight-week old female C57BL6/J mice were anesthetized with isoflurane and  
retro-orbitally infected with 3.6 x 10<sup>7</sup> colony forming units (CFUs) of *Staphylococcus aureus* LAC  
carrying a genomic sfGFP reporter under control of the sarA promoter. Mice were humanely  
sacrificed at 10 days post infection (DPI). Kidneys for imaging and microLESA experiments were  
aseptically removed and frozen on dry ice.

#### *MALDI IMS of Proteins*

MALDI IMS of proteins was performed on a modified Bruker SolariX 15T Fourier transform ion  
cyclotron resonance (FT-ICR) mass spectrometer (Bruker Daltonics, Billerica, MA, USA). The  
source pressure of the instrument was decreased to 950 mTorr to maximize the transmission  
efficiency of larger intact protein species by regulating the gas flow through the ESI port. Tissue  
preparation strategies and instrumental parameters are discussed in the supplemental information.  
In all experiments except the tissue thickness optimization, tissue was sectioned (12 µm thickness)  
at -15 °C using a CryoStar<sup>TM</sup> NX70 Cryostat (Thermo Fisher Scientific, San Jose, CA, USA),  
thaw mounted onto conductive indium-tin-oxide coated slides with custom printed fiducials in

black ink (Delta Technologies, Loveland, CO, USA)), and dried in a vacuum desiccator for at least 20 minutes prior to preparation for analysis. Tissue sections underwent a washing prior to any imaging, micro-digestion, or surface extraction to remove interfering lipids and salts. The wash steps were as follows: 70% ethanol (30s), 100% ethanol (30s), Carnoy's Wash (6:3:1 ethanol:chloroform:acetic acid), 100% ethanol (30s), water (30s), and 100% ethanol (30s) as described previously.<sup>52</sup>

For intact protein IMS, tissue was covered homogeneously with DHA using a robotic sprayer (TM Sprayer, HTX Technologies, Carrboro, NC, US) at a concentration of 15 mg/mL in 9:1, ACN:H<sub>2</sub>O (0.1% formic acid). The sprayer nozzle was set to spray at 85 °C using a carrier solvent of 9:1 ACN:H<sub>2</sub>O at a flow rate of 0.1 mL/min and a drying sheath gas of dry nitrogen set to 10 psi. Four passes of matrix were applied using alternating offsets (1 mm) and directional rotations (90 degrees) with a 2 mm track spacing. The spray velocity was set to 700 mm/min with a 2 s dry time between passes and 40 mm nozzle height. The matrix layer on the sample was recrystallized prior to MALDI analysis as previously described using 1.0 mL of 1:1, TFA:H<sub>2</sub>O at 37 °C for 3 minutes. The image was acquired in positive ion mode at 60 μm spatial resolution on a 15T FT-ICR MS. The instrument employs a Smartbeam II 2 kHz frequency tripled Nd:YAG (355 nm) laser, as well as an Apollo II dual MALDI/ESI ion source. Each pixel was the sum of 2000 laser shots, using the smallest laser focus (~50 μm), while random-walking the target within the 125 μm pixel. The mass spectrometer was externally calibrated prior to analysis using a protein mixture (insulin, cytochrome C, trypsinogen, and apomyoglobin). Data were collected from m/z 1,385 - 20,000 with a time-domain file size of 512K (FID length: 1.6078 s), yielding a resolving power of ~42,000 at m/z 5000. In order to generate an image with a higher mass range, the ion optics were tuned as follows: accumulation hexapole (1.4 MHz, 1700 Vpp), time-of-flight delay

(2.1 ms), funnel RF amplitude (200 Vpp), transfer optics (2 MHz, 380 Vpp), and ICR cell (sweep excitation power: 40%). The source pressure was lowered to 950 mTorr in order to maximize the transmission of heavier species.

#### *Bottom-Up LC-MS/MS and Data Analysis*

For the microLESA optimization experiments, an analytical column was packed with 22 cm of C18 reverse phase material (Jupiter, 3  $\mu\text{m}$  beads, 300 $\text{\AA}$ , Phenomenox) directly into a laser-pulled emitter tip (Sutter Instrument Company, Novato, CA, USA). Peptides were loaded on the capillary reverse phase analytical column (360  $\mu\text{m}$  O.D. x 100  $\mu\text{m}$  I.D.) using a Dionex Ultimate 3000 nanoLC and autosampler. The mobile phase solvents consisted of 0.1% formic acid, 99.9% water (solvent A) and 0.1% formic acid, 99.9% acetonitrile (solvent B). Peptides were eluted with a gradient at a flow rate of 400 nL/min. A 60-minute gradient was performed as follows: 1-2 min, 2% B (sample loading from autosampler); 2-44 min, 2-35% B; 44-49 min, 35-95% B; 49-49.5 min, 95% B; 49.5-50 min, 95-2% B; 50-60 min (column re-equilibration), 2% B. A Thermo Q Exactive Plus Orbitrap mass spectrometer (Thermo Scientific, San Jose, CA, USA), equipped with a nanoelectrospray ionization source, was used to analyze the eluting peptides. The instrument method consisted of MS1 using an MS AGC target value of  $3 \times 10^6$ , followed by up to 15 MS/MS scans of the most abundant ions detected in the preceding MS scan. A maximum MS/MS ion accumulation time of 60 ms was used with a MS2 AGC target of  $1 \times 10^5$  and an intensity threshold of  $5 \times 10^4$ . Dynamic exclusion was set to 10s, HCD collision energy was set to 27 normalized collisional energy, and peptide match and isotope exclusion were enabled.

For the microLESA experiments targeting the abscess in mouse infected with *S. aureus*, tryptic peptides from the tissue extracts were injected and gradient eluted on a pulled tip emitter column (360  $\mu\text{m}$  O.D. x 100  $\mu\text{m}$  I.D. x 35 cm) packed in-house with C18 material (Waters BEH C18, 1.7

$\mu\text{m}$ , 130 Å). The column was heated to 60 °C with a flow rate of 400 nL/min during operation using an Easy-nLC 1000 UHPLC (Thermo Scientific, San Jose, CA, USA), where the mobile phase A consisted of 0.1% formic acid, 99.9% water, and mobile phase B consisted of 0.1% formic acid, 99.9% acetonitrile. Peptides were eluted on the reverse phase column using a linear gradient of 2-20% B for 100 minutes, followed by 20-32% B for 20 minutes, and lastly 32-95% B for 1 minute. An Orbitrap Fusion Tribrid mass spectrometer (Thermo Scientific, San Jose, CA, USA) was used to mass analyze the eluting peptides. MS1 scans were acquired using the Orbitrap at 120k resolution, a mass range of 400-1600 m/z, an automatic gain control (AGC) target of  $1.0 \times 10^6$ , and a maximum injection time of 100 ms. The top 17 most abundant ions measured in the MS1 scans were then mass isolated using a quadrupole mass filter at 2 m/z window width to undergo fragmentation in the HCD cell using 35% normalized collision energy. The fragmented ions are subsequently mass analyzed in the linear ion trap using an AGC target of  $1 \times 10^4$ , a maximum injection time of 35 ms, and the normal scanning rate setting. Dynamic exclusion of 30 s was used for all MS2 scans. For identification of peptides from both instruments, tandem mass spectra were searched using Proteome Discoverer software (Vulcan Analytic, Birmingham, Alabama, USA) against a rat database created from the UniprotKB protein database ([www.uniprot.org](http://www.uniprot.org)). Variable modifications such as acetylation, phosphorylation, methionine oxidation, and deamidation were included in the database search. Proteins were identified with at least 2 unique peptides per protein, with a false discovery rate of 1%.

### **Acknowledgements**

I wish to acknowledge and thank Dr. Andy Weiss and Dr. Eric Skaar for their efforts in generating the infection models for the work discussed above. I also wish to thank Dr. Jim

Cassat, Nicole Putnam, and Aimee Wilde for their work in generating the fluorescently-labeled strain of bacteria utilized in the microLESA work.

## CHAPTER V

### CONSPECTUS

#### Overview

The development of next-generation, spatially targeted proteomic strategies has greatly improved the way in which we elucidate proteomic information from a tissue and has improved our identification strategies in MALDI IMS workflows. In the work detailed herein, both instrumental modifications and new sample preparation technologies were developed and implemented for protein analysis from tissue. First, protein ion transmission for high-performance MALDI IMS platforms was improved by optimizing the source pressure to maximize the effective potential wall confining ions through the first stage of a 15T FT-ICR MS. Additionally, the new spatially targeted surface sampling technology LESA was optimized and incorporated to complement MALDI IMS workflows to enable a high throughput approach to generate protein identifications from tissue incorporating top down or bottom up mass spectrometry. This technology was determined to be robust with regards to analytical figures of merit, but the standard LESA workflow is limited with regards to resolution, and is inadequate when studying foci smaller than 500  $\mu\text{m}$ . To overcome the challenges associated with a traditional LESA (*i.e.* large droplet diameter on tissue), a new method incorporating an enzymatic micro-digestion was developed. This new approach was applied to study the host/pathogen interface of a staphylococcus aureus infection. In this conspectus, the current state of the field as it relates to these technologies is discussed.



## Protein Ion Transmission in MALDI MS/IMS

MALDI IMS is continuing to grow with regards to applied research and technological development. For example, the development of high frequency lasers has generated instruments capable of acquiring tens of spectra per second.<sup>41</sup> The continued development of mass spectrometers with improved mass resolution and mass accuracy has driven the technologies popularity and IMS is now routinely utilized to study a number of different diseases such as cancers and diabetes.<sup>24, 177, 193, 210</sup> The proteome provides a unique environment to study which often reflects disruptions in health and the current state of a disease in a particular animal, and thus is a vital area for MALDI IMS. In order for the field to move forward and continue growing, challenges inherent to protein identification must be addressed. One of the limiting factors in protein MALDI MS, aside from fragmentation efficiency, is limited ion transmission within the mass spectrometer. Time-of-flight (TOF) mass spectrometers provide the greatest transmission range, relative to other mass spectrometers used in MALDI MS, and can routinely transmit and detect proteins beyond 35 kDa from tissue.<sup>145</sup> Although useful, these platforms lack the resolution necessary to isotopically resolve a protein distribution, and have limited mass accuracy making identification a challenge.

In work discussed in Chapter 2, a commercially available FT-ICR MS instruments are capable of transmitting and detecting protein ions up to ~12-14 kDa.<sup>40</sup> In order to increase the transmission range on this platform, the pressure region where the ion funnel is located (*i.e.* where ions are generated and initially transmitted) was regulated by modifying the ESI capillary to include the addition of a metering valve, as well isolation valves on the manifold pumping down the source region, and second rough pump to decrease pressure further, as highlighted in Chapter 2. A number of experimental parameters were tested and optimized, such as the effect of off-axis

gas flow on ion transmission. It was found that raising the capillary to its highest setting (*i.e.* out of the way of the MALDI plume) provided the lowest interference with the ions being generated. Chapter 2 also reviews the effects of systematically decreasing the pressure in the source region. Moving from the ‘normal’ operating pressure of 2.9 Torr, to a reduced 750 mTorr, generated an increase in protein ion abundance by 10 to 100 fold. This pronounced effect was attributed to a less dampened effective potential for ion radial confinement and enabled the detection of protein ions up to  $m/z$  24,000. Although the modifications have almost doubled our effective transmittable mass range, we are just beginning to push the envelope with regards to detecting average sized proteins found within a cell (*i.e.* mass > 35,000 Da), and an even greater increase in transmission will be needed to study the majority of the proteome. For example, yeast proteins are on average 466 amino acids long, corresponding to an average mass of 53 kDa.<sup>211</sup> Future work should focus around new instrumental modifications in the form of improved electronics. For example, RF generators capable of operating at lower frequencies are necessary for a higher mass transmission and could be introduced to enhance  $m.z$  sensitivity even further. Such research would enable a deeper study of the proteome by IMS and will be necessary to understand proteomic changes associated with disease.

### Protein Identification Using LESA

Protein identification in MALDI IMS is crucial in helping to understand the physiological role of biomolecular and cellular systems. Prior to the development of LESA, orthogonal approaches utilizing a tissue homogenate were most commonly employed to generate protein identifications for MALDI IMS workflows. Although this approach can generate thousands of protein IDs, this technique relies on a complete pulverization of tissue, losing the spatial integrity gained during an IMS acquisition. The optimization of LESA, highlighted in chapter 3, enables a

new high throughput approach to identifications from tissue. By dispensing and aspirating a small volume of liquid (0.5-2.0  $\mu\text{L}$ ), the user can extract peptides and proteins from tissue foci as small as 600  $\mu\text{m}$  in diameter. The LESA technology was first benchmarked with regards to analytical figures of merit, determining and optimizing such characteristics as sensitivity and resolution. The reproducibility of a robotic LESA extract was also examined, and it was found to be very reproducible with low RSD's (< 5%). One of the unique characteristics inherent to the liquid extraction is the rate at which it can be completed. The entire experiment involves an *in situ* enzymatic digestion, extraction, and chromatography/mass spectrometry. In total, one can generate thousands of protein identifications in as little as 16 hours, if digesting the tissue overnight, and a single *in situ* tissue digest provides countless LESA extracts. Similar spatially targeted approaches, such as a hydrogel extraction, require almost twice that amount of time.<sup>74</sup> The aforementioned experiment requires ~16 hr to cast a gel, ~1-2 hr for gel placement, ~14 hr for digestion, ~1-2 hr for peptide extraction, and ~1-2 hr for LC-MS/MS. In order to bypass the sample handling stages of a LESA, and gain an even greater increase in throughput, online HPLC was incorporated into the workflow. The new LESAplusLC experiment enables an all-in-one platform that is capable of extracting analytes and moving them onto an HPLC column for LC-MS analysis.

The LESA technology is also capable of being applied to both top-down and bottom-up MS studies, extending its applications to enhance our current MALDI protein IMS workflows. Extracting from whole body mouse pup in Chapter 3, LESA extracts were subjected to top-down mass spectrometry on an Orbitrap MS. The spectra were sequenced *de novo*, and select identifications were mapped back to an intact MALDI IMS data set collected from the same animal demonstrating its utility in aiding in protein ID in a MALDI IMS workflow. Due to these advantages of the LESA experiment, a number of labs are employing this technology to generate

molecular information from a number of substrates including food, paper,<sup>158</sup> and animals.<sup>212, 213</sup> Although this work advanced the applicability of LESA in IMS workflows, further work was needed to overcome the limited droplet diameter achievable on tissue.

#### microLESA and the Host/Pathogen Interface

Spatially targeted proteomic experiments are a powerful approach that allow one to place an ID with a region on tissue, and limitations in droplet diameter restrict what tissue foci can be analyzed using a standard LESA. Micro-spotting has proven to be useful approach to spot both enzyme and matrix for MALDI MS studies.<sup>151</sup> Previous research utilized a micro-digestion to deposit small volumes of enzyme to reduce the dimension of analysis (*i.e.* digestion area on tissue) for bottom-up LESA extractions.<sup>186</sup> Here, regions for micro-spotting were defined using MALDI IMS data and proteins were identified from regions as small as 250  $\mu\text{m}$ . In Chapter 4, a new workflow coined microLESA that incorporates both micro-enzymatic digestions and autofluorescence microscopy, was developed. MicroLESA allows for the reduction of the digestion area on tissue for a proteomic LESA analysis by incorporating liquid micro-spotting. Here, we are repeatedly dispensing a small (~260 pL) volume of trypsin on tissue, one drop at a time, which translates to a digestion spot of approximately 110  $\mu\text{m}$  in diameter on the surface of the sample. The use of a droplet-based digestion improves the resolution of the digested area, forgoing the robotically sprayed, *in situ* digest used in Chapter 3. Following an incubation period, tryptic peptides are collected using a standard LESA, ensuring the area of digestion is covered with the liquid extract. Endogenous peptides are accounted for by completing a control extract from a non-digested region of tissue. One of the greatest challenges in developing the new workflow focused on finding a non-destructive approach to visualize target foci for micro-spotting. Prior research incorporating MALDI IMS relied on a serial section of tissue for proteomic analysis,

and often tissue substructures are lost due to the extra sectioning required for this. The use of autofluorescence (AF) microscopy enables the generation of a non-destructive, high resolution, high contrast image to visualize tissue morphology, forgoing the need for additional serial sections of tissue for the digestion. In our work, this allowed for the clear visualization of the substructure present within a *staphylococcus aureus* infected mouse kidney. The incorporation of fluorescently labeled bacteria enables the visualization of the bacterial colonies, *ex vivo*, and allows the user to target these foci for micro-digestion. microLESA analysis of the infectious foci present in the kidney yielded thousands of protein identifications and many related to host-defense responses.

#### Outlook and Continued Development of Targeted Proteomic Technologies

Modifications to a 15T FT-ICR MS have effectively doubled the transmittable mass range for routine MALDI IMS of proteins from a tissue section. Although we are currently detecting protein ions at twice the mass that was previously achievable, we are still only beginning to detect a small amount of all of the possible proteoforms present within a cell. Future work needs to entail the use of RF generators that allow the ion funnel to operate at lower frequencies in order to continue to push the boundaries of high mass transmission. Currently, the funnel does not allow for the tuning of the RF operating frequency, and only the magnitude of the applied RF can be varied. Future work should also incorporate the analysis of different biomolecular classes from tissue, including small molecule metabolites, lipids, and peptides.

Liquid extraction surface analysis, coupled to mass spectrometry (both online and offline) has greatly improved the way that we generate complimentary information for MALDI IMS of proteins. One of the greatest challenges facing protein identification in MALDI IMS, utilizing electrospray ionization-based experiments to generate IDs, is the poor overlap of the ionized species detected between ESI and MALDI. Currently, only 10-30% of protein ions

detected and identified utilizing ESI are detected in MALDI IMS experiments, severely limiting the number of IDs one can generate from tissue. In order to overcome this challenge and generate more informative information from tissue, *in situ* enzymatic digestions enabling a robust peptide MALDI IMS must be optimized. MALDI IMS of peptides allows for the detection of species of the same biomolecular class (*i.e.* peptides) that we are identifying in our LESA and microLESA experiments, enabling a direct comparison of the two experiments and a greater probability for making a molecular identification based on peptide identifications. Current challenges facing MALDI IMS of peptides are trypsin application, trypsin activity, delocalization of species after trypsin application, and limited throughput when generating tandem mass spectra for identification.

MicroLESA has greatly improved the resolution of a bottom-up LESA experiment by incorporating both micro-digestions and autofluorescence microscopy. Currently, the technology is only being used to generate molecular identifications and no quantitative information is drawn from the resulting data. In order for this technology to improve and continue to grow, quantitation of the species being identified is critical and is the next step in the development of this approach. More often than not, proteins are expressed at increased or decreased levels during the progression of various diseases, and microLESA faces a number of challenges when trying to assess this metric. The digestion itself is quite variable, and the reliability of the data collected relies heavily on how stable the liquid droplet deposition is. The stability of the droplet is dictated by the solution of liquid, the analyte being dispensed, and the applied voltage and frequency to the Piezo nozzle. Dissolving trypsin in pure water enabled a stable droplet for our work. A number of approaches could be utilized for a more quantitative microLESA experiment. For example, acquiring data from a greater number of biological replicates enable one to analyze trends within the data,

focusing on abundant proteins that are always present within the extracts and their respective abundances (*i.e.* increased or decreased abundance) across different disease states.

## **Conclusions**

Advancements in MALDI IMS instrumentation and spatially targeted proteomic technologies have enabled new and improved approaches to generate proteomic information from a tissue sample. To fully elucidate the underlying biology that these images represent, it is important to employ methods for the identification of protein signals afforded from IMS experiments. Recent developments in orthogonal, spatially targeted proteomics technologies and methods have allowed for more robust identification of peptides and proteins, driving the continued use of protein IMS towards next-generation biological applications. There is a focus in the field towards combining technologies to maximize sensitivity and fragmentation efficiency at higher spatial resolutions. For example, instrument source modifications to allow for finer control over source pressure are improving sensitivity of intact protein analysis on high-performance imaging platforms. Additionally, the implementation of charge state independent ion activation techniques, such as ultraviolet photodissociation, may hold the key to allowing spatially targeted fragmentation of intact proteins directly from tissue using MALDI. The field of spatially targeted proteomics would benefit greatly from the integration of these technologies into the IMS workflow, and would enable a visualization of a greater fraction of the proteome and ultimately a better understanding of pathologically relevant processes. This will usher in a new era of systems biology by providing spatial contextualization of the dynamic molecular interactions and protein networks found in intact tissues, opening new possibilities for probing disease-perturbed systems and drug target discovery.

## References

1. Venter, J. C.; Adams, M. D.; Myers, E. W.; Li, P. W.; Mural, R. J.; Sutton, G. G.; Smith, H. O.; Yandell, M.; Evans, C. A.; Holt, R. A.; Gocayne, J. D.; Amanatides, P.; Ballew, R. M.; Huson, D. H.; Wortman, J. R.; Zhang, Q.; Kodira, C. D.; Zheng, X. Q. H.; Chen, L.; Skupski, M.; Subramanian, G.; Thomas, P. D.; Zhang, J. H.; Miklos, G. L. G.; Nelson, C.; Broder, S.; Clark, A. G.; Nadeau, C.; McKusick, V. A.; Zinder, N.; Levine, A. J.; Roberts, R. J.; Simon, M.; Slayman, C.; Hunkapiller, M.; Bolanos, R.; Delcher, A.; Dew, I.; Fasulo, D.; Flanigan, M.; Florea, L.; Halpern, A.; Hannenhalli, S.; Kravitz, S.; Levy, S.; Mobarry, C.; Reinert, K.; Remington, K.; Abu-Threideh, J.; Beasley, E.; Biddick, K.; Bonazzi, V.; Brandon, R.; Cargill, M.; Chandramouliswaran, I.; Charlab, R.; Chaturvedi, K.; Deng, Z. M.; Di Francesco, V.; Dunn, P.; Eilbeck, K.; Evangelista, C.; Gabrielian, A. E.; Gan, W.; Ge, W. M.; Gong, F. C.; Gu, Z. P.; Guan, P.; Heiman, T. J.; Higgins, M. E.; Ji, R. R.; Ke, Z. X.; Ketchum, K. A.; Lai, Z. W.; Lei, Y. D.; Li, Z. Y.; Li, J. Y.; Liang, Y.; Lin, X. Y.; Lu, F.; Merkulov, G. V.; Milshina, N.; Moore, H. M.; Naik, A. K.; Narayan, V. A.; Neelam, B.; Nusskern, D.; Rusch, D. B.; Salzberg, S.; Shao, W.; Shue, B. X.; Sun, J. T.; Wang, Z. Y.; Wang, A. H.; Wang, X.; Wang, J.; Wei, M. H.; Wides, R.; Xiao, C. L.; Yan, C. H.; Yao, A.; Ye, J.; Zhan, M.; Zhang, W. Q.; Zhang, H. Y.; Zhao, Q.; Zheng, L. S.; Zhong, F.; Zhong, W. Y.; Zhu, S. P. C.; Zhao, S. Y.; Gilbert, D.; Baumhueter, S.; Spier, G.; Carter, C.; Cravchik, A.; Woodage, T.; Ali, F.; An, H. J.; Awe, A.; Baldwin, D.; Baden, H.; Barnstead, M.; Barrow, I.; Beeson, K.; Busam, D.; Carver, A.; Center, A.; Cheng, M. L.; Curry, L.; Danaher, S.; Davenport, L.; Desilets, R.; Dietz, S.; Dodson, K.; Doup, L.; Ferriera, S.; Garg, N.; Gluecksmann, A.; Hart, B.; Haynes, J.; Haynes, C.; Heiner, C.; Hladun, S.; Hostin, D.; Houck, J.; Howland, T.; Ibegwam, C.; Johnson, J.; Kalush, F.; Kline, L.; Koduru, S.; Love, A.; Mann, F.; May, D.; McCawley, S.; McIntosh, T.; McMullen, I.; Moy, M.; Moy, L.; Murphy, B.; Nelson, K.; Pfannkoch, C.; Pratts, E.; Puri, V.; Qureshi, H.; Reardon, M.; Rodriguez, R.; Rogers, Y. H.; Romblad, D.; Ruhfel, B.; Scott, R.; Sitter, C.; Smallwood, M.; Stewart, E.; Strong, R.; Suh, E.; Thomas, R.; Tint, N. N.; Tse, S.; Vech, C.; Wang, G.; Wetter, J.; Williams, S.; Williams, M.; Windsor, S.; Winn-Deen, E.; Wolfe, K.; Zaveri, J.; Zaveri, K.; Abril, J. F.; Guigo, R.; Campbell, M. J.; Sjolander, K. V.; Karlak, B.; Kejariwal, A.; Mi, H. Y.; Lazareva, B.; Hatton, T.; Narechania, A.; Diemer, K.; Muruganujan, A.; Guo, N.; Sato, S.; Bafna, V.; Istrail, S.; Lippert, R.; Schwartz, R.; Walenz, B.; Yooseph, S.; Allen, D.; Basu, A.; Baxendale, J.; Blick, L.; Caminha, M.; Carnes-Stine, J.; Caulk, P.; Chiang, Y. H.; Coyne, M.; Dahlke, C.; Mays, A. D.; Dombroski, M.; Donnelly, M.; Ely, D.; Esparham, S.; Fosler, C.; Gire, H.; Glanowski, S.; Glasser, K.; Glodek, A.; Gorokhov, M.; Graham, K.; Gropman, B.; Harris, M.; Heil, J.; Henderson, S.; Hoover, J.; Jennings, D.; Jordan, C.; Jordan, J.; Kasha, J.; Kagan, L.; Kraft, C.; Levitsky, A.; Lewis, M.; Liu, X. J.; Lopez, J.; Ma, D.; Majoros, W.; McDaniel, J.; Murphy, S.; Newman, M.; Nguyen, T.; Nguyen, N.; Nodell, M.; Pan, S.; Peck, J.; Peterson, M.; Rowe, W.; Sanders, R.; Scott, J.; Simpson, M.; Smith, T.; Sprague, A.; Stockwell, T.; Turner, R.; Venter, E.; Wang, M.; Wen, M. Y.; Wu, D.; Wu, M.; Xia, A.; Zandieh, A.; Zhu, X. H., The sequence of the human genome. *Science* **2001**, *291* (5507), 1304-+.
2. Hanash, S., Disease proteomics. *Nature* **2003**, *422* (6928), 226-232.
3. Aebersold, R.; Agar, J. N.; Amster, I. J.; Baker, M. S.; Bertozzi, C. R.; Boja, E. S.; Costello, C. E.; Cravatt, B. F.; Fenselau, C.; Garcia, B. A.; Ge, Y.; Gunawardena, J.; Hendrickson, R. C.; Hergenrother, P. J.; Huber, C. G.; Ivanov, A. R.; Jensen, O. N.; Jewett, M. C.; Kelleher, N. L.; Kiessling, L. L.; Krogan, N. J.; Larsen, M. R.; Loo, J. A.; Loo, R. R. O.; Lundberg, E.; MacCoss, M. J.; Mallick, P.; Mootha, V. K.; Mrksich, M.; Muir, T. W.; Patrie, S. M.; Pesavento, J. J.; Pitteri, S. J.; Rodriguez, H.; Saghatelian, A.; Sandoval, W.; Schluter, H.; Sechi, S.; Slavoff, S. A.; Smith, L. M.; Snyder, M. P.; Thomas, P. M.; Uhlen, M.; Van Eyk, J. E.; Vidal, M.; Walt, D. R.; White, F. M.; Williams, E. R.; Wohlschlagler, T.; Wysocki, V. H.; Yates, N. A.; Young, N. L.; Zhang, B., How many human proteoforms are there? *Nature Chemical Biology* **2018**, *14* (3), 206-214.



4. El-Aneed, A.; Cohen, A.; Banoub, J., Mass Spectrometry, Review of the Basics: Electrospray, MALDI, and Commonly Used Mass Analyzers. *Applied Spectroscopy Reviews* **2009**, *44* (3), 210-230.
5. Tanaka, K.; Waki, H.; Ido, Y.; Akita, S.; Yoshida, Y.; Yoshida, T.; Matsuo, T., Protein and polymer analyses up to  $m/z$  100 000 by laser ionization time-of-flight mass spectrometry. *Rapid Commun. Mass Spectrom*: 1988; Vol. 2, pp 151-153.
6. Karas, M.; Bachmann, D.; Bahr, U.; Hillenkamp, F., MATRIX-ASSISTED ULTRAVIOLET-LASER DESORPTION OF NONVOLATILE COMPOUNDS. *International Journal of Mass Spectrometry and Ion Processes* **1987**, *78*, 53-68.
7. Sandrin, T. R.; Goldstein, J. E.; Schumaker, S., MALDI TOF MS profiling of bacteria at the strain level: A review. *Mass Spectrometry Reviews* **2013**, *32* (3), 188-217.
8. Monagas, M.; Quintanilla-Lopez, J. E.; Gomez-Cordoves, C.; Bartolome, B.; Lebron-Aguilar, R., MALDI-TOF MS analysis of plant proanthocyanidins. *Journal of Pharmaceutical and Biomedical Analysis* **2010**, *51* (2), 358-372.
9. Hu, Y. L.; Mechref, Y., Comparing MALDI-MS, RP-LC-MALDI-MS and RP-LC-ESI-MS glycomic profiles of permethylated N-glycans derived from model glycoproteins and human blood serum. *Electrophoresis* **2012**, *33* (12), 1768-1777.
10. Khattab, R.; Eskin, M.; Aliani, M.; Thiyam, U., Determination of Sinapic Acid Derivatives in Canola Extracts Using High-Performance Liquid Chromatography. *Journal of the American Oil Chemists Society* **2010**, *87* (2), 147-155.
11. Caprioli, R. M.; Farmer, T. B.; Gile, J., Molecular imaging of biological samples: Localization of peptides and proteins using MALDI-TOF MS. *Analytical Chemistry* **1997**, *69* (23), 4751-4760.
12. Kaspar, S.; Peukert, M.; Svatos, A.; Matros, A.; Mock, H. P., MALDI-imaging mass spectrometry - An emerging technique in plant biology. *Proteomics* **2011**, *11* (9), 1840-1850.
13. Powers, T. W.; Neely, B. A.; Shao, Y.; Tang, H. Y.; Troyer, D. A.; Mehta, A. S.; Haab, B. B.; Drake, R. R., MALDI Imaging Mass Spectrometry Profiling of N-Glycans in Formalin-Fixed Paraffin Embedded Clinical Tissue Blocks and Tissue Microarrays. *Plos One* **2014**, *9* (9).
14. Mirnezami, R.; Spagou, K.; Vorkas, P. A.; Lewis, M. R.; Kinross, J.; Want, E.; Shion, H.; Goldin, R. D.; Darzi, A.; Takats, Z.; Holmes, E.; Cloarec, O.; Nicholson, J. K., Chemical mapping of the colorectal cancer microenvironment via MALDI imaging mass spectrometry (MALDI-MSI) reveals novel cancer-associated field effects. *Molecular Oncology* **2014**, *8* (1), 39-49.
15. Ly, A.; Buck, A.; Balluff, B.; Sun, N.; Gorzolka, K.; Feuchtinger, A.; Janssen, K. P.; Kuppen, P. J. K.; van de Velde, C. J. H.; Weirich, G.; Erlmeier, F.; Langer, R.; Aubele, M.; Zitzelsberger, H.; McDonnell, L.; Aichler, M.; Walch, A., High-mass-resolution MALDI mass spectrometry imaging of metabolites from formalin-fixed paraffin-embedded tissue. *Nature Protocols* **2016**, *11* (8), 1428-1443.
16. Dilillo, M.; Ait-Belkacem, R.; Esteve, C.; Pellegrini, D.; Nicolardi, S.; Costa, M.; Vannini, E.; de Graaf, E. L.; Caleo, M.; McDonnell, L. A., Ultra-High Mass Resolution MALDI Imaging Mass Spectrometry of Proteins and Metabolites in a Mouse Model of Glioblastoma. *Scientific Reports* **2017**, *7*.
17. Anderson, D. M. G.; Ablonczy, Z.; Koutalos, Y.; Spraggins, J.; Crouch, R. K.; Caprioli, R. M.; Schey, K. L., High Resolution MALDI Imaging Mass Spectrometry of Retinal Tissue Lipids. *Journal of the American Society for Mass Spectrometry* **2014**, *25* (8), 1394-1403.
18. Gustafsson, O. J. R.; Briggs, M. T.; Condina, M. R.; Winderbaum, L. J.; Pelzing, M.; McColl, S. R.; Everest-Dass, A. V.; Packer, N. H.; Hoffmann, P., MALDI imaging mass spectrometry of N-linked glycans on formalin-fixed paraffin-embedded murine kidney. *Analytical and Bioanalytical Chemistry* **2015**, *407* (8), 2127-2139.
19. Kaletas, B. K.; van der Wiel, I. M.; Stauber, J.; Dekker, L. J.; Guzel, C.; Kros, J. M.; Luider, T. M.; Heeren, R. M. A., Sample preparation issues for tissue imaging by imaging MS. *Proteomics* **2009**, *9* (10), 2622-2633.

20. Yang, J. H.; Caprioli, R. M., Matrix Sublimation/Recrystallization for Imaging Proteins by Mass Spectrometry at High Spatial Resolution. *Analytical Chemistry* **2011**, *83* (14), 5728-5734.
21. Aichler, M.; Walch, A., MALDI Imaging mass spectrometry: current frontiers and perspectives in pathology research and practice. *Laboratory Investigation* **2015**, *95* (4), 422-431.
22. Gessel, M. M.; Norris, J. L.; Caprioli, R. M., MALDI imaging mass spectrometry: Spatial molecular analysis to enable a new age of discovery. *Journal of Proteomics* **2014**, *107*, 71-82.
23. Sidransky, D.; Irizarry, R.; Califano, J. A.; Li, X. B.; Ren, H. N.; Benoit, N.; Mao, L., Serum protein MALDI profiling to distinguish upper aerodigestive tract cancer patients from control subjects. *Journal of the National Cancer Institute* **2003**, *95* (22), 1711-1717.
24. Albrethsen, J., The first decade of MALDI protein profiling: A lesson in translational, biomarker research. *Journal of Proteomics* **2011**, *74* (6), 765-773.
25. Villanueva, J.; Philip, J.; Entenberg, D.; Chaparro, C. A.; Tanwar, M. K.; Holland, E. C.; Tempst, P., Serum peptide profiling by magnetic particle-assisted, automated sample processing and MALDI-TOF mass spectrometry. *Analytical Chemistry* **2004**, *76* (6), 1560-1570.
26. Gamez-Pozo, A.; Sanchez-Navarro, I.; Nistal, M.; Calvo, E.; Madero, R.; Diaz, E.; Camafeita, E.; de Castro, J.; Lopez, J. A.; Gonzalez-Baron, M.; Espinosa, E.; Vara, J. A. F., MALDI Profiling of Human Lung Cancer Subtypes. *Plos One* **2009**, *4* (11).
27. Ryan, D. J.; Spraggins, J. M.; Caprioli, R. M., Protein identification strategies in MALDI imaging mass spectrometry: a brief review. *Current opinion in chemical biology* **2018**, *48*, 64-72.
28. van Hove, E. R. A.; Smith, D. F.; Heeren, R. M. A., A concise review of mass spectrometry imaging. *Journal of Chromatography A* **2010**, *1217* (25), 3946-3954.
29. Bich, C.; Touboul, D.; Brunelle, A., Biomedical studies by TOF-SIMS imaging. *Biointerphases* **2015**, *10* (1).
30. Wiseman, J. M.; Ifa, D. R.; Song, Q. Y.; Cooks, R. G., Tissue imaging at atmospheric pressure using desorption electrospray ionization (DESI) mass spectrometry. *Angewandte Chemie-International Edition* **2006**, *45* (43), 7188-7192.
31. Vestal, M. L.; Juhasz, P.; Martin, S. A., DELAYED EXTRACTION MATRIX-ASSISTED LASER-DESORPTION TIME-OF-FLIGHT MASS-SPECTROMETRY. *Rapid Communications in Mass Spectrometry* **1995**, *9* (11), 1044-1050.
32. Mamyrin, B. A.; Karataev, V. I.; Shmikk, D. V.; Zagulin, V. A., The mass-reflectron, a new nonmagnetic time-of-flight mass spectrometer with high resolution. *Soviet Physics* **1973**, *37* (45).
33. Du, L.; Yang, X. H.; Li, W. Q.; Li, H. Y.; Feng, S. B.; Zeng, R.; Yu, B.; Xiao, L. X.; Liu, Y.; Tu, M.; Nie, H. Y., Time-of-flight secondary ion mass spectrometry analyses of vancomycin. *Biointerphases* **2018**, *13* (3).
34. Annan, R. S.; Carr, S. A., Phosphopeptide analysis by matrix-assisted laser desorption time-of-flight mass spectrometry. *Analytical Chemistry* **1996**, *68* (19), 3413-3421.
35. Llombart, V.; Trejo, S. A.; Bronsoms, S.; Morancho, A.; Ma, F. F.; Faura, J.; Garcia-Berrocoso, T.; Simats, A.; Rosell, A.; Canals, F.; Hernandez-Guillamon, M.; Montaner, J., Profiling and identification of new proteins involved in brain ischemia using MALDI-imaging-mass-spectrometry. *Journal of Proteomics* **2017**, *152*, 243-253.
36. Li, Y.; Shrestha, B.; Vertes, A., Atmospheric pressure molecular imaging by infrared MALDI mass spectrometry. *Analytical Chemistry* **2007**, *79* (2), 523-532.
37. Nemes, P.; Barton, A. A.; Li, Y.; Vertes, A., Ambient molecular imaging and depth profiling of live tissue by infrared laser ablation electrospray ionization mass spectrometry. *Analytical Chemistry* **2008**, *80* (12), 4575-4582.
38. Djidja, M. C.; Claude, E.; Snel, M. F.; Scriven, P.; Francese, S.; Carolan, V.; Clench, M. R., MALDI-Ion Mobility Separation-Mass Spectrometry Imaging of Glucose-Regulated Protein 78 kDa

- (Grp78) in Human Formalin-Fixed, Paraffin-Embedded Pancreatic Adenocarcinoma Tissue Sections. *Journal of Proteome Research* **2009**, *8* (10), 4876-4884.
39. Marshall, A. G.; Hendrickson, C. L.; Jackson, G. S., Fourier transform ion cyclotron resonance mass spectrometry: A primer. *Mass Spectrometry Reviews* **1998**, *17* (1), 1-35.
40. Spraggins, J. M.; Rizzo, D. G.; Moore, J. L.; Rose, K. L.; Hammer, N. D.; Skaar, E. P.; Caprioli, R. M., MALDI FTICR IMS of Intact Proteins: Using Mass Accuracy to Link Protein Images with Proteomics Data. *Journal of the American Society for Mass Spectrometry* **2015**, *26* (6), 974-985.
41. Spraggins, J. M.; Rizzo, D. G.; Moore, J. L.; Noto, M. J.; Skaar, E. P.; Caprioli, R. M., Next-generation technologies for spatial proteomics: Integrating ultra-high speed MALDI-TOF and high mass resolution MALDI FTICR imaging mass spectrometry for protein analysis. *Proteomics* **2016**, *16* (11-12), 1678-1689.
42. Boersema, P. J.; Taouatas, N.; Altelaar, A. F. M.; Gouw, J. W.; Ross, P. L.; Pappin, D. J.; Heck, A. J. R.; Mohammed, S., Straightforward and de Novo Peptide Sequencing by MALDI-MS/MS Using a Lys-N Metalloendopeptidase. *Molecular & Cellular Proteomics* **2009**, *8* (4), 650-660.
43. Mekecha, T. T.; Amunugama, R.; McLuckey, S. A., Ion trap collision-induced dissociation of human hemoglobin alpha-chain cations. *Journal of the American Society for Mass Spectrometry* **2006**, *17* (7), 923-931.
44. Reid, G. E.; McLuckey, S. A., 'Top down' protein characterization via tandem mass spectrometry. *Journal of Mass Spectrometry* **2002**, *37* (7), 663-675.
45. Zhang, Y. Y.; Fonslow, B. R.; Shan, B.; Baek, M. C.; Yates, J. R., Protein Analysis by Shotgun/Bottom-up Proteomics. *Chemical Reviews* **2013**, *113* (4), 2343-2394.
46. Catherman, A. D.; Skinner, O. S.; Kelleher, N. L., Top Down proteomics: Facts and perspectives. *Biochemical and Biophysical Research Communications* **2014**, *445* (4), 683-693.
47. Wells, J. M.; McLuckey, S. A., Collision-induced dissociation (CID) of peptides and proteins. *Biological Mass Spectrometry* **2005**, *402*, 148-185.
48. Wysocki, V. H.; Tsaprailis, G.; Smith, L. L.; Brechi, L. A., Special feature: Commentary - Mobile and localized protons: a framework for understanding peptide dissociation. *Journal of Mass Spectrometry* **2000**, *35* (12), 1399-1406.
49. Syka, J. E. P.; Coon, J. J.; Schroeder, M. J.; Shabanowitz, J.; Hunt, D. F., Peptide and protein sequence analysis by electron transfer dissociation mass spectrometry. *Proceedings of the National Academy of Sciences of the United States of America* **2004**, *101* (26), 9528-9533.
50. Schey, K. L.; Hachey, A. J.; Rose, K. L.; Grey, A. C., MALDI imaging mass spectrometry of Pacific White Shrimp *L. vannamei* and identification of abdominal muscle proteins. *Proteomics* **2016**, *16* (11-12), 1767-1774.
51. Alberts, D.; Pottier, C.; Smargiasso, N.; Baiwir, D.; Mazzucchelli, G.; Delvenne, P.; Kriegsmann, M.; Kazdal, D.; Warth, A.; De Pauw, E.; Longuespee, R., MALDI Imaging-Guided Microproteomic Analyses of Heterogeneous Breast Tumors-A Pilot Study. *Proteomics Clinical Applications* **2018**, *12* (1).
52. Yajima, Y.; Hiratsuka, T.; Kakimoto, Y.; Ogawa, S.; Shima, K.; Yamazaki, Y.; Yoshikawa, K.; Tamaki, K.; Tsuruyama, T., Region of Interest analysis using mass spectrometry imaging of mitochondrial and sarcomeric proteins in acute cardiac infarction tissue. *Scientific Reports* **2018**, *8*.
53. Svensson, M.; Boren, M.; Skold, K.; Falth, M.; Sjogren, B.; Andersson, M.; Svenningsson, P.; Andren, P. E., Heat Stabilization of the Tissue Proteome: A New Technology for Improved Proteomics. *Journal of Proteome Research* **2009**, *8* (2), 974-981.
54. Wu, C. C.; MacCoss, M. J.; Howell, K. E.; Yates, J. R., A method for the comprehensive proteomic analysis of membrane proteins. *Nature Biotechnology* **2003**, *21* (5), 532-538.
55. Overmyer, K. A.; Tyanova, S.; Hebert, A. S.; Westphall, M. S.; Cox, J.; Coon, J. J., Multiplexed proteome analysis with neutron-encoded stable isotope labeling in cells and mice. *Nature Protocols* **2018**, *13* (2), 293-306.

56. Ficarro, S. B.; McClelland, M. L.; Stukenberg, P. T.; Burke, D. J.; Ross, M. M.; Shabanowitz, J.; Hunt, D. F.; White, F. M., Phosphoproteome analysis by mass spectrometry and its application to *Saccharomyces cerevisiae*. *Nature Biotechnology* **2002**, *20* (3), 301-305.
57. Wisztorski, M.; Quanico, J.; Franck, J.; Fatou, B.; Salzet, M.; Fournier, I., Droplet-Based Liquid Extraction for Spatially-Resolved Microproteomics Analysis of Tissue Sections. *Imaging Mass Spectrometry: Methods and Protocols* **2017**, *1618*, 49-63.
58. Lefcoski, S.; Kew, K.; Reece, S.; Torres, M. J.; Parks, J.; Bras, L. E. D.; Virag, J. A. I., Anatomical-Molecular Distribution of EphrinA1 in Infarcted Mouse Heart Using MALDI Mass Spectrometry Imaging. *Journal of the American Society for Mass Spectrometry* **2018**, *29* (3), 527-534.
59. Grey, A. C.; Schey, K. L., Age-Related Changes in the Spatial Distribution of Human Lens alpha-Crystallin Products by MALDI Imaging Mass Spectrometry. *Investigative Ophthalmology & Visual Science* **2009**, *50* (9), 4319-4329.
60. Pote, N.; Alexandrov, T.; Le Faouder, J.; Laouirem, S.; Leger, T.; Mebarki, M.; Belghiti, J.; Camadro, J. M.; Bedossa, P.; Paradis, V., Imaging Mass Spectrometry Reveals Modified Forms of Histone H4 as New Biomarkers of Microvascular Invasion in Hepatocellular Carcinomas. *Hepatology* **2013**, *58* (3), 983-994.
61. Groseclose, M. R.; Massion, P. R.; Chaurand, P.; Caprioli, R. M., High-throughput proteomic analysis of formalin-fixed paraffin-embedded tissue microarrays using MALDI imaging mass spectrometry. *Proteomics* **2008**, *8* (18), 3715-3724.
62. Stauber, J.; MacAleese, L.; Franck, J.; Claude, E.; Snel, M.; Kaletas, B. K.; Wiel, I.; Wisztorski, M.; Fournier, I.; Heeren, R. M. A., On-Tissue Protein Identification and Imaging by MALDI-Ion Mobility Mass Spectrometry. *Journal of the American Society for Mass Spectrometry* **2010**, *21* (3), 338-347.
63. Toue, S.; Sugiura, Y.; Kubo, A.; Ohmura, M.; Karakawa, S.; Mizukoshi, T.; Yoneda, J.; Miyano, H.; Noguchi, Y.; Kobayashi, T.; Kabe, Y.; Suematsu, M., Microscopic imaging mass spectrometry assisted by on-tissue chemical derivatization for visualizing multiple amino acids in human colon cancer xenografts. *Proteomics* **2014**, *14* (7-8), 810-819.
64. Keough, T.; Lacey, M. P.; Youngquist, R. S., Derivatization procedures to facilitate de novo sequencing of lysine-terminated tryptic peptides using postsorce decay matrix-assisted laser desorption/ionization mass spectrometry. *Rapid Communications in Mass Spectrometry* **2000**, *14* (24), 2348-2356.
65. Samyn, B.; Debyser, G.; Sergeant, K.; Devreese, B.; Van Beeumen, J., A case study of de novo sequence analysis of N-sulfonated peptides by MALDI TOF/TOF mass spectrometry. *Journal of the American Society for Mass Spectrometry* **2004**, *15* (12), 1838-1852.
66. Franck, J.; El Ayed, M.; Wisztorski, M.; Salzet, M.; Fournier, I., On-Tissue N-Terminal Peptide Derivatizations for Enhancing Protein Identification in MALDI Mass Spectrometric Imaging Strategies. *Analytical Chemistry* **2009**, *81* (20), 8305-8317.
67. Holst, S.; Heijs, B.; de Haan, N.; van Zeijl, R. J. M.; Briaire-de Bruijn, I. H.; van Pelt, G. W.; Mehta, A. S.; Angel, P. M.; Mesker, W. E.; Tollenaar, R. A.; Drake, R. R.; Bovee, J.; McDonnell, L. A.; Wuhrer, M., Linkage-Specific in Situ Sialic Acid Derivatization for N-Glycan Mass Spectrometry Imaging of Formalin-Fixed Paraffin-Embedded Tissues. *Analytical Chemistry* **2016**, *88* (11), 5904-5913.
68. Quanico, J.; Franck, J.; Wisztorski, M.; Salzet, M.; Fournier, I., Combined MALDI Mass Spectrometry Imaging and Parafilm-Assisted Microdissection-Based LC-MS/MS Workflows in the Study of the Brain. *Neuroproteomics: Methods and Protocols, 2nd Edition* **2017**, *1598*, 269-283.
69. Liu, E. Y.; Jung, S.; Weitz, D. A.; Yi, H. M.; Choi, C. H., High-throughput double emulsion-based microfluidic production of hydrogel microspheres with tunable chemical functionalities toward biomolecular conjugation. *Lab on a Chip* **2018**, *18* (2), 323-334.
70. Li, J. Y.; Mooney, D. J., Designing hydrogels for controlled drug delivery. *Nature Reviews Materials* **2016**, *1* (12).

71. Liu, H.; Wang, C. Y.; Li, C.; Qin, Y. G.; Wang, Z. H.; Yang, F.; Li, Z. H.; Wang, J. C., A functional chitosan-based hydrogel as a wound dressing and drug delivery system in the treatment of wound healing. *Rsc Advances* **2018**, *8* (14), 7533-7549.
72. Harris, G. A.; Nicklay, J. J.; Caprioli, R. M., Localized in Situ Hydrogel-Mediated Protein Digestion and Extraction Technique for on-Tissue Analysis. *Analytical Chemistry* **2013**, *85* (5), 2717-2723.
73. Nicklay, J. J.; Harris, G. A.; Schey, K. L.; Caprioli, R. M., MALDI Imaging and in Situ Identification of Integral Membrane Proteins from Rat Brain Tissue Sections. *Analytical Chemistry* **2013**, *85* (15), 7191-7196.
74. Rizzo, D. G.; Prentice, B. M.; Moore, J. L.; Norris, J. L.; Caprioli, R. M., Enhanced Spatially Resolved Proteomics Using On-Tissue Hydrogel Mediated Protein Digestion. *Analytical Chemistry* **2017**, *89* (5), 2948-2955.
75. Schey, K. L.; Anderson, D. M.; Rose, K. L., Spatially-Directed Protein Identification from Tissue Sections by Top-Down LC-MS/MS with Electron Transfer Dissociation. *Analytical Chemistry* **2013**, *85* (14), 6767-6774.
76. Bruins, A. P.; Covey, T. R.; Henion, J. D., Ion spray interface for combined liquid chromatography/atmospheric pressure ionization mass spectrometry. *Anal. Chem.* **1987**, *59*, 2642-2646.
77. Ford, M. J.; Van Berkel, G. J., An improved thin-layer chromatography/mass spectrometry coupling using a surface sampling probe electrospray ion trap system. *Rapid Communications in Mass Spectrometry* **2004**, *18* (12), 1303-1309.
78. Prentice, B. M.; Ryan, D. J.; Van de Plas, R.; Caprioli, R. M.; Spraggins, J. M., Enhanced Ion Transmission Efficiency up to m/z 24 000 for MALDI Protein Imaging Mass Spectrometry. *Anal. Chem.*, **2018**; Vol. 90, pp 5090-5099.
79. Dole, M.; Mack, L. L.; Hines, R. L.; Mobley, R. C.; Ferguson, L. D.; Alice, M. B., Molecular beams of macroions. *J. Chem. Phys.* **1968**, *49*, 2240-2249.
80. Mack, L. L.; Kralik, P.; Rheude, A.; Dole, M., Molecular beams of macroions II. *J. Chem. Phys.* **1970**, *52*, 4977-4986.
81. Yamashita, M.; Fenn, J. B., Electrospray ion source. Another variation on the free-jet theme. *J Phys Chem* **1984**, *88*, 4451-4459.
82. Fenn, J. B.; Mann, M.; Meng, C. K.; Wong, S. F.; Whitehouse, C. M., Electrospray ionization for mass spectrometry of large biomolecules. *Science* **1989**, *246* (4926), 64-71.
83. Chowdhury, S. K.; Katta, V.; Chait, B. T., An electrospray-ionization mass spectrometer with new features. *Rapid Commun. Mass Spectrom.* **1990**, *4*, 81-87.
84. Wilm, M. S.; Mann, M., Electrospray and Taylor-cone theory, Dole's beam of macromolecules at last? *Int. J. Mass Spectrom. Ion Processes* **1994**, *136*, 167-180.
85. Wilm, M.; Mann, M., Analytical properties of the nanoelectrospray ion source. *Anal. Chem.* **1996**, *68* (1), 1-8.
86. Shaffer, S. A.; Tang, K.; Anderson, G. A.; Prior, D. C.; Udseth, H. R.; Smith, R. D., A novel ion funnel for focusing ions at elevated pressure using electrospray ionization mass spectrometry. *Rapid Commun. Mass Spectrom.* **1997**, *11*, 1813-1817.
87. Shaffer, S. A.; Prior, D. C.; Anderson, G. A.; Udseth, H. R.; Smith, R. D., An ion funnel interface for improved ion focusing and sensitivity using electrospray ionization mass spectrometry. *Anal. Chem.* **1998**, *70* (19), 4111-4119.
88. Kim, T.; Tolmachev, A. V.; Harkewicz, R.; Prior, D. C.; Anderson, G.; Udseth, H. R.; Smith, R. D.; Bailey, T. H.; Rakov, S.; Futrell, J. H., Design and implementation of a new electrodynamic ion funnel. *Anal. Chem.* **2000**, *72* (10), 2247-2255.
89. Second, T. P.; Blethrow, J. D.; Schwartz, J. C.; Merrihew, G. E.; MacCoss, M. J.; Swaney, D. L.; Russell, J. D.; Coon, J. J.; Zabrouskov, V., Dual-pressure linear ion trap mass spectrometer improving the analysis of complex protein mixtures. *Anal. Chem.* **2009**, *81* (18), 7757-7765.

90. Fernandez-Lima, F.; Kaplan, D. A.; Suetering, J.; Park, M. A., Gas-phase separation using a trapped ion mobility spectrometer. *International Journal for Ion Mobility Spectrometry* **2011**, *14* (2-3), 93-98.
91. May, J. C.; Goodwin, C. R.; Lareau, N. M.; Leaptrot, K. L.; Morris, C. B.; Kurulugama, R. T.; Mordehai, A.; Klein, C.; Barry, W.; Darland, E.; Overney, G.; Imatani, K.; Stafford, G. C.; Fjeldsted, J. C.; McLean, J. A., Conformational ordering of biomolecules in the gas phase: nitrogen collision cross sections measured on a prototype high resolution drift tube ion mobility-mass spectrometer. *Anal. Chem.* **2014**, *86* (4), 2107-2116.
92. Lynn, E. C.; Chung, M. C.; Han, C. C., Characterizing the transmission properties of an ion funnel. *Rapid Commun. Mass Spectrom.* **2000**, *14* (22), 2129-2134.
93. Tolmachev, A. V.; Kim, T.; Udseth, H. R.; Smith, R. D.; Bailey, T. H.; Futrell, J. H., Simulation-based optimization of the electrodynamic ion funnel for high sensitivity electrospray ionization mass spectrometry. *Int. J. Mass Spectrom.* **2000**, *203* (1-3), 31-47.
94. Julian, R. R.; Mabbett, S. R.; Jarrold, M. F., Ion funnels for the masses: experiments and simulations with a simplified ion funnel. *J. Am. Soc. Mass Spectrom.* **2005**, *16* (10), 1708-1712.
95. Page, J. S.; Tolmachev, A. V.; Tang, K. Q.; Smith, R. D., Theoretical and experimental evaluation of the low m/z transmission of an electrodynamic ion funnel. *J. Am. Soc. Mass Spectrom.* **2006**, *17* (4), 586-592.
96. Kelly, R. T.; Tolmachev, A. V.; Page, J. S.; Tang, K. Q.; Smith, R. D., The ion funnel: theory, implementations, and applications. *Mass Spectrom. Rev.* **2010**, *29* (2), 294-312.
97. Ibrahim, Y.; Tang, K. Q.; Tolmachev, A. V.; Shvartsburg, A. A.; Smith, R. D., Improving mass spectrometer sensitivity using a high-pressure electrodynamic ion funnel interface. *J. Am. Soc. Mass Spectrom.* **2006**, *17* (9), 1299-1305.
98. Dehmelt, H. G., Radiofrequency spectroscopy of stored ions I: storage. In *Adv. At. Mol. Phys.*, Bates, D. R.; Estermann, I., Eds. Academic Press: New York, 1967; Vol. 3, pp 53-72.
99. Gerlich, D., Inhomogeneous rf fields: a versatile tool for the study of processes with slow ions. In *State-Selected and State-to-State Ion-Molecule Reaction Dynamics. Part 1: Experiment*, Ng, C.-Y.; Baer, M., Eds. John Wiley & Sons, Inc.: 1992; Vol. LXXXII.
100. Schmidt, A.; Bahr, U.; Karas, M., Influence of pressure in the first pumping stage on analyte desolvation and fragmentation in nano-ESI MS. *Anal. Chem.* **2001**, *73* (24), 6040-6046.
101. van den Heuvel, R. H. H.; van Duijn, E.; Mazon, H.; Synowsky, S. A.; Lorenzen, K.; Versluis, C.; Brouns, S. J. J.; Langridge, D.; van der Oost, J.; Hoyes, J.; Heck, A. J. R., Improving the performance of a quadrupole time-of-flight instrument for macromolecular mass spectrometry. *Anal. Chem.* **2006**, *78* (21), 7473-7483.
102. Landreh, M.; Liko, I.; Uzdavinys, P.; Coincon, M.; Hopper, J. T. S.; Drew, D.; Robinson, C. V., Controlling release, unfolding and dissociation of membrane protein complexes in the gas phase through collisional cooling. *Chem. Commun.* **2015**, *51* (85), 15582-15584.
103. Rosati, S.; Rose, R. J.; Thompson, N. J.; van Duijn, E.; Damoc, E.; Denisov, E.; Makarov, A.; Heck, A. J. R., Exploring an orbitrap analyzer for the characterization of intact antibodies by native mass spectrometry. *Angew. Chem.-Int. Edit.* **2012**, *51* (52), 12992-12996.
104. van de Waterbeemd, M. V.; Fort, K. L.; Boll, D.; Reinhardt-Szyba, M.; Routh, A.; Makarov, A.; Heck, A. J. R., High-fidelity mass analysis unveils heterogeneity in intact ribosomal particles. *Nat. Methods* **2017**, *14* (3), 283-+.
105. Li, H. L.; Nguyen, H. H.; Loo, R. R. O.; Campuzano, I. D. G.; Loo, J. A., An integrated native mass spectrometry and top-down proteomics method that connects sequence to structure and function of macromolecular complexes. *Nature Chem.* **2018**, *10* (2), 139-148.
106. Karas, M.; Kruger, R., Ion formation in MALDI: The cluster ionization mechanism. *Chem. Rev.* **2003**, *103* (2), 427-439.

107. Knochenmuss, R.; Zenobi, R., MALDI ionization: The role of in-plume processes. *Chem. Rev.* **2003**, *103* (2), 441-452.
108. Knochenmuss, R., Ion formation mechanisms in UV-MALDI. *Analyst* **2006**, *131* (9), 966-986.
109. Spraggins, J. M. R., David G.; Moore, Jessica L.; Rose, Kristie L.; Hammer, Neal D.; Skaar, Eric P.; Caprioli, Richard M., MALDI FTICR IMS of intact proteins: using mass accuracy to link protein images with proteomics data. *J. Am. Soc. Mass Spectrom.* **2015**, *26*, 974-985.
110. Baykut, G.; Jertz, R.; Witt, M., Matrix-assisted laser desorption/ionization Fourier transform ion cyclotron resonance mass spectrometry with pulsed in-source collision gas and in-source ion accumulation. *Rapid Commun. Mass Spectrom.* **2000**, *14* (14), 1238-1247.
111. Belov, M. E.; Gorshkov, M. V.; Udseth, H. R.; Anderson, G. A.; Tolmachev, A. V.; Prior, D. C.; Harkewicz, R.; Smith, R. D., Initial implementation of an electrodynamic ion funnel with Fourier transform ion cyclotron resonance mass spectrometry. *J. Am. Soc. Mass Spectrom.* **2000**, *11* (1), 19-23.
112. Kellersberger, K. A.; Tan, P. V.; Laiko, V. V.; Doroshenko, V. M.; Fabris, D., Atmospheric pressure MALDI-Fourier transform mass spectrometry. *Anal. Chem.* **2004**, *76* (14), 3930-3934.
113. Tan, P. V.; Laiko, V. V.; Doroshenko, V. M., Atmospheric pressure MALDI with pulsed dynamic focusing for high-efficiency transmission of ions into a mass spectrometer. *Anal. Chem.* **2004**, *76* (9), 2462-2469.
114. Smith, D. F.; Aizikov, K.; Duursma, M. C.; Giskes, F.; Spaanderman, D. J.; McDonnell, L. A.; O'Connor, P. B.; Heeren, R. M. A., An external matrix-assisted laser desorption ionization source for flexible FT-ICR mass spectrometry imaging with internal calibration on adjacent samples. *J. Am. Soc. Mass Spectrom.* **2011**, *22* (1), 130-137.
115. Karas, M.; Hillenkamp, F., Laser desorption ionization of proteins with molecular masses exceeding 10,000 daltons. *Anal. Chem.* **1988**, *60* (20), 2299-2301.
116. Tanaka, K.; Waki, N.; Ido, Y.; Akita, S.; Yoshida, Y.; Yoshida, T., Protein and polymer analyses up to  $m/z$  100,000 by laser ionization time-of-flight mass spectrometry. *Rapid Commun. Mass Spectrom.* **1988**, *2*, 151-153.
117. Spraggins, J.; Rizzo, D.; Moore, J.; Noto, M.; Skaar, E.; Caprioli, R., Next-generation technologies for spatial proteomics: Integrating ultra-high speed MALDI-TOF and high mass resolution MALDI FTICR imaging mass spectrometry for protein analysis. *Proteomics* **2016**, *16* (11-12), 1678-1689.
118. Castro, J. A.; Koster, C.; Wilkins, C., Matrix-assisted laser desorption/ionization of high-mass molecules by Fourier-transform mass spectrometry. *Rapid Commun. Mass Spectrom.* **1992**, *6* (4), 239-241.
119. Koster, C.; Castoro, J. A.; Wilkins, C. L., High-resolution matrix-assisted laser desorption/ionization of biomolecules by Fourier transform mass spectrometry. *J. Am. Chem. Soc.* **1992**, *114* (19), 7572-7574.
120. Easterling, M. L.; Mize, T. H.; Amster, I. J., Routine part-per-million mass accuracy for high-mass ions: Space-charge effects in MALDI FT-ICR. *Anal. Chem.* **1999**, *71* (3), 624-632.
121. Kim, T.; Udseth, H. R.; Smith, R. D., Improved ion transmission from atmospheric pressure to high vacuum using a multicapillary inlet and electrodynamic ion funnel interface. *Anal. Chem.* **2000**, *72* (20), 5014-5019.
122. Zenobi, R.; Knochenmuss, R., Ion formation in MALDI mass spectrometry. *Mass Spectrom. Rev.* **1998**, *17* (5), 337-366.
123. Konig, S.; Kollas, O.; Dreisewerd, K., Generation of highly charged peptide and protein ions by atmospheric pressure matrix-assisted infrared laser desorption/ionization ion trap mass spectrometry. *Anal. Chem.* **2007**, *79* (14), 5484-5488.
124. Sampson, J. S.; Hawkridge, A. M.; Muddiman, D. C., Development and characterization of an ionization technique for analysis of biological macromolecules: Liquid matrix-assisted laser desorption electrospray ionization. *Anal. Chem.* **2008**, *80* (17), 6773-6778.

125. Sampson, J. S.; Muddiman, D. C., Atmospheric pressure infrared (10.6  $\mu\text{m}$ ) laser desorption electrospray ionization (IR-LDESI) coupled to a LTQ Fourier transform ion cyclotron resonance mass spectrometer. *Rapid Commun. Mass Spectrom.* **2009**, *23* (13), 1989-1992.
126. McEwen, C. N.; Larsen, B. S.; Trimpin, S., Laserspray ionization on a commercial atmospheric pressure-MALDI mass spectrometer ion source: selecting singly or multiply charged ions. *Anal. Chem.* **2010**, *82* (12), 4998-5001.
127. Spengler, B.; Hubert, M., Scanning microprobe matrix-assisted laser desorption ionization (SMALDI) mass spectrometry: instrumentation for sub-micrometer resolved LDI and MALDI surface analysis. *J. Am. Soc. Mass Spectrom.* **2002**, *13* (6), 735-748.
128. Hopfgartner, G.; Varesio, E.; Stoekli, M., Matrix-assisted laser desorption/ionization mass spectrometric imaging of complete rat sections using a triple quadrupole linear ion trap. *Rapid communications in mass spectrometry : RCM* **2009**, *23* (6), 733-736.
129. Spraggins, J. M.; Caprioli, R. M., High-speed MALDI-TOF imaging mass spectrometry: rapid ion image acquisition and considerations for next generation instrumentation. *J. Am. Soc. Mass Spectrom.* **2011**, *22* (6), 1022-1031.
130. Trim, P.; Djidja, M.-C.; Atkinson, S.; Oakes, K.; Cole, L.; Anderson, D.; Hart, P.; Francese, S.; Clench, M., Introduction of a 20 kHz Nd:YVO<sub>4</sub> laser into a hybrid quadrupole time-of-flight mass spectrometer for MALDI-MS imaging. *Anal. Bioanal. Chem.* **2010**, *397* (8), 3409-3419.
131. Prentice, B. M.; Chumbly, C. W.; Caprioli, R. M., High-speed MALDI TOF/TOF imaging mass spectrometry using continuous raster sampling. *J. Mass Spectrom.* **2015**, *50* (4), 703-710.
132. Van de Plas, R. Y., Junhai; Spraggins, Jeffery; Caprioli, Richard M., Image fusion of mass spectrometry and microscopy: a multimodality paradigm for molecular tissue mapping. *Nat. Methods* **2015**, *12* (4), 366-372.
133. Alford, J. M.; Williams, P. E.; Trevor, D. J.; Smalley, R. E., Metal cluster ion cyclotron resonance. Combining supersonic metal cluster beam technology with FT-ICR. *Int. J. Mass Spectrom.* **1986**, *72* (1-2), 33-51.
134. Kofel, P.; Allemann, M.; Kellerhals, H.; Wanczek, K. P., Time-of-flight ICR spectrometry. *Int. J. Mass Spectrom. Ion Processes* **1986**, *72* (1-2), 53-61.
135. Deutschens, F.; Yang, J.; Caprioli, R. M., High spatial resolution imaging mass spectrometry and classical histology on a single tissue section. *J. Mass Spectrom.* **2011**, *46* (6), 568-571.
136. Hankin, J. A.; Barkley, R. M.; Murphy, R. C., Sublimation as a method of matrix application for mass spectrometric imaging. *J. Am. Soc. Mass Spectrom.* **2007**, *18* (9), 1646-1652.
137. Yang, J.; Caprioli, R. M., Matrix sublimation/recrystallization for imaging proteins by mass spectrometry at high spatial resolution. *Anal. Chem.* **2011**, *83* (14), 5728-5734.
138. Caprioli, R. M.; Farmer, T. B.; Gile, J., Molecular imaging of biological samples: localization of peptides and proteins using MALDI-TOF MS. *Anal. Chem.* **1997**, *69*, 4751-4760.
139. Moore, J. L.; Becker, K. W.; Nicklay, J. J.; Boyd, K. L.; Skaar, E. P.; Caprioli, R. M., Imaging mass spectrometry for assessing temporal proteomics: Analysis of calprotectin in *Acinetobacter baumannii* pulmonary infection. *Proteomics* **2014**, *14* (7-8), 820-828.
140. Meding, S.; Nitsche, U.; Balluff, B.; Elsner, M.; Rauser, S.; Schone, C.; Nipp, M.; Maak, M.; Feith, M.; Ebert, M. P.; Friess, H.; Langer, R.; Hofler, H.; Zitzelsberger, H.; Rosenberg, R.; Walch, A., Tumor Classification of Six Common Cancer Types Based on Proteomic Profiling by MALDI Imaging. *Journal of Proteome Research* **2012**, *11* (3), 1996-2003.
141. Castellino, S.; Groseclose, M. R.; Wagner, D., MALDI imaging mass spectrometry: bridging biology and chemistry in drug development. *Bioanalysis* **2011**, *3* (21), 2427-2441.
142. Karlsson, O.; Hanrieder, J., Imaging mass spectrometry in drug development and toxicology. *Archives of Toxicology* **2017**, *91* (6), 2283-2294.



143. Stauber, J.; Lemaire, R.; Franck, J.; Bonnel, D.; Croix, D.; Day, R.; Wisztorski, M.; Fournier, I.; Salzet, M., MALDI Imaging of formalin-fixed paraffin-embedded tissues: Application to model animals of Parkinson disease for biomarker hunting. *Journal of Proteome Research* **2008**, *7* (3), 969-978.
144. El Ayed, M.; Bonnel, D.; Longuespee, R.; Castellier, C.; Franck, J.; Vergara, D.; Desmons, A.; Tasiemski, A.; Kenani, A.; Vinatier, D.; Day, R.; Fournier, I.; Salzet, M., MALDI imaging mass spectrometry in ovarian cancer for tracking, identifying, and validating biomarkers. *Medical Science Monitor* **2010**, *16* (8), BR233-BR245.
145. Cornett, D. S.; Reyzer, M. L.; Chaurand, P.; Caprioli, R. M., MALDI imaging mass spectrometry: molecular snapshots of biochemical systems. *Nature Methods* **2007**, *4* (10), 828-833.
146. Goodwin, R. J. A.; Pennington, S. R.; Pitt, A. R., Protein and peptides in pictures: Imaging with MALDI mass spectrometry. *Proteomics* **2008**, *8* (18), 3785-3800.
147. Maier, S. K.; Hahne, H.; Gholami, A. M.; Balluff, B.; Meding, S.; Schoene, C.; Walch, A. K.; Kuster, B., Comprehensive Identification of Proteins from MALDI Imaging. *Molecular & Cellular Proteomics* **2013**, *12* (10), 2901-2910.
148. Wildburger, N. C.; Wood, P. L.; Gumin, J.; Lichti, C. F.; Emmett, M. R.; Lang, F. F.; Nilsson, C. L., ESI-MS/MS and MALDI-IMS Localization Reveal Alterations in Phosphatidic Acid, Diacylglycerol, and DHA in Glioma Stem Cell Xenografts. *Journal of Proteome Research* **2015**, *14* (6), 2511-2519.
149. Wenke, J. L.; Rose, K. L.; Spraggins, J. M.; Schey, K. L., MALDI Imaging Mass Spectrometry Spatially Maps Age-Related Deamidation and Truncation of Human Lens Aquaporin-0. *Investigative Ophthalmology & Visual Science* **2015**, *56* (12), 7398-7405.
150. Monroe, E. B.; Annangudi, S. R.; Hatcher, N. G.; Gutstein, H. B.; Rubakhin, S. S.; Sweedler, J. V., SIMS and MALDI MS imaging of the spinal cord. *Proteomics* **2008**, *8* (18), 3746-3754.
151. Groseclose, M. R.; Andersson, M.; Hardesty, W. M.; Caprioli, R. M., Identification of proteins directly from tissue: in situ tryptic digestions coupled with imaging mass spectrometry. *Journal of Mass Spectrometry* **2007**, *42* (2), 254-262.
152. Taverna, D.; Norris, J. L.; Caprioli, R. M., Histology-Directed Microwave Assisted Enzymatic Protein Digestion for MALDI MS Analysis of Mammalian Tissue. *Analytical Chemistry* **2015**, *87* (1), 670-676.
153. Patrie, S. M.; Robinson, D. E.; Meng, F. Y.; Du, Y.; Kelleher, N. L., Strategies for automating top-down protein analysis with Q-FTICR MS. *International Journal of Mass Spectrometry* **2004**, *234* (1-3), 175-184.
154. Kertesz, V.; Van Berkel, G. J., Liquid Microjunction Surface Sampling Coupled with High-Pressure Liquid Chromatography-Electrospray Ionization-Mass Spectrometry for Analysis of Drugs and Metabolites in Whole-Body Thin Tissue Sections. *Analytical Chemistry* **2010**, *82* (14), 5917-5921.
155. Kertesz, V.; Van Berkel, G. J., Fully automated liquid extraction-based surface sampling and ionization using a chip-based robotic nanoelectrospray platform. *Journal of Mass Spectrometry* **2010**, *45* (3), 252-260.
156. Sarsby, J.; Martin, N. J.; Lalor, P. F.; Bunch, J.; Cooper, H. J., Top-Down and Bottom-Up Identification of Proteins by Liquid Extraction Surface Analysis Mass Spectrometry of Healthy and Diseased Human Liver Tissue. *Journal of the American Society for Mass Spectrometry* **2014**, *25* (11), 1953-1961.
157. Rao, W.; Celiz, A. D.; Scurr, D. J.; Alexander, M. R.; Barrett, D. A., Ambient DESI and LESA-MS Analysis of Proteins Adsorbed to a Biomaterial Surface Using In-Situ Surface Tryptic Digestion. *Journal of the American Society for Mass Spectrometry* **2013**, *24* (12), 1927-1936.
158. Sarsby, J.; Griffiths, R. L.; Race, A. M.; Bunch, J.; Randall, E. C.; Creese, A. J.; Cooper, H. J., Liquid Extraction Surface Analysis Mass Spectrometry Coupled with Field Asymmetric Waveform Ion Mobility Spectrometry for Analysis of Intact Proteins from Biological Substrates. *Analytical Chemistry* **2015**, *87* (13), 6794-6800.

159. Van Berkel, G. J.; Kertesz, V., Continuous-flow liquid microjunction surface sampling probe connected on-line with high-performance liquid chromatography/mass spectrometry for spatially resolved analysis of small molecules and proteins. *Rapid Communications in Mass Spectrometry* **2013**, *27* (12), 1329-1334.
160. Kertesz, V.; Calligaris, D.; Feldman, D. R.; Changelian, A.; Laws, E. R.; Santagata, S.; Agar, N. Y. R.; Van Berkel, G. J., Profiling of adrenocorticotrophic hormone and arginine vasopressin in human pituitary gland and tumor thin tissue sections using droplet-based liquid-microjunction surface-sampling-HPLC-ESI-MS-MS. *Analytical and Bioanalytical Chemistry* **2015**, *407* (20), 5989-5998.
161. Martin, N. J.; Griffiths, R. L.; Edwards, R. L.; Cooper, H. J., Native Liquid Extraction Surface Analysis Mass Spectrometry: Analysis of Noncovalent Protein Complexes Directly from Dried Substrates. *Journal of the American Society for Mass Spectrometry* **2015**, *26* (8), 1320-1327.
162. Eikel, D.; Henion, J., Liquid extraction surface analysis (LESA) of food surfaces employing chip-based nano-electrospray mass spectrometry. *Rapid Communications in Mass Spectrometry* **2011**, *25* (16), 2345-2354.
163. Bailey, M. J.; Randall, E. C.; Costa, C.; Salter, T. L.; Race, A. M.; de Puit, M.; Koeberg, M.; Baumert, M.; Bunch, J., Analysis of urine, oral fluid and fingerprints by liquid extraction surface analysis coupled to high resolution MS and MS/MS - opportunities for forensic and biomedical science. *Analytical Methods* **2016**, *8* (16), 3373-3382.
164. Wisztorski, M.; Desmons, A.; Quanicco, J.; Fatou, B.; Gimeno, J. P.; Franck, J.; Salzet, M.; Fournier, I., Spatially-resolved protein surface microsampling from tissue sections using liquid extraction surface analysis. *Proteomics* **2016**, *16* (11-12), 1622-1632.
165. Lamont, L.; Baumert, M.; Ogrinc Potocnik, N.; Allen, M.; Vreeken, R.; Heeren, R. M. A.; Porta, T., Integration of Ion Mobility MSE after Fully Automated, Online, High-Resolution Liquid Extraction Surface Analysis Micro-Liquid Chromatography. *Anal Chem* **2017**.
166. Mu, H.; Ohashi, R.; Yang, H.; Wang, X. W.; Li, M.; Lin, P.; Yao, Q. Z.; Chen, C. Y., Thymosin beta 10 inhibits cell migration and capillary-like tube formation of human coronary artery endothelial cells. *Cell Motility and the Cytoskeleton* **2006**, *63* (4), 222-230.
167. Hall, A. K., DEVELOPMENTAL REGULATION OF THYMOSIN-BETA-10 MESSENGER-RNA IN THE HUMAN BRAIN. *Molecular Brain Research* **1991**, *9* (1-2), 175-177.
168. Junge, W.; Nelson, N., ATP Synthase. *Annual Review of Biochemistry*, Vol 84 **2015**, *84*, 631-657.
169. Lee, L. W.; Yatsu, F. M., ATP SYNTHESIS BY MITOCHONDRIA OF BRAIN SYNAPTOSOMES. *Journal of Neurochemistry* **1974**, *23* (5), 1081-1082.
170. Bosch, A.; Suau, P., CHANGES IN-CORE HISTONE VARIANT COMPOSITION IN DIFFERENTIATING NEURONS - THE ROLES OF DIFFERENTIAL TURNOVER AND SYNTHESIS RATES. *European Journal of Cell Biology* **1995**, *68* (3), 220-225.
171. Chen, R.; Kang, R.; Fan, X. G.; Tang, D., Release and activity of histone in diseases. *Cell Death & Disease* **2014**, *5*.
172. Bunn, H. F., SUBUNIT ASSEMBLY OF HEMOGLOBIN - AN IMPORTANT DETERMINANT OF HEMATOLOGIC PHENOTYPE. *Blood* **1987**, *69* (1), 1-6.
173. Finkelstein, F. O.; Story, K.; Firaneck, C.; Mendelssohn, D.; Barre, P.; Takano, T.; Soroka, S.; Mujais, S., Health-Related Quality of Life and Hemoglobin Levels in Chronic Kidney Disease Patients. *Clinical Journal of the American Society of Nephrology* **2009**, *4* (1), 33-38.
174. Deutskens, F.; Yang, J. H.; Caprioli, R. M., High spatial resolution imaging mass spectrometry and classical histology on a single tissue section. *Journal of Mass Spectrometry* **2011**, *46* (6), 568-571.
175. Jones, E. E.; Powers, T. W.; Neely, B. A.; Cazares, L. H.; Troyer, D. A.; Parker, A. S.; Drake, R. R., MALDI imaging mass spectrometry profiling of proteins and lipids in clear cell renal cell carcinoma. *Proteomics* **2014**, *14* (7-8), 924-935.

176. Labas, V.; Spina, L.; Belleannee, C.; Teixeira-Gomes, A. P.; Gargaros, A.; Dacheux, F.; Dacheux, J. L., Analysis of epididymal sperm maturation by MALDI profiling and top-down mass spectrometry. *Journal of Proteomics* **2015**, *113*, 226-243.
177. Na, C. H.; Hong, J. H.; Kim, W. S.; Shanta, S. R.; Bang, J. Y.; Park, D.; Kim, H. K.; Kim, K. P., Identification of Protein Markers Specific for Papillary Renal Cell Carcinoma Using Imaging Mass Spectrometry. *Molecules and Cells* **2015**, *38* (7), 624-629.
178. Kim, W.; Bennett, E. J.; Huttlin, E. L.; Guo, A.; Li, J.; Possemato, A.; Sowa, M. E.; Rad, R.; Rush, J.; Comb, M. J.; Harper, J. W.; Gygi, S. P., Systematic and Quantitative Assessment of the Ubiquitin-Modified Proteome. *Molecular Cell* **2011**, *44* (2), 325-340.
179. Pelkonen, L.; Sato, K.; Reinisalo, M.; Kidron, H.; Tachikawa, M.; Watanabe, M.; Uchida, Y.; Urtti, A.; Terasaki, T., LC-MS/MS Based Quantitation of ABC and SLC Transporter Proteins in Plasma Membranes of Cultured Primary Human Retinal Pigment Epithelium Cells and Immortalized ARPE19 Cell Line. *Molecular Pharmaceutics* **2017**, *14* (3), 605-613.
180. Steurer, S.; Seddiqi, A. S.; Singer, J. M.; Bahar, A. S.; Eichelberg, C.; Rink, M.; Dahlem, R.; Huland, H.; Sauter, G.; Simon, R.; Minner, S.; Burandt, E.; Stahl, P. R.; Schlomm, T.; Wurlitzer, M.; Schluter, H., MALDI Imaging on Tissue Microarrays Identifies Molecular Features Associated with Renal Cell Cancer Phenotype. *Anticancer Research* **2014**, *34* (5), 2255-2261.
181. Meding, S.; Balluff, B.; Elsner, M.; Schone, C.; Rauser, S.; Nitsche, U.; Maak, M.; Schafer, A.; Hauck, S. M.; Ueffing, M.; Langer, R.; Hofler, H.; Friess, H.; Rosenberg, R.; Walch, A., Tissue-based proteomics reveals FXD3, S100A11 and GSTM3 as novel markers for regional lymph node metastasis in colon cancer. *Journal of Pathology* **2012**, *228* (4), 459-470.
182. Datta, S.; Malhotra, L.; Dickerson, R.; Chaffee, S.; Sen, C. K.; Roy, S., Laser capture microdissection: Big data from small samples. *Histology and Histopathology* **2015**, *30* (11), 1255-1269.
183. Cahill, J. F.; Kertesz, V.; Weiskittel, T. M.; Vavrek, M.; Freddo, C.; Van Berkel, G. J., Online, Absolute Quantitation of Propranolol from Spatially Distinct 20- and 40- $\mu$ m Dissections of Brain, Liver, and Kidney Thin Tissue Sections by Laser Microdissection-Liquid Vortex Capture-Mass Spectrometry. *Analytical Chemistry* **2016**, *88* (11), 6026-6034.
184. Mollee, P.; Boros, S.; Loo, D.; Ruelcke, J. E.; Lakis, V. A.; Cao, K. A. L.; Renaut, P.; Hill, M. M., Implementation and evaluation of amyloidosis subtyping by laser-capture microdissection and tandem mass spectrometry. *Clinical Proteomics* **2016**, *13*.
185. Ryan, D. J.; Nei, D.; Prentice, B. M.; Rose, K. L.; Caprioli, R. M.; Spraggins, J. M., Protein identification in imaging mass spectrometry through spatially targeted liquid micro-extractions. *Rapid Communications in Mass Spectrometry* **2018**, *32* (5), 442-450.
186. Quanico, J.; Franck, J.; Cardon, T.; Leblanc, E.; Wisztorski, M.; Salzet, M.; Fournier, I., NanoLC-MS coupling of liquid microjunction microextraction for on-tissue proteomic analysis. *Biochimica Et Biophysica Acta-Proteins and Proteomics* **2017**, *1865* (7), 891-900.
187. DeLeo, F. R.; Otto, M.; Kreiswirth, B. N.; Chambers, H. F., Community-associated methicillin-resistant *Staphylococcus aureus* Reply. *Lancet* **2010**, *376* (9743), 767-767.
188. Graham, P. L.; Lin, S. X.; Larson, E. L., A US population-based survey of *Staphylococcus aureus* colonization. *Annals of Internal Medicine* **2006**, *144* (5), 318-325.
189. Cheng, A. G.; DeDent, A. C.; Schneewind, O.; Missiakas, D., A play in four acts: *Staphylococcus aureus* abscess formation. *Trends in Microbiology* **2011**, *19* (5), 225-232.
190. DeLeo, F. R.; Diep, B. A.; Otto, M., Host Defense and Pathogenesis in *Staphylococcus aureus* Infections. *Infectious Disease Clinics of North America* **2009**, *23* (1), 17-+.
191. Guggenberger, C.; Wolz, C.; Morrissey, J. A.; Heesemann, J., Two Distinct Coagulase-Dependent Barriers Protect *Staphylococcus aureus* from Neutrophils in a Three Dimensional in vitro Infection Model. *Plos Pathogens* **2012**, *8* (1).

192. Kehl-Fie, T. E.; Skaar, E. P., Nutritional immunity beyond iron: a role for manganese and zinc. *Current Opinion in Chemical Biology* **2010**, *14* (2), 218-224.
193. Cassat, J. E.; Moore, J. L.; Wilson, K. J.; Stark, Z.; Prentice, B. M.; Van de Plas, R. V.; Perry, W. J.; Zhang, Y. F.; Virostko, J.; Colvin, D. C.; Rose, K. L.; Judd, A. M.; Reyzer, M. L.; Spraggins, J. M.; Grunenwald, C. M.; Gore, J. C.; Caprioli, R. M.; Skaar, E. P., Integrated molecular imaging reveals tissue heterogeneity driving host-pathogen interactions. *Science Translational Medicine* **2018**, *10* (432).
194. Tong, S. Y. C.; Davis, J. S.; Eichenberger, E.; Holland, T. L.; Fowler, V. G., Staphylococcus aureus Infections: Epidemiology, Pathophysiology, Clinical Manifestations, and Management. *Clinical Microbiology Reviews* **2015**, *28* (3), 603-661.
195. Patterson, N. H.; Tuck, M.; Lewis, A.; Kaushansky, A.; Norris, J.; Van de Plas, R.; Caprioli, R. M., Next Generation Histology-Directed Imaging Mass Spectrometry Driven by Autofluorescence Microscopy. *Analytical Chemistry* **2018**, *90* (21), 12404-12413.
196. Patterson, N. H.; Tuck, M.; Van de Plas, R.; Caprioli, R. M., Advanced Registration and Analysis of MALDI Imaging Mass Spectrometry Measurements through Autofluorescence Microscopy. *Analytical Chemistry* **2018**, *90* (21), 12395-12403.
197. Patterson, N. H.; Tuck, M.; Van de Plas, R.; Caprioli, R. M., Advanced Registration and Analysis of MALDI Imaging Mass Spectrometry Measurements through Autofluorescence Microscopy. *Analytical Chemistry* **2018**, *90* (21), 12395-12403.
198. Patterson, N. H.; Tuck, M.; Lewis, A.; Kaushansky, A.; Norris, J.; Van de Plas, R.; Caprioli, R. M., Next Generation Histology-Directed Imaging Mass Spectrometry Driven by Autofluorescence Microscopy. *Analytical Chemistry* **2018**, *90* (21), 12404-12413.
199. Casadonte, R.; Caprioli, R. M., Proteomic analysis of formalin-fixed paraffin-embedded tissue by MALDI imaging mass spectrometry. *Nature Protocols* **2011**, *6* (11), 1695-1709.
200. Corbin, B. D.; Seeley, E. H.; Raab, A.; Feldmann, J.; Miller, M. R.; Torres, V. J.; Anderson, K. L.; Dattilo, B. M.; Dunman, P. M.; Gerads, R.; Caprioli, R. M.; Nacken, W.; Chazin, W. J.; Skaar, E. P., Metal chelation and inhibition of bacterial growth in tissue abscesses. *Science* **2008**, *319* (5865), 962-965.
201. Stapels, D. A. C.; Ramyar, K. X.; Bischoff, M.; von Kockritz-Blickwede, M.; Milder, F. J.; Ruyken, M.; Eisenbeis, J.; McWhorter, W. J.; Herrmann, M.; van Kessel, K. P. M.; Geisbrecht, B. V.; Rooijackers, S. H. M., Staphylococcus aureus secretes a unique class of neutrophil serine protease inhibitors. *Proceedings of the National Academy of Sciences of the United States of America* **2014**, *111* (36), 13187-13192.
202. Rooijackers, S. H. M.; Milder, F. J.; Bardoel, B. W.; Ruyken, M.; van Strijp, J. A. G.; Gros, P., Staphylococcal complement inhibitor: Structure and active sites. *Journal of Immunology* **2007**, *179* (5), 2989-2998.
203. Skaar, E. P.; Schneewind, O., Iron-regulated surface determinants (Isd) of Staphylococcus aureus: stealing iron from heme. *Microbes and Infection* **2004**, *6* (4), 390-397.
204. Clohessy, P. A.; Golden, B. E., CALPROTECTIN-MEDIATED ZINC CHELATION AS A BIOSTATIC MECHANISM IN HOST-DEFENSE. *Scandinavian Journal of Immunology* **1995**, *42* (5), 551-556.
205. Hood, M. I.; Skaar, E. P., Nutritional immunity: transition metals at the pathogen-host interface. *Nature Reviews Microbiology* **2012**, *10* (8), 525-537.
206. Ludwig, B.; Bender, E.; Arnold, S.; Huttemann, M.; Lee, I.; Kadenbach, B., Cytochrome c oxidase and the regulation of oxidative phosphorylation. *Chembiochem* **2001**, *2* (6), 392-403.
207. Wikstrom, M. K. F., PROTON PUMP COUPLED TO CYTOCHROME-C OXIDASE IN MITOCHONDRIA. *Nature* **1977**, *266* (5599), 271-273.

208. Lauderdale, K. J.; Malone, C. L.; Boles, B. R.; Morcuende, J.; Horswill, A. R., Biofilm Dispersal of Community-Associated Methicillin-Resistant *Staphylococcus aureus* on Orthopedic Implant Material. *Journal of Orthopaedic Research* **2010**, *28* (1), 55-61.
209. Chen, J.; Yoong, P.; Ram, G.; Torres, V. J.; Novick, R. P., Single-copy vectors for integration at the SaPI1 attachment site for *Staphylococcus aureus*. *Plasmid* **2014**, *76*, 1-7.
210. Grove, K. J.; Voziyan, P. A.; Spraggins, J. M.; Wang, S. W.; Pauksakon, P.; Harris, R. C.; Hudson, B. G.; Caprioli, R. M., Diabetic nephropathy induces alterations in the glomerular and tubule lipid profiles. *Journal of Lipid Research* **2014**, *55* (7), 1375-1385.
211. Kozlowski, L. P., Proteome-pl: proteome isoelectric point database. *Nucleic Acids Research* **2017**, *45* (D1), D1112-D1116.
212. Hall, Z.; Chu, Y. J.; Griffin, J. L., Liquid Extraction Surface Analysis Mass Spectrometry Method for Identifying the Presence and Severity of Nonalcoholic Fatty Liver Disease. *Analytical Chemistry* **2017**, *89* (9), 5161-5170.
213. Griffiths, R. L.; Dexter, A.; Creese, A. J.; Cooper, H. J., Liquid extraction surface analysis field asymmetric waveform ion mobility spectrometry mass spectrometry for the analysis of dried blood spots. *Analyst* **2015**, *14* (20), 6879-6885.

# Daniel J. Ryan

Work: (615) 343-3403

Cell: (910)-545-4180

[daniel.ryan@vanderbilt.edu](mailto:daniel.ryan@vanderbilt.edu)

## Permanent Address

4608 Wyoming Avenue, Unit B  
Nashville, TN 37209

## University Address

Vanderbilt University, Department of Chemistry  
7330 Stevenson Center, Station B, 351822  
Nashville, TN 37235

## EDUCATION & TRAINING

### Doctor of Philosophy, Analytical Chemistry

Vanderbilt University, Nashville, Tennessee

Advisor: Professor Richard M. Caprioli, Jeffrey M. Spraggins

2015 – June 2019

### Bachelor of Science, Chemistry, Minors: Mathematics, Honors: Summa Cum Laude

University of North Carolina at Charlotte, Charlotte, North Carolina

Advisor: Professor Brian T. Cooper

2011 – May 2015

## PUBLICATIONS

5. **Daniel J. Ryan**, Nathan H. Patterson, Nicole E. Putnam, Aimee D. Wilde, James E. Cassat, Eric P. Skaar, Richard M. Caprioli, Jeffrey M. Spraggins. MicroLESA: Integrating Autofluorescence Microscopy, In Situ Micro-Digestions, and Liquid Extraction Surface Analysis for High Spatial Resolution Targeted Proteomic Studies. *Anal. Chem.* **2019**.
4. Eric C. Spivey, Josiah C. McMillen, **Daniel J. Ryan**, Jeffrey M. Spraggins, Richard M. Caprioli. Combining MALDI-2 and Transmission Geometry Laser Optics to Achieve High Sensitivity for Ultra-High Spatial Resolution Surface Analysis, *J. Mass Spectrom.* **2019**, 54: 366-370.
3. **Daniel J. Ryan**; Jeffrey M. Spraggins; Richard M. Caprioli. Protein Identifications in MALDI Imaging Mass Spectrometry: A Review, *Curr. Opin. Chem. Biol.* **2018**, 48: 64-72.
2. Boone M. Prentice; **Daniel J. Ryan**; Raf Van de Plas; Richard M. Caprioli; Jeffrey M. Spraggins. Enhanced Ion Transmission Efficiency of Proteins up to m/z 22,000 on a 15T FT-ICR MS for MALDI Imaging Applications. *Anal. Chem.* **2018**, 90, 5090-5099.
1. **Daniel J. Ryan**, David Nei, Boone M. Prentice, Kristie L. Rose, Richard M. Caprioli, Jeffrey M. Spraggins. Protein identification in imaging mass spectrometry through spatially targeted liquid micro-extractions. *Rapid Commun. Mass Spectrom.* **2018**, 32; 442-450.

## PRESENTATIONS (*presenter underlined*)

12. **Daniel J. Ryan**, Heath N. Patterson, James E. Cassar, Eric P. Skarr, Richard M. Caprioli, Jeffrey M. Spraggins “Analysis of *Staphylococcus aureus* Infections through Spatially Targeted Micro-Proteomics” *67<sup>th</sup> ASMS Conference on Mass Spectrometry & Allied Topics*, Atlanta, GA, June 2019.
11. **Daniel J. Ryan**, Heath N. Patterson, Jeffrey M. Spraggins, Richard M. Caprioli, “microLESA: Combining Fluorescence-Guided, Micro-Digestions with Liquid Surface Extractions” *Chemical Biology Association of Students Monthly Seminar Series*, Nashville, TN, May 2019.
10. **Daniel J. Ryan**, Heath N. Patterson, Jeffrey M. Spraggins, Richard M. Caprioli, “Advanced Surface Sampling Technologies: Combining Fluorescence-Guided, Micro-Digestions with Liquid Surface Extractions” *International Mass Spectrometry Conference*, Florence, Italy, August 2018.
9. Boone M Prentice; **Daniel J. Ryan**; Raf Van de Plas; Jeffrey M. Spraggins; Richard M. Caprioli, “Enhanced ion funnel transmission efficiency up to m/z 24,000 for MALDI FT-ICR protein imaging mass spectrometry”. *66<sup>th</sup> ASMS Conference on MS & Allied Topics*, San Diego, CA, June 2018.
8. **Daniel J. Ryan**, Jeffrey M. Spraggins, Boone M. Prentice, Richard M. Caprioli, “High Spatial Resolution MALDI IMS on a 9.4T FTICR Through the Addition of a Second Laser Enabling Simplistic Beam Alignment and Dual Modes of Operation” *Imaging Mass Spectrometry Society Inaugural Conference*, Boston, MA, October 2017.
7. **Daniel J. Ryan**, David Nei, Boone M. Prentice, Jeffrey M. Spraggins, Richard M. Caprioli, “Linking Protein Identifications to Imaging Mass Spectrometry through Spatially Resolved Proteomics” *AbbVie Analytical Research Symposium*, Chicago, IL, August 2017.

6. **Daniel J. Ryan**, David Nei, Boone M. Prentice, Jeffrey M. Spraggins, Richard M. Caprioli, "Spatially Resolved Proteomics to Improve Protein Identification in Imaging Mass Spectrometry" *Vanderbilt Institute of Chemical Biology Symposium*, Nashville, TN, August 2017.
5. **Daniel J. Ryan**, David Nei, Boone M. Prentice, Jeffrey M. Spraggins, Richard M. Caprioli, "Histology Directed Liquid Surface Extractions coupled Directly to Liquid Chromatography for Improving Identification Strategies in Advanced IMS Applications" *65<sup>th</sup> ASMS Conference on MS & Allied Topics*, Indianapolis, IN, June 2017.
4. Jeffrey M. Spraggins, Raf Van de Plas, Jessica L. Moore, **Daniel J. Ryan**, Richard M. Caprioli, "Maximizing performance of spatial proteomics through the fusion of ultra-high speed MALDI-TOF and high mass resolution MALDI FTICR IMS," *64<sup>th</sup> ASMS Conference on MS & Allied Topics*, San Antonio, TX, June 2016.
3. **Daniel J. Ryan**, Boone M. Prentice, Raf Van de Plas, Jeffrey M. Spraggins, Richard M. Caprioli, "Histology-Directed Lipid Identification: Advanced Imaging Mass Spectrometry and Liquid Extraction Technologies Enable Spatially Specific Tandem Mass Spectrometry" *64<sup>th</sup> ASMS Conference on MS & Allied Topics*, San Antonio, TX, June 2016.
2. **Daniel J. Ryan**, Brittany Gray, Daniel Rabinovich, "Expanding the Octet: A look into Hypervalent Compounds," *2013 University of North Carolina Charlotte Undergraduate Research Conference*, Charlotte, NC, June 2013.
1. **Daniel J. Ryan**, Brittany Gray, Daniel Rabinovich, "Synthesis of New Hypervalent Compounds," *State of North Carolina Undergraduate Research and Creativity Symposium*, Duke University, Durham, NC, May 2012.

## HONORS, AWARDS, & FUNDING

**2019 Warren Fellowship**

*Summer 2019*

**2018 Journal of Mass Spectrometry Symposium Award**

*Spring 2018*

**Vanderbilt Institute of Chemical Biology Fellowship**

*Fall 2015 – Spring 2016*

**Suma cum laude, BS Chemistry**

*Spring 2015*

**Dean's list**

*Fall 2011 – Spring 2015*

## LABORATORY EXPERIENCE

**Graduate Dissertation Research** (Vanderbilt University, Dept. of Biochemistry)

*2015 - present*

- o Research emphasizing the fundamental development and technological advancements of protein identification for imaging mass spectrometry (IMS) under the direction of Professor Richard M. Caprioli
  - Optimized and incorporated the use of enhanced robotic liquid surface extractions to aid in protein identification strategies in MALDI IMS experiments through the use of online LC-MS, top-down, and bottom-up mass spectrometry.
  - Developed a new targeted proteomic workflow coined 'microLESA' by combining autofluorescence microscopy and robotic, micro-enzymatic digestions to target tissue foci on the order of ~120 µm for digestion and mass spectrometry analysis.
  - Designed the addition and implementation of a second, high speed laser to improve spatial resolution in FTICR MALDI IMS to <10 µm.
  - Enhanced protein ion transmission on a 15T FT-ICR mass spectrometer by modifying the source region in order to optimize the pressure and improve transmission efficiency, allowing for the detection of species up to *m/z* 22,000 Da.

**Undergraduate Research** (University of North Carolina at Charlotte, Dept. of Chemistry)

*Fall 2013 - Spring 2015*

- o Establishing methods of derivatization to test the accuracy of the new metabolomics deconvolution software ADAP 2.0 through the use of GC-MS under the supervision of Dr. Brian Cooper.

**Undergraduate Research** (University of North Carolina at Charlotte, Dept. of Chemistry)

*Fall 2012 - Spring 2013*

- o Synthesis and reactivity of a new bis(picoly)selone ligand, including the preparation of silver(I) complexes and hypervalent halogen (Br<sub>2</sub>, I<sub>2</sub>) derivatives

## TECHNICAL EXPERTISE

### Instrumentation

- o Extensive experience in troubleshooting and fixing a variety of instruments on several platforms
  - 15T FT-ICR MS (Bruker Solarix)
  - 9.4T FT-ICR MS (Bruker Solarix)
  - MALDI TOF MS (Bruker RapiFlex)
  - Orbitrap Elite (Thermo Velos Pro)
  - TriVersa NanoMate Surface Sampler (Advion)
  - scieFLEXARRAYER Liquid Dispenser (Sciencion AG)

### Utilities/Software

- o Microsoft Office
- o PowerPoint
- o SIMION
- o Autodesk Inventor
- o flexImaging, flexControl
- o Xcalibur
- o PMi Byonic
- o Bruker Data Analysis

## TEACHING & MENTORING EXPERIENCE

- Workshop Assistant (Vanderbilt University, Department of Biochemistry, MSRC)** *April 2018*
- Advanced Imaging Mass Spectrometry (AIMS) Laboratory Course- “Surface Sampling Technologies”
  - Taught laboratory skills to 30 scientists (technicians, graduate students, postdocs, principal investigators)
- Invited Panelist (American Society for Mass Spectrometry Annual Conference 2017 [ASMS])** *June 2017*
- GSC “Graduate Student Panel: Experiences and Advice” Event
  - Q&A for ~20 undergraduate students regarding professional and academic scientific work experiences
- Workshop Assistant (Vanderbilt University, Department of Biochemistry, MSRC)** *April 2017*
- Advanced Imaging Mass Spectrometry (AIMS) Laboratory Course- “Liquid Extraction Surface Analysis”
  - Taught laboratory skills to 27 scientists (technicians, graduate students, postdocs, principal investigators)
- Workshop Assistant (Vanderbilt University, Department of Biochemistry, MSRC)** *April 2016*
- AIMS Laboratory Course- “FTICR Instrumentation and Applications”
  - Taught laboratory skills to 26 scientists (technicians, graduate students, postdocs, principal investigators)
- Lecture Series (Vanderbilt University, Department of Biochemistry, MSRC)** *Fall 2015 - present*
- Lecturer: “Ion Optics and Ion Transmission”, “Ultraviolet Photodissociation and Ion Spectroscopy”
- Teaching Assistant (University of North Carolina at Charlotte, Department of Chemistry)** *Spring 2015*
- Physical Chemistry: Thermodynamics
  - Assisted in course instruction for 28 undergraduate students
  - Course instruction included exam administration, grading assignments (quizzes, labs, homework), leading review sessions, and holding office review hours for students
- Laboratory Assistant (University of North Carolina at Charlotte, Department of Chemistry)** *Fall 2014*
- Quantitative Analysis
  - Assisted in the execution of the laboratory course instruction with the professor for 30 undergraduate students
  - Managed laboratory assignments such as assisting and demonstrating various experiments, and ensuring experiments were prepared for each course.
- Teaching Assistant (University of North Carolina at Charlotte, Department of Chemistry)** *Fall 2014*
- Physical Chemistry: Quantum Mechanics
  - Assisted in course instruction for 28 undergraduate students
  - Course instruction included exam administration, grading assignments (quizzes, labs, homework), leading review sessions, and holding office review hours for students